MASARYKOVA UNIVERZITA
Přírodovědecká fakulta
Ústav teoretické fyziky a astrofyziky

Diplomová práce

Brno 2024 Bc. Kateřina Neumannová

MASARYKOVA
UNIVERZITA
PŘÍRODOVĚDECKÁ FAKULTA
ÚSTAV TEORETICKÉ FYZIKY A ASTROFYZIKY

Mira variable stars in globular clusters

Diplomová práce

Bc. Kateřina Neumannová

Vedoucí práce: doc. Ernst Paunzen, Dr.rer.nat **Brno 2024**

Bibliografický záznam

Autor:	Bc. Kateřina Neumannová Přírodovědecká fakulta, Masarykova univerzita Ústav teoretické fyziky a astrofyziky
Název práce:	Mira variable stars in globular clusters
Studijní program:	Fyzika
Studijní obor:	Astrofyzika
Vedoucí práce:	doc. Ernst Paunzen, Dr.rer.nat
Akademický rok:	2023/2024
Počet stran:	viii + 77
Klíčová slova:	Kulová hvězdokupa; Proměnná hvězda; Metalicita, Mirida

Bibliographic Entry

Author:	Bc. Kateřina Neumannová Faculty of Science, Masaryk University Department of Theoretical Physics and Astrophysics

Title of Thesis:	
Degree Programme:	Physics
Field of Study:	Astrophysics
Supervisor:	doc. Ernst Paunzen, Dr.rer.nat
Academic Year:	2023/2024
Number of Pages:	viii + 77
Keywords:	Globular cluster; Variable star; Metallicity, Mira

Abstrakt

Cílem této práce bylo studovat miridy ve výduti a v halo naší galaxie včetně těch, které se nacházejí v kulových hvězdokupách. Získali jsme data pro 1608 mirid ve výduti, z toho 308 se nachází v 15 kulových hvězdokupách. Pro hvězdy v halo jsme získali 1954 mirid, z toho 4 se nachází ve 3 kulových hvězdokupách. Miridy ve výduti vykazují bimodální distribuci metalicity s vrcholem pro –0,4 dex a +0,5 dex, zatímco miridy v halo mají největší četnost pouze pro metalicitu +0,5 dex. Při studiu závislosti periody na metalicitě se neukázal žádný trend, ale perioda mirid ve výduti je v průměru o 30 dnů delší než pro miridy v halo. Rozdělení typu mirid na O/C (kyslíkové/uhlíkové) bylo určeno z programu Upsilon, světelných křivek, barevně barevného nebo barevně magnitudového diagramu, s tím, že ve výduti hojně převládají O miridy oproti C miridám. Závislost logaritmu periody o základu 10 na magnitudě v infračervené části spektra nám dává lineární závislost s tím, že při využití filtru v optické části spektra se závislost převrací. Kulové hvězdokupy Ter 6 a Djor 1 ve výduti vykazují vysokou extinkci ve srovnání s ostatními kulovými hvězdokupami. Pohyblivý barevný diagram magnitudy vykazuje v případě halo i výdutě vysoké amplitudy změn jasnosti související se silnými pulzacemi mirid. Kromě toho miridy v halo se nachází ve dvou oblastech na diagramu, přičemž jedna se nachází v oblasti velmi nízkých teplot, zatímco druhá v oblasti velmi vysokých teplot. Po korekci ovlivnění extinkcí zůstávají hodnoty zbavené zčervenání pro halo i výduť v souladu s původními závislostmi, což potvrzuje stabilitu našich analýz.

Abstract

The aim of this thesis was to study Miras in the bulge and halo of our galaxy, including those in globular clusters. We obtained data for 1608 Miras in the bulge of which 308 are located in 15 globular clusters. For the stars in the halo, we obtained data for 1954 Miras of which 4 are located in 3 globular clusters. Miras in the bulge show a bimodal metallicity distribution with a peak for –0.4 dex and +0.5 dex, while Miras in the halo have the highest abundance only for +0.5 dex metallicity. When studying the dependence of period on metallicity, no trend is shown, but the period of Miras in bulge is on average 30 days longer than for Miras in halo. The O/C (Oxygen/Carbon) distribution of Miras type was determined from Upsilon, light curves, color-color or color-magnitude diagrams, with O Miras being more abundant in bulge than C Miras. The dependence of the logarithm of the base 10 period on magnitude in the infrared part of the spectrum gives us a linear dependence, with the dependence inverting when a filter is used in the optical part of the spectrum. The globular clusters Ter 6 and Djor 1 in the bulge show high extinction compared to other globular clusters. Moving color–magnitude diagrams show high amplitudes of luminosity changes associated with strong Miras pulsations in both the halo and bulge cases. In addition, Miras in the halo are located in two regions on the diagram, one in the very low effective temperature region, while the other in the very high effective temperature region. After correcting for extinction effects, the dereddened values for both halo and bulge remain consistent with the original dependencies, confirming the stability of our analyses.

MUNI
SCI

MASARYKOVA UNIVERZITA
PŘÍRODOVĚDECKÁ FAKULTA
KOTLÁŘSKÁ 2, 611 37 BRNO
IČ: 00216224
DIČ: CZ00216224

ZADÁNÍ
DIPLOMOVÉ PRÁCE

Akademický rok: 2023/2024

Ústav:	Ústav teoretické fyziky a astrofyziky
Studentka:	Bc. Kateřina Neumannová
Program:	Fyzika
Specializace:	Astrofyzika

Ředitel *ústavu* PřF MU Vám ve smyslu Studijního a zkušebního řádu MU určuje diplomovou práci s názvem:

Název práce:	Mira variable stars in globular clusters
Název práce anglicky:	Mira variable stars in globular clusters
Jazyk závěrečné práce:	angličtina

Oficiální zadání:
The class of Mira variables will be investigated by archival data, and if possible, with own observations. For this, suitable candidates from the newest catalogues of star clusters using Gaia data will be chosen and analysed.

Literatura:
BUDDING, E. a Osman DEMIRCAN. *An introduction to astronomical photometry*. 2nd ed. Cambridge: Cambridge University Press, 2007. xvi, 434. ISBN 9780521847117.

MIKULÁŠEK, Zdeněk a Miloslav ZEJDA. *Proměnné hvězdy*. ÚTFA PřF MU. Brno, 2009.

Vedoucí práce:	doc. Ernst Paunzen, Dr.rer.nat
Datum zadání práce:	11. 1. 2022
V Brně dne:	13. 9. 2023

Zadání bylo schváleno prostřednictvím IS MU.

Bc. Kateřina Neumannová, 11. 1. 2022
doc. Ernst Paunzen, Dr.rer.nat, 13. 1. 2022
Mgr. Dušan Hemzal, Ph.D., 25. 1. 2022

Poděkování

Na tomto místě bych chtěla poděkovat mému vedoucímu doc. Ernst Paunzen, Dr.rer.nat za cenné rady a vedení mé práce, také za jeho vstřícný přístup po dobu psaní mé práce. Zároveň bych chtěla poděkovat všem, kteří mě v průběhu mého studia a psaní práce podpořili, a to především mé rodině a přátelům.

Prohlášení

Prohlašuji, že jsem svoji diplomovou práci vypracovala samostatně pod vedením vedoucího práce s využitím informačních zdrojů, které jsou v práci citovány.

Brno 2024

. . . . . .

Bc. Kateřina Neumannová

Contents

Introduction

Among the first observed and documented globular clusters was Omega Centauri, which was first classified as a star and in the 19th century by John Herschel as a cluster. Today, we know of approximately 157 globular clusters in the Galaxy. Globular clusters are very old gravitationally bound of population II stars. These objects are found in the halo and bulge of the Galaxy. They are very stable and their members show similar ages and metallicities. By studying them, we are therefore able to estimate the age of the Universe, its evolution or the composition of the primordial stars. Thanks to the large number of stars in a relatively small area, we are also able to study the dynamics of stars and the gravitational interactions between them. We may then apply this to the study of larger gravitationally bound groups such as galaxies.

Mira variable stars are old pulsating stars that are found in globular clusters, among other places. This type of low and intermediate-mass stars are found on the asymptotic giant branch (AGB). The first Mira type star observed was Omicron Ceti, which was nicknamed the Wonderful, hence the Latin name Mira. Among the first observers to note its change in brightness was David Fabricius in the 16th century, but it was not until several centuries later that it was classified as a proper variable star type. The study of these stars is very useful because of their well-defined relationship between period and luminosity. This allows us to use Miras as a standard candle, especially when studying old elliptical galaxies or the halo of our Galaxy. It is also essential to study Miras because the Sun will most likely become a Mira in the later stages of its evolution, and studying Miras will therefore allow us to better understand the processes occurring in our parent star.

The purpose of this thesis was to investigate Mira variable stars in the galactic halo and bulge and to classify these Miras into globular clusters. Subsequently, it was crucial to investigate the correlations and properties between these stars, determine type of Miras and understand their behaviour. This thesis deals with the general properties of these stars available from surveys and articles and is not intended to find new Miras or to replace articles focusing on a small sample of Miras with a particular issue. This thesis is intended to provide insight into the behaviour and properties of these stars in general terms, looking for their common/different properties depending on location in the Galaxy or cluster.

In the first two chapters Globular clusters and Mira variable stars we discuss the theoretical description of globular clusters and Miras, based on already-known information, and put them in context. In the following chapter Methodology we deal with the acquisition, collection, selection and processing of real data. As the main part, see chapter Analysis, we first analyze and explore the dependencies from the processed data for Miras in the bulge and then for Miras in the halo. Finally, in the chapter Conclusion and summary we summarize our results and put them in context with each other.

Globular clusters

1.2 Definition and general information

Globular clusters (GCs) can be defined as dense gravitationally bound groups of thousands to millions of stars (1). Our Galaxy is thought to contain about 160 globular clusters (2), which are located in the Galactic halo and bulge. Because GCs are strongly bound by gravity, they are very stable objects and are even as old as the universe itself (1).

Figure 1.2.1: Example of globular cluster — Omega Centauri (11)

The age of a cluster can be determined from the Hertzsprung–Russell (HR) diagram or from the color–magnitude diagram (CMD) since the stars in the GC have similar ages and places of formation. It is known that stars with the highest mass (luminosity) evolve the fastest, and thus leave the main sequence (defined as the region in the HR where stars have fusion to He in their cores) first. Gradually, the less massive ones follow. The departure from the main sequence can be observed as a "bend" – a turnoff point, where we observe a relatively short main sequence in GCs, which in itself suggests that these are old objects (9), see figure 1.2.2. This turnoff point, which corresponds to a certain luminosity and

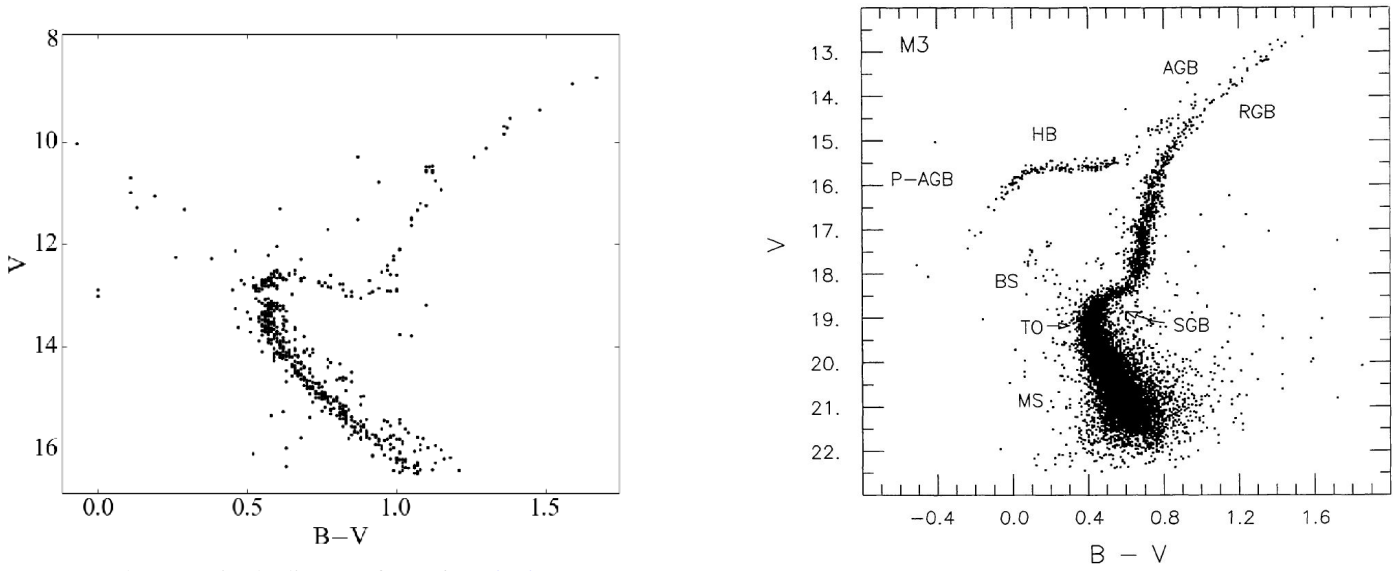

(a) Color-magnitude diagram for M67 (Viani, 2017)

(b) Color-magnitude diagram for M3 (Renzini, 1988)

Figure 1.2.2: Color-magnitude diagram for open cluster M67 (3.6 – 4.8 Gyr (Viani, 2017)) and for globular cluster M3 (11.4 Gyr (Forbes, 2010)). We can see that the main sequence in the older globular cluster is more condensed, whereas in the younger open cluster, it is more extended. But the turnoff point may be affected by the number of stars in the cluster, or by not including low magnitudes, or by a filter in which stars may not be visible.

color (or effective temperature), is a direct function of the age of the cluster (Carroll, 2017). A slightly more accurate method is isochrone fitting, where we have a theoretical isochrone curve for a certain age and metallicity of the stars, which we compare with specific observed/measured values (Angus, 2019). Thus, by comparing the positions of stars with different isochrones on the HR diagram, it is also possible to estimate the age and metallicity of the stellar population in clusters, which approaches up to 12.5 Gyr for GCs (Forbes, 2018).

Previously, it was assumed that the stars in a globular cluster formed simultaneously and from the same molecular cloud, and thus would have similar properties (age, chemical composition, place of origin). However, there is now emerging evidence that some globular clusters (especially those in the halo) contain multiple stellar populations (Mackey, 2004). This is also supported by the fact, we observe a bimodal distribution of metallicities, where the younger population is slightly more metal-rich than the older one (Mackey, 2004). Explanations could be that there was an accretion of a dwarf galaxy by our Galaxy (Bellazzini, 2003), an encounter with a molecular cloud that triggered further star formation (Kruijssen, 2015), or close encounters that could have led to a mixing of matter/clouds and thus the formation of new stars (Kruijssen, 2015). These theories are supported by studies that have determined that up to 50% of the mass of a galaxy's stellar halo is due to mergers with dwarf galaxies that contain a cluster (Mackey, 2004).

Currently, there is no known evidence of active star formation in globular clusters. It is thought that all the dust was depleted to form the first stars or was blown out of the cluster

by massive first-generation stars that exploded as supernovae (3), (Charbonnel, 2012). Thus, we have to rely only on theoretical scenarios and models which help explain the formation of globular clusters. Two scenarios are the most supported. The first scenario is the formation of GCs in a period close to the reionization period in haloes of the dark matter (Peebles, 1968). The second scenario of GC formation is the natural star formation process in regions of higher pressure in galactic discs, where GC formation may be enhanced when galaxies or clusters merge with each other (Kruijssen, 2015).

In general, globular clusters contain old stars of population II with low metallicity. They can be found in all types of galaxies, whereas in ours they are found in the galactic halo and bulge and some crossing the Galactic plane, for example because the have highly eccentric orbits. Halo and bulge differ in several ways. While GCs in the bulge follow circular orbits, GCs in the halo follow very eccentric elliptical orbits (4). The difference is also evident in the abundance, where GCs in the halo have a lower abundance of heavier elements compared to those found in the bulge (3). This may be due to the fact that most of the gas was expelled from the GC halo before it was enriched by the supernova explosion (3). While this gas existed in most of Galaxy bulge.

The first observations of a globular cluster Omega Centauri, date back to ancient Greece, where it was thought to be a star. However, it was not until the early 19th century that John Herschel reclassified it as a cluster, as he was already able to distinguish some stars from one another (5). Observing individual stars in star clusters is complicated by the high density and concentration of stars. Another problem is interstellar extinction, which is particularly evident in bulge observations. Breakthroughs in GC observation have come with the use of space telescopes such as Hubble (7) and JWST (8), which have been able to detect individual stars in a cluster accurately (5). These telescopes have given us a detailed view of the structure and composition of clusters and a better understanding of the processes that take place within them.

1.3 Dynamics of globular cluster

As mentioned, globular clusters are high-density objects that contain thousands to millions of stars. The stellar density of a cluster can be affected by various factors, such as the cluster's age, mass, location and other physical parameters. For this reason, the American astronomer Ivan R. King introduced the parameters; core radius and tidal radius, which describe the real density distribution of stars in a cluster (also called density law) (King, 1962). These parameters are collectively called King models, and they are a good fit to describe the structure of a GC. Sometimes the half-mass radius, half-light radius, and Jacobi radius are added to these parameters for an even more detailed description.

The core radius (r_c), sometimes called the King radius, is the radius where the surface brightness drops to half its central value (Carlson, 2001). It measures the degree of concentration at the centre of the cluster and it is the internal energy of the system (King, 1962). Core radius has several meanings, however, depending on the purpose it is intended to serve. The definition we have given here is used by theorists. Numerical N-body simulations define the core radius as a function of the density radius (the density-weighted average of the distance of the star from the mean value of the density (Mardling, 2001), or from the point of highest density in the cluster (Aarseth, 2003). It has also been found that

the core radius increases with the age of the cluster. There is a segregation of stars, with heavier stars and binaries having lower velocities on average, falling to the centre, while lighter stars are moved to the outer parts of the cluster. The denser core of the cluster is consequently more prone to collisions that impart thermal kinetic energy to the cluster, resulting in an increase in pressure and subsequent expansion of the cluster (16).

A similar quantity is the half-light radius (r_e), which is defined as the distance from which we can see half the light of the cluster, see figure 1.3.1a. This quantity is usually larger than the core radius and is independent of the concentration of stars and therefore the size of the cluster (Carlson, 2001).

The tidal radius (r_t), also called the King tidal radius, is the radius at which the gravity of the Galaxy has a greater effect on the stars in a cluster than the cluster itself. Thus, we measure the boundary density at the edge of the cluster, as is shown in figure 1.3.1b, which is able to help us determine the boundary mass of the Galaxy (Carlson, 2001). It has been observed that there is a decrease in the tidal radius of the cluster during its lifetime, the main source of which is evaporation (the escape of low-mass stars from the cluster). The difference between the Jacobi radius and the tidal radius stems from the nature of their measurements - the tidal radius is determined by direct measurement, while the Jacobi radius is a theoretical estimate derived from certain assumptions in the theoretical assumptions. (Binney, 2008).

All these quantities are important for understanding the evolution and predicting the behaviour of clusters. They can give us information about the size of a cluster, its mass or even the mass of the Galaxy. They allow us to get information about how densely stars are grouped in the centre of the cluster and how they interact with their surroundings.

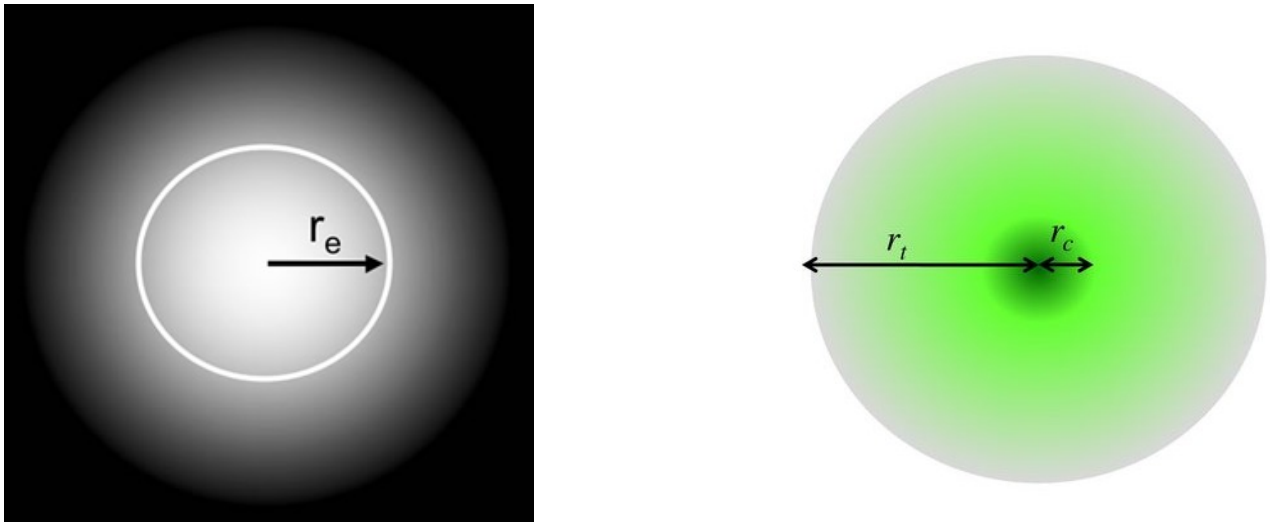

(a) Half-light radius for cluster (38)

(b) Core radius and tidal radius for cluster (39)

Figure 1.3.1: Diagram showing the approximate radii from the centre of the cluster, corresponding to core, tidal and half-light radii.

1.4 Variable stars in globular clusters

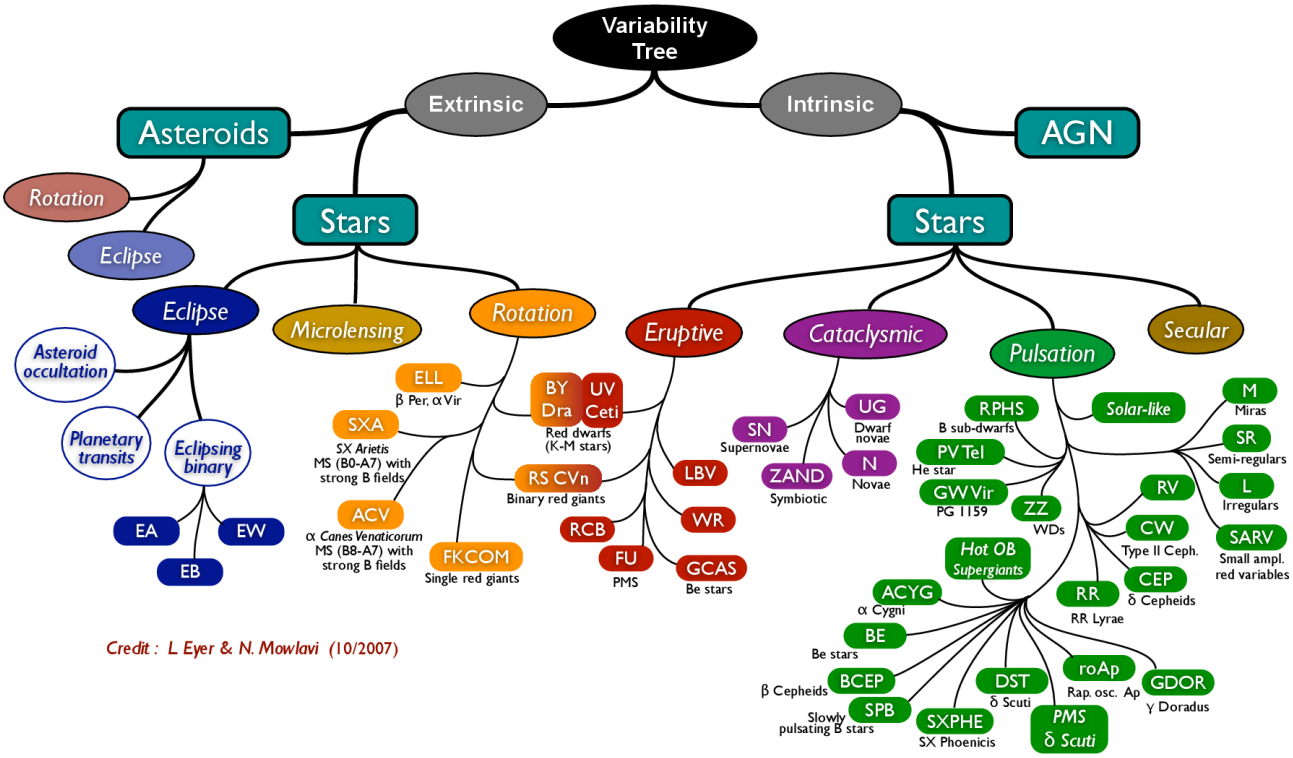

Figure 1.4.1: Classification of variable stars (Eyer, 2007)

Variable stars are stars whose brightness changes over time. These changes can be periodic, semi-periodic or irregular and take place on a time scale of milliseconds (pulsars) (10) to thousand of years (Percy, 1978).

There may be several reasons for their variability. The basic classification of variable stars is according to the cause of the change in their brightness. They are divided into intrinsic and extrinsic variable stars. An illustrative distribution of variable stars is shown in Fig. 1.4.1.

Extrinsic variable stars are stars where the total flux of light coming from the star does not change, but only the amount of light we are able to detect on Earth changes. This may be due to the star's rotation (due to rapid rotation, the star's surface becomes flattened, and/or we can also observe spots on its surface) or the star may be occulting (e.g. exoplanets).

On the other hand, intrinsic variable stars are real variable stars, meaning that there are physical changes to the star itself. There can be several reasons for this, which is why these stars are divided into three basic groups; pulsating, eruptive and cataclysmic variable stars. Pulsating variable stars exhibit surface layer changes where all or part of the star expands and contracts (12). For example, pulsating variable stars can include; RR Lyrae, W Virginis, Delta Cephei, Mira variables. As the name suggests, eruptive variable stars include stars that show a change in brightness due to eruptions and/or ejections of material on the stellar surface. There can also occur interactions with interstellar matter (10). These include, e.g.; Herbig Ae/Be and Wolf-Rayet stars. Cataclysmic variables are binary

systems where a mass transfer from a classical star (usually the main sequence type) to a white dwarf occurs, converting potential energy into X-rays during the process (13). Into this type of variable stars, we can also include explosive variable stars, where explosions caused by thermonuclear reactions, such as supernovae explosions, or explosions caused by the merging of two stars (10).

Among the earliest observers of variable stars were the ancient Egyptians, who have preserved records of the observations of the occulting variable star Algol (Jetsu, 2015). Somewhat later, in the 17th century, David Fabricius observed the variable star Omicron Ceti (Mira), which he fondly believed to be a nova. Some 40 years later, Johannes Holwards determined its period of brightness changes to be 11 months (10). In June 2022 we have identified 58035 variable stars (14).

Variable stars can be found in all parts of the Galaxy. It is therefore not exceptional that they are also found in GC. In the 20th century, 90% of variable stars in GC were of the RR Lyrae type (Clement, 2017). With the invention of the CCD detector in the late 20th century, it became possible to detect fainter stars, even those with a weaker change in brightness over time. Thus, there has been an increase in variable stars of the Slow variables (Mira variables, Semi-regular variables), Eclipsing binaries and SX Phoenicis (SX Phe) type, although RR Lyrae type stars are still the most numerous group (Clement, 2017). According to the article by (Clement, 2001) variable stars of the W Virginis, Cepheids and RV Tauri types can also be found in globular clusters but not in the abundant numbers as the previous ones. The complete evolution of the amount of variable stars in globular clusters is in table 1.4.2.

Variables	1939	1955	1973	2001	2016
RR Lyrae	613	1114	1202	1842	>2925
Type II Cep, RV Tau	27	32	37	60	>85
Slow Vars: L, M, SR	15	53	71	117	>475
SX Phe	0	0	0	117	>325
Eclipsing, ELL	1	2	2	96	>400

Figure 1.4.2: The number of different types of variable stars in globular clusters (Clement, 2017)

There are several reasons why we observe these variable stars in globular clusters. One reason is that globular clusters contain already evolved stars that are in the giant or post-AGB branch, which is fulfilled by variable stars such as RR Lyrae, Mira, RV Tauri and W Virginis. The selection effect also plays a role, where we can better detect brighter stars with more pronounced brightness changes, such as the variable star type SX Phe.

The study of variable stars is very important to astronomers because we can use them to determine, for example, the distances in the Universe or its age. They can also help us understand how the Universe is expanding, how a star has evolved or how it will evolve. Thus variable stars are an important tool for understanding the behaviour of the Universe, and the other stars, including our Sun (15).

Mira variable stars

2.1 General information

Mira variables are pulsating variable cool giants located on the asymptotic giant branch (AGB) of HR diagram, 2.1.1. Low to intermediate-mass stars, typically with an initial mass of 1–2 $M_\odot$, enter the Miras phase on the AGB (Meyers, 2001). They have a high luminosity (10^3 $L_\odot$) and a low effective temperature of up to 4000 K (Meyers, 2001). Because of the already advanced stage of evolution, during which the star's size increases, Miras have radii reaching up to 2 AU, where the low effective temperatures in the atmospheres can lead to the formation of silicate or graphite dust at its edge (Reid, 2002). Periods of luminosity variation range from 80 days to 1000 days, where, due to the high period dispersion, semiregular variable stars or irregular variable stars are sometimes included in this type of variable stars (Willson, 2012). It is generally assumed that semiregular variable stars are predecessors of Miras, so they are slightly lower on the HR diagram in the AGB than Miras. They also have shorter periods, smaller amplitudes of change in brightness, and pulsate in multiple modes (ussualy three or more) (Bedding, 1998).

In addition to their long periods, Miras are characterized by high observed amplitudes of luminosity variations, especially in the optical, where variations reach values of up to 11 mag (Meyers, 2001). In contrast, amplitudes of at most 1 mag are observed in the infrared due to the fact that the dust surrounding the stars does not absorb infrared light, and also because the effective temperature changes during pulsations are mainly visible in the optical part of spectra (17).

It has also been found that most Miras have an asymmetric shape, where the exact reason is not fully understood. It is thought that the cause may be non-radial pulsations or an asymmetric dust cloud around the star. Last but not least, the reason may be the strong stellar wind, which is typical for AGB stars and reaches values of up to 10^{-5} $M_\odot$ per year for Miras (Ragland, 2006).

As of 2017, the GCVS catalogue states that approximately 8500 Miras are known, which corresponds to about 15% of all variable stars in this catalogue (18).

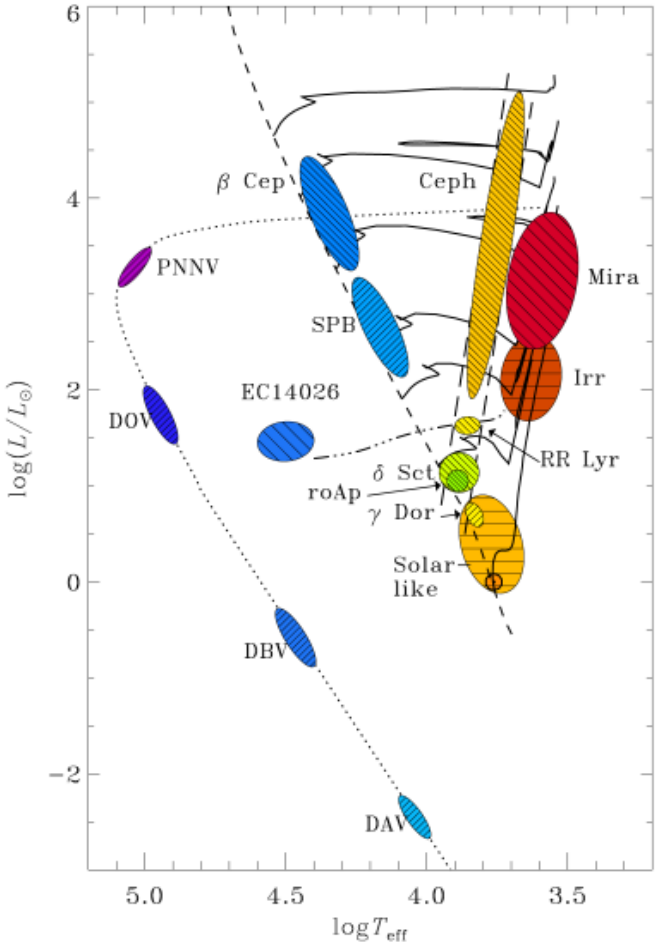

Figure 2.1.1: Location of variable stars on the HR diagram. Mira variables are located next to instability strip (17).

2.2 History and observation

The first observed Mira variable star was Omega Ceti, nicknamed Mira (the "wonderful"), whose first systematic observation dates back to the 16th century by the Dutch astronomer David Fabricius. However, he mistakenly thought it was a nova. It was only a few years later that Johannes Wolward identified it as a variable star and defined its period as 11 months. In the 17th century, its value was specified by Ismael Bouillaud, who set its period to 333 days, where its actual period is 332 days. In the 19th century, Seth Chandler investigated the causes of changes in period and in light curves. It was not until the 20th century, with the arrival of modern technology and improved knowledge of physics, that Theodore Stern and Leon Campbell proposed a fairly accurate statistical method for determining period changes, which is still being improved using the numerical modelling of stars (17).

Miras can be easily observed with amateur telescopes due to the high luminosities and apparent visual magnitudes of these stars. As a result, we have long observational records that are able to give us an insight into the behaviour and evolution of these stars and also

low to intermediate-mass stars in general. With their advanced stage of evolution, during stellar winds, we are able to observe Miras on longer timescales. Their metallicities are able to give us insights into the past of the Universe and its composition. Last but not least, they are important for the description and evolution of our Sun, which will most likely also enter the Miras phase.

2.3 Evolution of low-mass stars (Mira-like type)

Miras are stars well over 7 Gyr (Feast, 2008) old that have passed through the main sequence (MS), red giant branch (RGB), horizontal branch (HB) and now asymptotic giant branch (AGB) phases. After the core of the main sequence (MS), the star began to run out of H (which was burned to He by the pp-process), the thermonuclear reactions in the core were unable to resist the gravity of the surrounding layers and the core began to shrink, denser and the core temperature increase. A H shell ignites around the core, which covers the star's luminosity, and even surpasses its previous luminosity. Some of the energy is radiated, but some is captured by the stellar envelope and used to expand it. The core becomes denser, fully He and even degenerate (resisting further shrinking). The star moves from the MS to the RGB phase.

The effective temperature and mass of the core increase (in degenerate gas the pressure does not depend on the temperature) and so does the energy production. Once it reaches approximately 100 million K (19), a He flash occurs – an explosive ignition of the He reaction using the triple-alpha process. The He burning into carbon and oxygen occurs. The nucleus expands and degeneration stops. The expansion of the core causes that a layer of burning H to reach the higher, cooler layers of the star and the rate of reactions drops. This causes shrinkage and heating of the star, which goes into the HB on the HR diagram.

The He reactions are fast, carbon and oxygen start to build up in the core, after which we have an inactive core that starts to shrink again. Above it, we have a layer of burning He and burning H, which were able to reignite their reactions by re-shrinking and heating the star. A degenerate core of carbon and oxygen is formed, and the star re-inflates and goes into the asymptotic giant branch (AGB) phase, where the illustration of the inner part of a star in the AGB branch is in Fig. 2.3.1.

It remains in this phase for barely 10^5 years (Habing, 1997), during which pulsations, stellar wind and explosive He reactions (thermal pulses) in the shell around the core occur. We have two phases of AGB; early AGB (E-AGB) and thermally pulsing AGB (TP-AGB). E-AGB is the initial phase in which He is burned to carbon and oxygen in the shell around the nucleus. In the later TP-AGB phase, thermal pulses occur. The upper H shell burns, the product of which is He, which accumulates in the lower He shell. Over time, the He shell ignites explosively (He shell flash), causing the star to expand, cool, and grow in luminosity over hundreds of years. The H shell stops burning. But after a while, the H shell is re-ignited (due to He burning and convection) and the process repeats. During the heat pulses, an s-process (slow neutron capture) occurs in the centre, which produces elements heavier than iron and rare nuclides (such as 99Tc). These reach the surface of the star by powerful convection (sometimes called dredge-up), where they are carried away by the stellar wind. In addition to thermal pulses with periods of hundreds to thousands of years, pulsations lasting hundreds of days on average occur during this phase (see the

pulsation chapter for more details).

The stellar wind carries material away from the star, which rapidly cools and surrounds the star. Eventually, the star loses all of its envelope, leaving a stellar core remnant of electron-degenerate carbon and/or oxygen core – the future white dwarf, and an envelope – the planetary nebula.

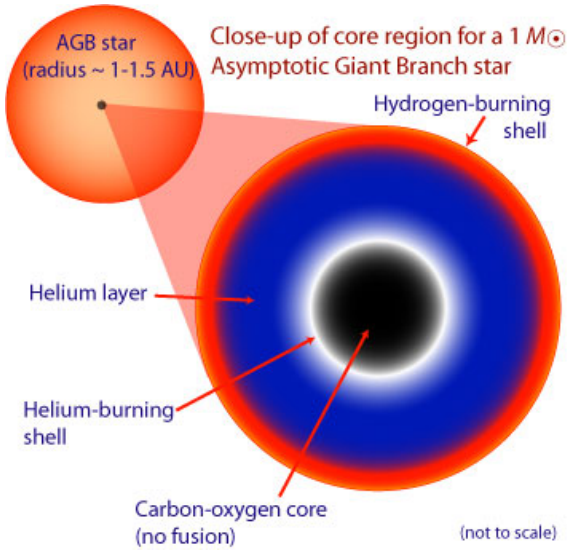

Figure 2.3.1: Thermonuclear reactions in low mass AGB star (e6).

2.4 Classification of Miras

According to the spectral type, there are three types of Miras; C, M and S type. Type C, as the name suggests, includes carbon stars that contain CN and C absorption bands, but carbon Miras are not numerous in our Galaxy. Another spectral type is the S type, where we observe ZrO and LaO absorption bands. Most Miras fall into the M type, which contains oxygen compounds, mainly TiO, TiO_2 and H_20 (Reid, 2002).

This classification is determined by the carbon-oxygen (C/O) ratio. If the C/O $>$ 1, these are carbon Miras, if the C/O ratio is $<$ 1 these are oxygen type Miras (Willson, 2012). If the oxygen-carbon ratio is balanced these are S type Miras.

If we have an excess of carbon over oxygen, the carbon is bound in CO and the rest can be observed as CN or C_2 molecular bands. Otherwise, all the carbon is bound in CO, which is optically invisible, and the excess oxygen is found in the compound TiO_2. If the ratio is balanced, we observe other bands such as ZrO, and LaO (Keenan, 1954) in addition to those mentioned above.

Various factors such as initial mass, age and metallicity affect whether a Mira star is an O type or a C type. In galaxies/regions with higher metallicity, we observe more oxygen Miras, in contrast to the higher abundance of carbon Miras (Magellanic Cloud) in regions with lower metallicity (Feast , 2006). In stars with lower metallicity, which have fewer heavier elements, there is less He and carbon, which limits the production of oxygen in the core of the star. This means that oxygen, in the form of oxygen compounds, will be less

available in these regions. Another reason we can give is dredge-up, which results in a lower abundance of oxygen relative to carbon. By alternately igniting the H and He shells of the star, massive convection occurs, bringing carbon to the surface. In the case of more massive stars, we get the CNO cycle, which occurs at higher temperatures. This causes the carbon to burn up (also known as hot-bottom burning) before it reaches the surface (Groenewegen , 1995,1). Another phenomenon that occurs is the change in the C/O ratio during pulsations, and thus during the inflation/shrinkage of the star, where the increase in C/O occurs (Willson, 2012).

In addition to the absorption bands already mentioned, we can observe emission lines of H and lithium at Miras. The H emission lines arise as a result of shock waves from the expanding stellar atmosphere (mass elements in the outer layers of the stellar atmosphere move faster than the surroundings), as a result of changing thermal pulses (Fabas, 2011). The previously mentioned hot-bottom burning can explain why we observe lithium in the spectrum. This is because the H-burning shell layer generates lithium by fusion, which is then carried upward by convection (Uttenthaler, 2011).

	C/O	Bands
M type	< 1	TiO, H_2O
S type	~ 1	ZrO, LaO
C type	> 1	CN, C

(a) Table showing the distribution of Miras with their basic characteristics related to the text above.

$\frac{M}{M_\odot}$	$\frac{t_M}{10^3 \text{ let}}$	$\frac{t_S}{10^3 \text{ let}}$	$\frac{t_C}{10^3 \text{ let}}$	N_c	N_{tot}
1,0	232	0	0	-	3
1,55	355	0	37	6	6
2,0	352	91	367	7	10
3,0	437	185	1667	9	31
4,0	55	83	183	11	22
5,0	140	0	0	-	29

(b) The length of the star's stay in M, S and C type Miras. M is the initial mass of the star, t is the time spent in the individual phases, N_c is the number of thermal pulses needed to transform the star into a carbon star and N_tot is the total number of pulses, (Polster, 2006).

Figure 2.4.1: Tables containing characteristics and properties of M, S and C Miras.

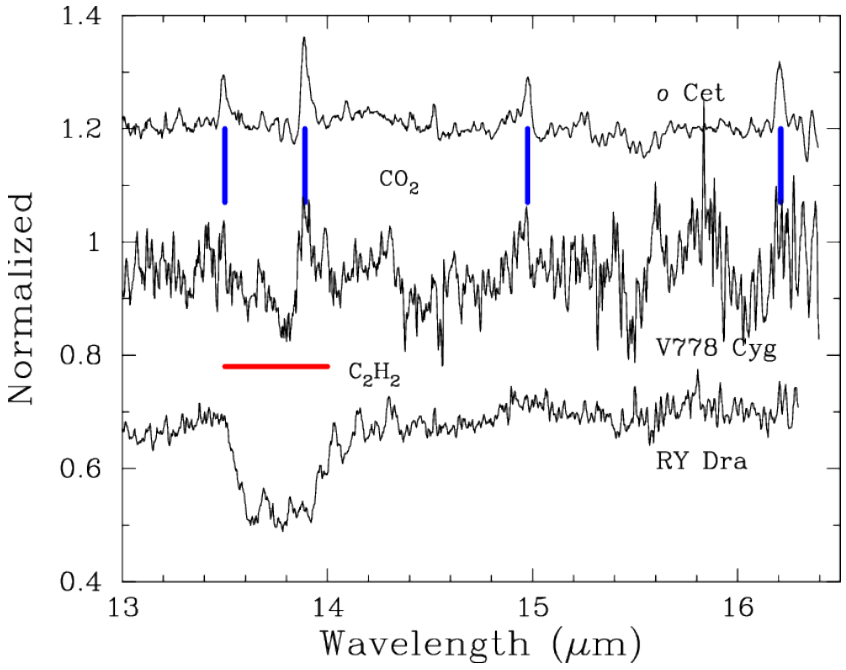

Figure 2.4.2: Normalized spectra of V778 Cyg - S Mira type, o Cet - M Mira type, and RY Dra - C Mira type. For o Cet and V778 Cyg, we can observe strong emission CO_2 lines, which are a sign of oxygen-rich molecules in stars. The absorption lines of C_2H_2 close to 13.7 µm indicate dust emission in the outer atmosphere diluted by the silicate dust. The deeper the absorption the stronger mass loss rate (Yamamura, 2000).

2.5 Periods and light curves

As mentioned in the previous text, the period of light changes of Miras is 80-1000 days. However, the shape of the light curve is not always periodic; it varies from cycle to cycle (Meyers, 2001).

Carbon Miras and Miras with longer periods have the most irregular light curves. Carbon Miras have slow irregular changes in brightness that are caused by the circumstellar envelope that prevents the throughpass of radiation (20). These irregular changes are visible in 2.5.2. Miras with periods longer than 200 days have higher amplitudes and steeper light curve gradients with "bumps", as is shown in figure 2.5.1. The bumps can be explained as a 2:1 period resonance between the fundamental and first harmonic modes (20). A 2:1 period means that the first harmonic mode has twice the frequency of the fundamental mode. Thus, when there is an oscillation of the Miras luminosity (fundamental mode), the first harmonic mode represents an oscillation of twice the frequency. Also, a relationship has been found for calculating the period of the luminosity changes in the fundamental and first harmonic modes, see 2.1 and 2.2, where P is the period, M is the mass, and R is the radius of the star (Willson, 2012). In the fundamental mode, the star pulsates radially – the entire star expands and then contracts, while in the first harmonic mode, part of the star expands while another part contracts. The first harmonic mode also has a shorter wavelength and therefore a shorter period. It is also shown that if the distance between two maxima of the light curve is smaller than the period of the brightness changes, the next

maximum will be brighter, and the reverse is also true (Mattei, 1997).

The equations were taken from (Willson, 2012).

$$P = 0.012\text{d}\, R^{1.86}\, M^{-0.73} \tag{2.1}$$

$$P = 0.04\text{d}\, R^{1.5}\, M^{-0.5} \tag{2.2}$$

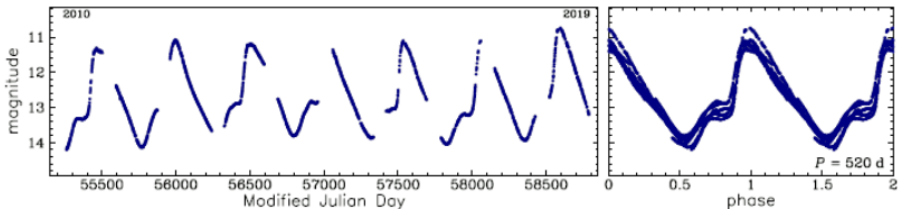

Figure 2.5.1: Light curve in the I-band of oxygen Mira variable star. We can notice a more regular phase curve, but there are also noticeable bumps (20).

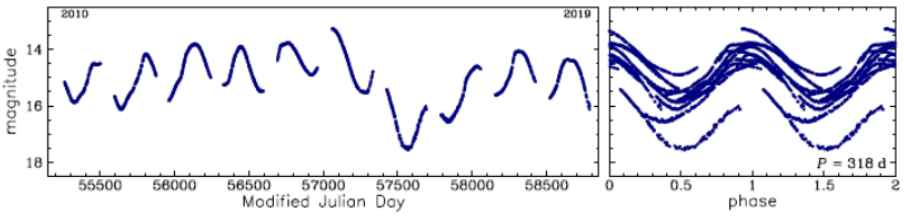

Figure 2.5.2: Light curve in the I-band of carbon Mira variable star. It is obvious that the phase curve is more irregular than for oxygen Mira (20).

2.6 Pulsation of Miras

The specific cause of pulsations causing light changes on the order of hundreds of days is not precisely known and is debated. However, there are several theories that can explain the pulsations of Miras, and thus its shrinkage and expansion during the cycle.

Wood (2006) and Darun (2017) claim that the pulsations are caused by convection in the vast atmospheres of these stars. Due to the low effective temperature of the stars, the He and H layers are located lower down, so the region of convection, which is very large in these stars and extends from the deeper layers to the surface, is thus able to affect the pulsations. They also found that convection can have both a damping and an excitation mechanism for pulsations. A confirmation of their theories is that Miras often pulsate at the fundamental frequency or first harmonic, which is associated with convective mass flow in the star.

Another theory, but one that has fewer supporters, is that of a close planetary companion in the region of the extended envelope of the star (Berlioz-Arthaud, 2003). One of its shortcomings is that it cannot reliably explain the variations in the Miras periods, their large spread and generally long periods.

The most widely supported theory explaining pulsations is κ-mechanism. This mechanism is well known for pulsating stars in the instability strip, such as RR Lyrae and Cepheids. However, for Miras, the H shell is important, unlike for stars in the instability strip where the H shell plays an important role. In this theory, expansion/shrinkage of the star is supposed to occur due to ionization and recombination. When the H shell is heated to a sufficient temperature, ionization occurs. The star is shrunk, and with higher effective temperatures, the density of the gas increases. This causes a decrease in opacity, the region becomes more transparent to radiation as light interacts less with the ionised atoms. So the star inflates due to the increased pressure. As the shell's radiation is emitted, a shock wave is created, which in turn causes emission lines in the spectrum. The inflation causes the pressure on the star to decrease and the effective temperature to decrease, the atoms recombine and the opacity increases. The amount of radiation, which can no longer resist gravity, is reduced as the star contracts. This process repeats itself over and over again (Boyd, 2021) and (Adams, 2013).

A final, widely supported model that explains the pulsations is the χ Cygni model, described in figure 2.6.1, and supported by the article (Reid, 2002). Named after the Mira variable of the χ Cygni star. The H shell, whose mechanism we explained in the paragraph above, plays an important role, as well as TiO molecules, which are abundant in M and S Miras. TiO molecules have a high efficiency of absorbing radiation in the optical part of the spectrum, so they are an important source of opacity, and they are also strongly dependent on temperature change. When the effective temperature drops, i.e. when the opacity is high, we can observe these emission lines in the atmosphere of the star, but at the maximum, these lines disappear (Herbig, 1965). At the maximum, the star is smaller, hotter, and more transmissive in the optical part of the spectrum, and the Ti is in atomic form. At the same time, these molecules are important for the formation and maintenance of pulsations, because they are dependent on the temperature and pressure in the atmosphere of a star. Changes in the amount of TiO molecules in Miras atmosphere cause an imbalance in energy that then leads to pressure pulses, and it is these pulses that

cause the star to periodically change its brightness at different intensities.

If we are interested in qualitative values, during the pulsations the surface temperature of the star changes from about 1900 K to 1400 K (15%), and the radius is able to increase/decrease by about 1.8 $R_{\odot}$ (20%) (Reid, 2002).

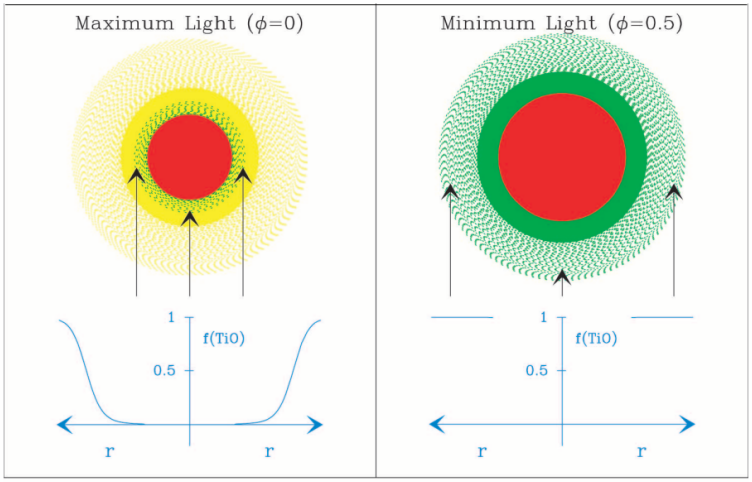

Figure 2.6.1: χ Cygni model of the pulsating star Miras. The arrows show the observed surface of the star. The star is shown on the left at its maximum light. The star is visible in the optical wavelengths, has a smaller radius, and has a higher effective temperature than at minimum light. Ti is in atomic form and we can see the surface of the star. In minimum light (right) the star has a high luminosity and the radius of the star is at its maximum. The effective temperature has dropped and the Ti atom exists in the molecular form TiO (green color) and the star is opaque in the visible spectrum. f(TiO) means the fraction (amount) of Ti in TiO and is plotted against the radius in blue. At a radius approx. 1.8 $R_{\odot}$ has TiO enough density to become invisible in visible light - we may not see the star (Reid, 2002).

Methodology

3.1 CMD of variable stars and long variable stars (Miras)

Already at the beginning of the 20th century, independently, Hertzsprung and Russell created a diagram for stars showing the dependence of absolute magnitude/luminosity on effective temperature/spectral classification (23). Where stars with higher effective temperatures and luminosity are located in the upper left part of the diagram. This diagram shows, among other things, the stages of stellar evolution through which we have been able to come closer to understanding stellar evolution. This diagram was immediately followed up by other astronomers such as Eggen, who studied where the Cepheids are located on the HR diagram - now called the instability strip (Eggen, 1951). In addition, he also studied where other types of variable stars are located on this diagram, using Cepheids located in star clusters. However, this diagram requires knowing the distance of the stars from us or we must have stars that we know are at approximately the same distance, such as in globular clusters. The accuracy of the absolute magnitude of the magnitude is determined by several factors such as the number of measurements and its accuracy.

Because of these limitations, a related and equivalent chart was created - the color–magnitude diagram (CMD), sometimes also called the observation diagram. This diagram shows either absolute or relative magnitude on the y-axis. The x-axis shows the difference in magnitude between two spectral filters (colors) (24). For historical reasons, the most commonly used color difference is $B-V$ or $U-B$, where U is ultraviolet, B is blue and V is a visible color filter (Johnson, 1953). However, nowadays most shows have their own color filters, for example, Gaia, uses the G, BP and RP color magnitudes (25). In general, the higher the color value, the redder and cooler the star. Thus, a cool star is brighter in red than in blue (Deliyannis, 2019).

This whole paragraph is inspired by the article (Eyer, 2019).

Eggen, in addition to the classical CMD, created a modified color diagram for Cepheids, called the moving CMD (Eggen, 1951). This diagram shows Cepheids during changes in luminosity due to pulsations and showed the Cepheids moving on this diagram. This work, however, was followed up in a larger paper containing data from Gaia DR2. This illustrated the moving CMD for stars falling into most variable star types, such as RR Lyrae, Miras, ZZ Cetes, Cepheids, SX Phoenicis Stars RS Canum Venaticorum and others. They claimed that the brightest and reddest regions on the diagram are populated by long-period stars (such as Miras), and these regions have a high probability of variability. At the same time, long-period variable stars show large variations in amplitudes correlated with redder (cooler) colors. According to this paper, main sequence stars, located in the brightest and hottest part of the sequence, also have a high probability of variability. The

pulsating stars appear bluer in the diagram 3.1.1 when they are brighter in G magnitude and thus, according to these stars, are mainly affected by brightness changes. If changes in radius were dominant, we would expect to see more changes in absolute magnitude without significant color changes. Among other things, the chart shows that variable stars such as Delta Scuti are bluer when they are brighter while Be/Gamma Cassiopeiae are bluer when they are fainter.

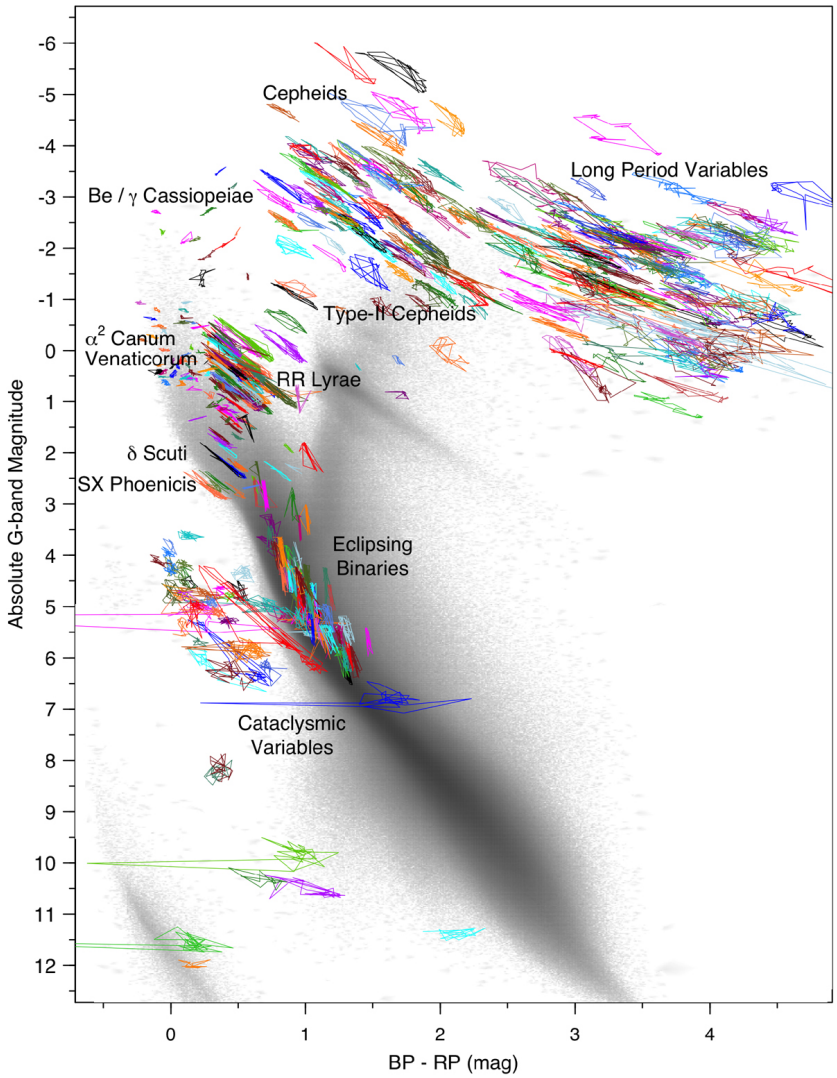

Figure 3.1.1: Moving color-magnitude diagram for variable stars. The grey color belongs evolutionary track of stars (Eyer, 2019).

Several things can affect the position of stars in the CMD, such as interstellar reddening (Deliyannis, 2019), chemical composition (Harris, 1976), and rotation and inclination of the rotation axis (Bastian, 2009). Interstellar reddening mainly affects objects that are located in the galactic disc, and therefore stars that are outside the disc or further away from the disc appear brighter to us. An example is the RR Lyrae stars, which are less reddened than the classical Cepheids (Eyer, 2019).

The CMD and moving CMD are useful diagrams that can help us refine the classification

of variable star types, or help us discover some new types of variable stars. They can help us to understand the instability strip, its location, and its dependence on chemical composition. Last but not least, they can tell us something about the behaviour and phenomena taking place in variable stars, the correlations between different types of variable stars, or shed light on their evolution.

3.2 Archives, time series (IPAC, IRSA, ZTF)

Figure 3.2.1: IRSA archive containing catalogues ZTF, PTF, 2MASS, etc. (Masci, 2018).

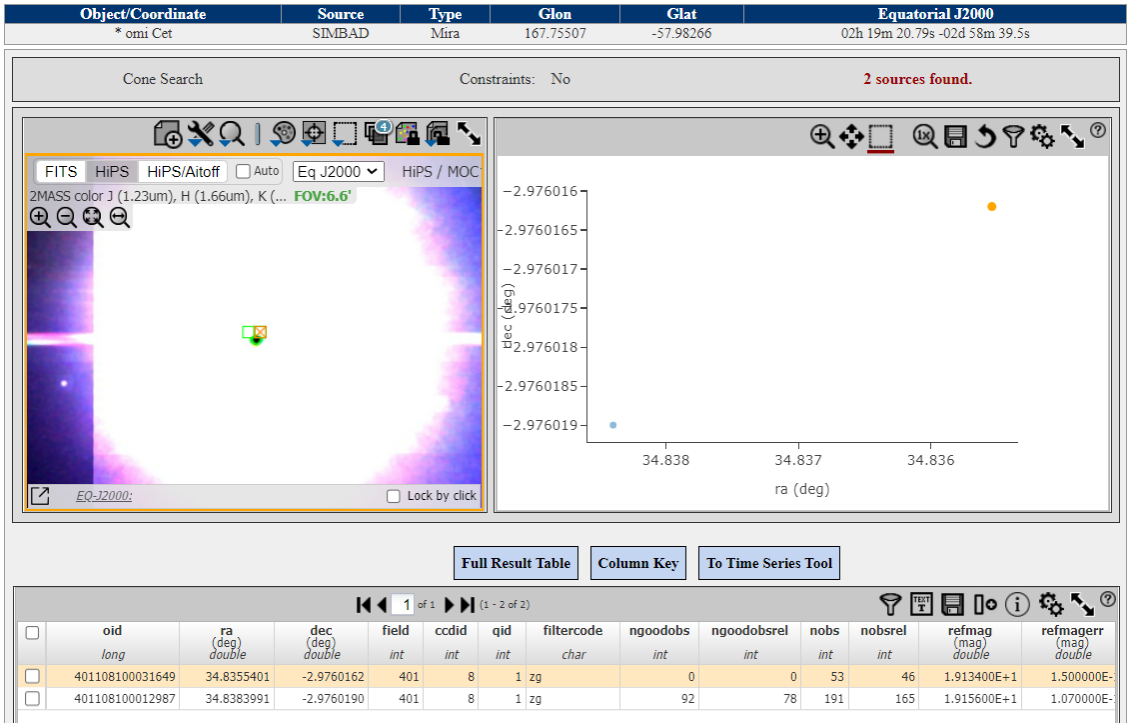

Figure 3.2.2: Example of search ZTF time series for Omicron Ceti (variable star). We can notice 2 found sources with similar coordinates in the same color filter. (Masci, 2018).

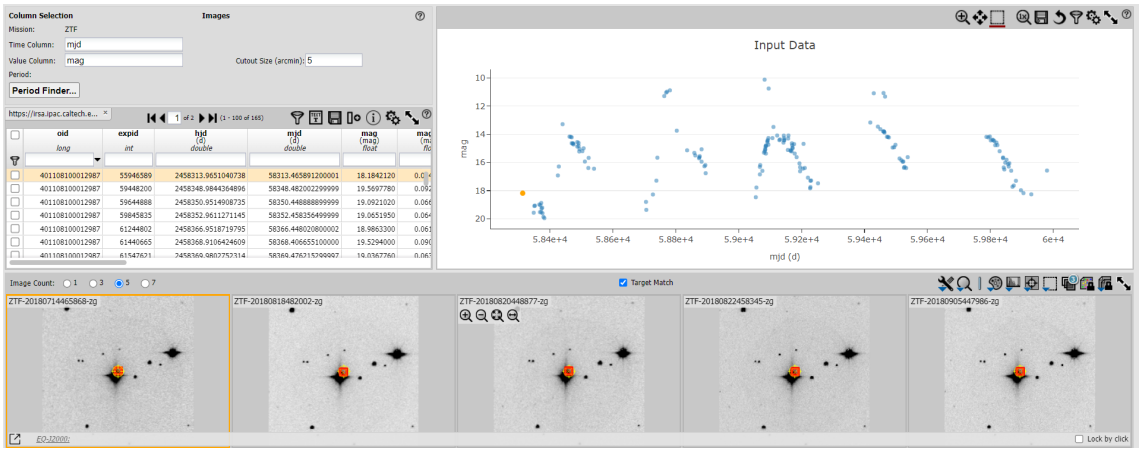

Figure 3.2.3: Time series tool for Omicron Ceti. On the top right is a light curve for Omicron Ceti. On the top left are input data and the period calculator (finder). At the bottom is displayed a star for each point in the light curve. (Masci, 2018).

To study variable stars, it is useful to know the light curves – the record of brightness changes over long time scales, ideally over multiple periods and in multiple filters. For long-period variable stars, which is where Miras falls, it is desirable to have photometric data over decades or more.

This is one of the reasons why an IPAC (Infrared Processing and Analysis Center) science centre was established at Caltech in the late 20th century to process and analyze

IRAS (Infrared Astronomical Satellite) data (26). Over time, as it grew and added more functions, an offshoot of IRSA (Infrared Science Archive) was set up to manage, process and make the data more accessible to scientists (27). Until then, everything was handled by IPAC, which currently has mainly a research function and technical support. Sometime later, IRSA became an important data source for some space and ground-based missions such as Herschel, Spitzer, Planck, ZTF, and PTF, see figure 3.2.1, and provided tools for data processing and distribution, mostly in the infrared and microwave spectrum (28).

The Zwicky Transient Facility (ZTF) is a project that performs time series surveys of the sky in the visible spectrum and detects various variable stars, eclipsing binary stars, supernovae, asteroids and more (Masci, 2018). It uses the 48-inch Schmid Palomar telescope to scan the entire visible northern sky (a Northern-equatorial sky survey) with the r, g and i (red, green, infrared) filters. This data is transmitted to IRSA where it is further processed and made available to users. There is a user interface where we have access as normal users to up to 50% of all measured data. For the ZTF lightcurve interface we have, among other things, a tool to analyse and display light curves, in multiple filters, calculate periods, manually remove and add photometric data and other statistical functions. The data contains for each star information about the filter, mjd, mag, error values, mean values and more, see figure 3.2.2 and 3.2.3. All these values can be filtered and downloaded in bulk for multiple stars and then further processed.

With IRSA and IPAC we have the ability to get time series data from several terrestrial and space-based surveys in one place in different filters. This therefore allows scientists to access the data quickly and easily, and to quickly check the data and then process it.

3.3 Data acquisition

3.3.1 Selecting of Mira variable stars

The AAVSO International Variable Star Index VSX catalogue (Watson, 2015) was used to retrieve Mira variable stars, identifying over 28 000 of them in our Galaxy. In addition to identifying Miras with their coordinates, the catalogue also provided us with information on the period of luminosity changes for Miras.

The next step was to classify and select the Miras, according to their location in the Galaxy – halo and bulge, as globular clusters are located in these parts. To determine the boundary of the galactic bulge, we took as its centre the coordinates of Sagittarius A* – a massive black hole, with coordinates 17 h 45 m 40.0409 s, $-29°0'28.118''$ (J2000) (Reid, 2004), which we transformed into galactic coordinates (galactic longitude – glon and galactic latitude – glat) for our purposes. The range for glon and glad bulge was inspired by paper by Minniti (2017) and the figure from source (30). We finally adopted a range of 344–374 (+14) deg for glon, and from -15 to 15 deg for glat, where this selection left us with only 1608 Miras, which are located in the galactic bulge.

To determine the limit of stars located only in the Galactic halo, we used sources (31) and (32). For the glon, we took its full range, i.e. 0–360 deg, because we are interested in both the inner and outer halo and in the whole Galaxy. For the glat, we took the range 20 deg to 90 deg for the upper hemisphere, and -90 deg to -20 deg for the lower hemisphere. This range narrowed down the number of Miras to 1954, which are located

in the galactic halo.

As can be seen in Fig. 3.3.1, these Miras are evenly distributed throughout the halo, so there is no region in which these variable stars are more closely spaced than elsewhere. On the other hand, we can notice in Fig. 3.3.2 that Miras in bulge are mostly located in the southern hemisphere of Galaxy. A very similar distribution of Miras in galactic bulge was shown in the article Qin (2018), where they use Miras as standard candles for determining distances, such as Cepheids.

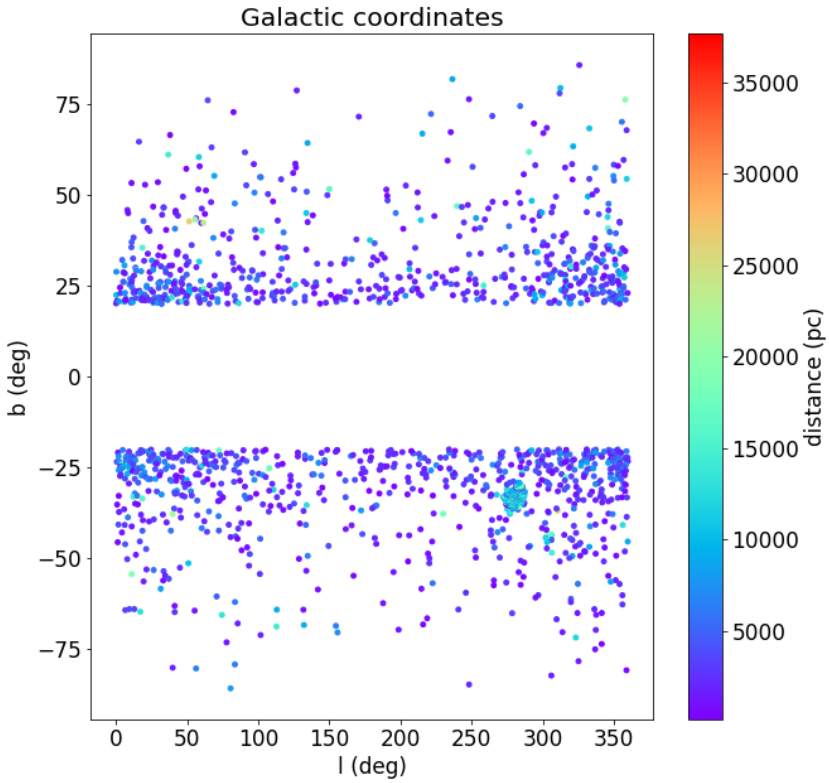

Figure 3.3.1: Distribution of Miras in the galactic halo. The colors distinguish the distances at which the Miras are from us. It is clear that most of them are located up to a distance of 5000 pc.

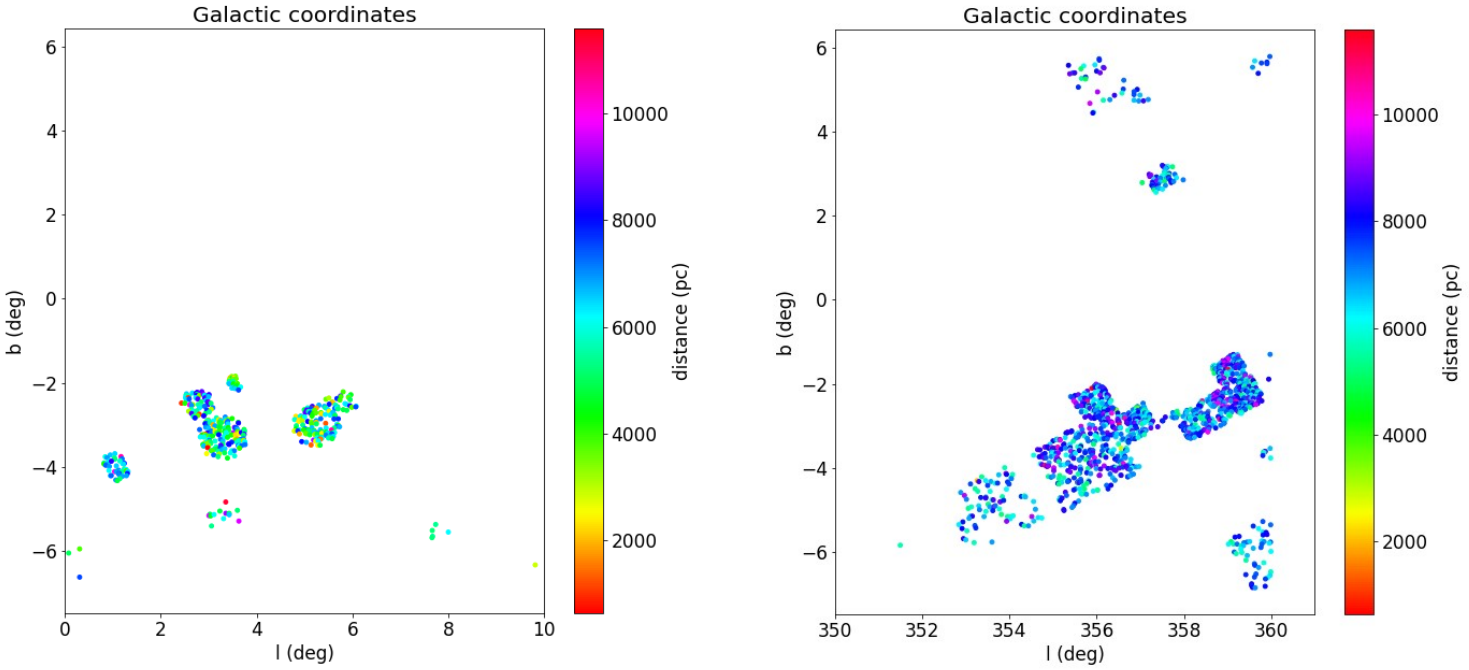

Figure 3.3.2: Distribution of Miras in the galactic bulge. The colors distinguish the distances at which the Miras are from us. In the left figure, the values of glon are lower than in the right panel. Also, these stars are closer to us, as we expect, with a medium distance from as of 4000 pc. In the right panel, these Miras are mostly 8000 pc away from us.

3.3.2 Mira variable stars in globular clusters

The next essential step was to determine whether these Miras are located in one of the 160 globular clusters, whose list and coordinates were taken from the catalogue (33) and the proper motion (μ) for these globular clusters was taken from (34). The proper motion for the stars was obtained from the Gaia DR2 catalogue in Vizier (Eyer, 2019), along with the standard error for each star. Similar values of the proper motion of a cluster and a star can be an indication that the star is a member of a globular cluster. This occurs because its members are gravitationally bound to each other, moving collectively in the same direction and at the same speed within space.

Data obtained from (Eyer, 2019) include proper motion in the right ascension (Ra) involving the cosine of the declination angle and proper motion in declination (Dec). Cos δ stands out here because proper motion in the direction of Ra is measured in units of time However, because of the geometry of the celestial sphere, we must take into account the fact that the Ra circles are tapered towards the poles. The factor cos δ is used to correctly express the proper motion in the rectangular direction with respect to the different Dec. This factor corrects the velocity of motion depending on the position in the sky. The total proper motion can then be calculated in the standard Pythagorean theorem as 3.3, where $\mu_{\alpha\star}$ is proper motion in Ra and μ_δ is proper motion in Dec.

$$\mu = \sqrt{\mu_{\alpha\star}^2 + \mu_\delta^2} \tag{3.3}$$

The total proper motion for Miras was calculated in the same way as for the cluster, and the deviation for each star was taken as 5 sigma (5 times the standard error of the star measurement). This deviation indicates the range in which a given star is likely to be due to measurement inaccuracies. The 5 sigma value is a frequently used statistical criterion for determining the confidence level or probability of a measurement. By subtracting and adding this value to the proper motion value of the star, we have determined the range of proper motion within which the proper motion value of the cluster must lie. Another condition for assigning a star to a cluster was that the stellar coordinates in Ra and Dec should be within 1 deg of the cluster coordinate. By satisfying these conditions, we obtained 304 Miras out of the original 1608 stars located in the bulge of the Galaxy. These Miras are distributed in 15 different globular clusters, with the largest number of Miras in Terzan 6, NGC 5453, and Djor 1. In contrast, in the Galactic halo in which we found 1954 Miras, only 4 of them are located in globular clusters, namely NGC 6093 (2 Miras), Arp 2, and Terzan 8, see their basic properties in figures 3.3.4 and 3.3.5.

We can also check whether a star belongs to a globular cluster using a density profile, where the number of stars should decrease with the square of the distance from the cluster centre. Unfortunately, we could not perform this test for the halo because of the low number of Miras in the cluster and the same for most Miras in the bulge. This test was therefore only indicative even though we got satisfactory results for a few clusters. In the case of more stars, it would have a higher significance, so we mention it only marginally.

Before we started looking at individual Miras in globular clusters, it was necessary to analyse the number of Miras as a function of core and half-light radius. The reason was to see if our Miras data are biased by the fact that a given cluster is well resolved or is closer to us, or has a really high star density. Another thing that Miras and other long period variable stars may be affected by is time bias, which we have no way of checking since our data is obtained from many papers. However, based on the 3.3.3, we conclude that our Miras are not biased by the apparent density of stars, since their number is evenly distributed over all radii.

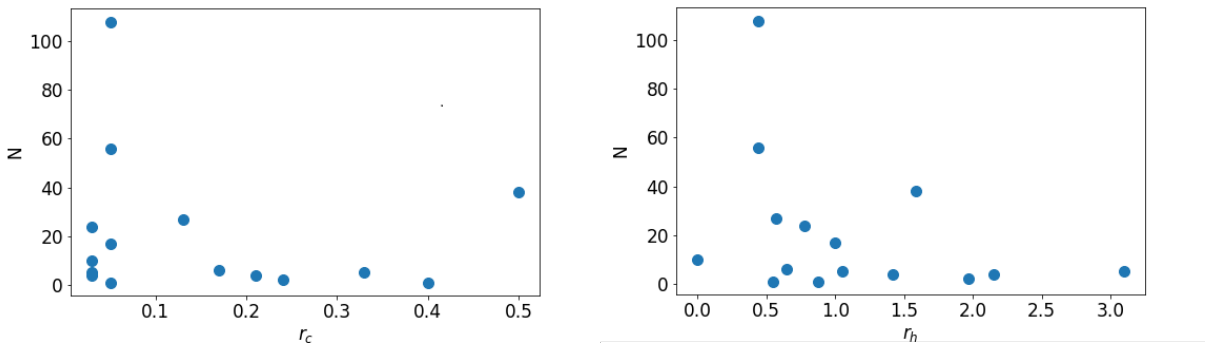

Figure 3.3.3: Occurance rate of Miras in relation to r_c and r_h. The Miras are located in various dense clusters and at all angular distances.

Cluster	count	Ra (deg)	Dec (deg)	l (deg)	b (deg)	[Fe/H]	E(B-V)	r_ c	r_h	R_Sun	R_GC
BH_261	1	273.5275	-28.635	3.362	-5.27	-1.30	0.36	0.40	0.55	6.12	2.20
Djor_1	38	266.8696	-33.0664	356.675	-2.484	-1.51	1.58	0.50	1.59	9.88	1.82
Djor_2	5	270.4544	-27.8258	2.763	-2.508	-0.65	0.94	0.33	1.05	8.76	0.80
HP_1	5	262.7717	-29.9817	357.425	2.115	-1.00	1.12	0.03	3.10	7.00	1.26
NGC_6304	4	258.6344	-29.462	355.826	5.376	-0.45	0.54	0.21	1.42	6.15	2.19
NGC_6316	6	259.1554	-28.1401	357.175	5.764	-0.45	0.54	0.17	0.65	11.15	3.16
NGC_6355	1	260.9935	-26.3528	359.585	5.429	-1.37	0.77	0.05	0.88	8.65	0.93
NGC_6441	27	267.5544	-37.0514	353.532	-5.006	-0.46	0.47	0.13	0.57	12.73	4.78
NGC_6453	56	267.7155	-34.5985	355.718	-3.872	-1.50	0.64	0.05	0.44	10.07	2.10
NGC_6522	17	270.892	-30.034	1.025	-3.926	-1.34	0.48	0.05	1.00	7.29	1.04
NGC_6540	10	271.5357	-27.7653	3.285	-3.313	-1.35	0.66	0.03		5.91	2.34
NGC_6558	4	272.574	-31.7645	0.199	-6.023	-1.32	0.44	0.03	2.15	7.47	1.08
NGC_6626	2	276.137	-24.8698	7.798	-5.581	-1.32	0.40	0.24	1.97	5.37	3.02
Ter_6	108	267.6933	-31.2754	358.571	-2.162	-0.56	2.35	0.05	0.44	7.27	0.97
Ter_9	24	270.4117	-26.8397	3.603	-1.989	-1.05	1.76	0.03	0.78	5.77	2.46

Figure 3.3.4: Basic information about globular clusters located in the galactic bulge that contain Miras. Data were taken from the Harris catalogue, where count is the number of Miras belonging to a given cluster, r_c is a core radius in arcmin, r_h is half-light radius in arcmin, R_Sun is distance from Sun (kiloparsecs) and R_GC is distance from the Galactic center (kpc).

Cluster	count	Ra (deg)	Dec (deg)	l (deg)	b (deg)	[Fe/H]	E(B-V)	r_ c	r_h	R_Sun	R_GC
Arp_2	1	292.1838	-30.3556	8.545	-20.785	-1.75	0.10	1.19	1.77	28.73	21.39
NGC_6093	2	244.26	-22.9761	352.673	19.463	-1.75	0.18	0.15	0.61	10.34	3.95
Ter_8	1	295.435	-33.9995	5.759	-24.559	-2.16	0.12	1.00	0.95	27.54	20.43

Figure 3.3.5: Basic information about globular clusters located in the galactic halo that contain Miras. Data were taken from the Harris catalogue.

3.3.3 Stellar Characteristics of Miras

From the final Miras coordinates already obtained, we could start searching for stellar characteristics such as metallicity, effective temperature and parallax. These data were crucial for a better understanding of Miras and their use in the next part of the thesis. The parallax for each star was obtained from the Gaia EDR3 catalogue (Gaia, 2021), while the metallicity and effective temperature were taken from the Gaia DR2 catalogue (Eyer, 2019). At the same time, thanks to the knowledge of the period, we were able to calculate the bolometric absolute magnitude (M_{bol}) using the formula 3.4. This relation was taken from an article (Andriantsaralaza, 2022), which claims that this relation can be generally applied to Miras in our Galaxy. This calculation yields a very useful parameter since it takes into account all the light emitted by the star (at all wavelengths) and is not limited to light in the visible spectrum. Moreover, M_{bol} is not affected by atmospheric absorption and scattering, giving us a more accurate estimate of the luminosity than a magnitude measured only in the visible part of the spectrum. From this relationship, we can therefore derive the commonly known relationship for luminosity (L) in units of L_{Sun}, see equation 3.5. The value $3.846 \cdot 10^{26}$ is the luminosity of the Sun and the value $3.0128 \cdot 10^{28}$ is the zero point luminosity in units of watt. Zero point luminosity is the luminosity that a star with M_{bol} equal to zero would have and was determined by the IAU in 2015, as was L_{Sun}

(Mamajek, 2015).

$$M_{\text{bol}} = -3.31(\log P - 2.5) - 4.317 \tag{3.4}$$

$$L/L_{\text{Sun}} = \frac{3.0128 \cdot 10^{28} \cdot 10^{-0.4 M_{\text{bol}}}}{3.846 \cdot 10^{26}} \tag{3.5}$$

3.3.4 Looking for filters and color indexes

We decided to compare the obtained Miras effective temperature with the effective temperature calculated from the color index. This comparison will reveal any discrepancies between the two effective temperature retrieval methods and will also complement the effective temperatures since the Gaia DR2 catalogue provided us with effective temperatures for about a third of our stars (Eyer, 2019). For this purpose, we needed to obtain Miras magnitudes in different color bands/filters. The search for colors was also crucial for the follow-up part of the thesis, where we investigated the correlations between different astrophysical quantities.

Since Miras are rather cooler stars emitting mostly at longer wavelengths, we focused on filters corresponding to this. We used catalogues such as the 2MASS Point Source Catalogue for J and K band (Skrutskie, 2000), The AllWISE data release ($W1$ – 3.35μm, $W2$ – 4.6μm, $W3$ – 11.6μm, $W4$ – 22.1μm) from Cutri (2014), Gaia DR3 (BP – band mean magnitude, RP – band mean magnitude and G – band mean magnitude), (Gaia, 2022). Among other things, we used the Gaia DR3 VariSumarry catalogue (Eyer, 2023), which provides the minimum and maximum magnitudes for the G, BP and RP bands. This allows us to observe how the color, and therefore the effective temperature, of a variable star changes during the period at which the brightness changes.

The last source from which we obtained information about the colors was the ZTF catalogue, which we mentioned in section 3.2. The data, which included among others mjd, mag and filtercode, were downloaded separately for halo and bulge, with a tolerance of 10 arcsec from our specified coordinates. For Miras, which is located in the galactic bulge, we extracted data for 207 stars from the 1608 stars we entered in the ZTF catalogue, 25 of which are located in clusters. For 1954 Miras, which are located in a halo, we obtained data for 855 stars, of which 2 are located in clusters. The ZTF catalogue has an interactive interface that allows us to visualize the data we are looking for and to see where they are located in the Galaxy. This interface therefore serves as a quick check to confirm whether we have indeed selected data from the Galactic bulge/halo. Data for the halo was more represented in the ZTF than for our bulge stars, but we also retrieved data for the halo in the g, r, and i filters, while for the bulge most of the data was only in the g and r filters. A large amount of the stars had data available in both the g and r filters. This allowed us to calculate the effective temperature (T_{eff}) of a given star from their difference using the relation 3.6 (Fukugita, 2011).

$$T_{\text{eff}} = \frac{1.09}{(g-r)+1.47} \cdot 10^4 [K] \tag{3.6}$$

The obtained values of modified Julian date (mjd), mag, mag error for each star were used to verify that our stars are indeed variable stars of the Miras type. For this, we used UPSILoN (AUtomated Classification of Periodic Variable Stars using MachIne LearNing) (Kim, 2016). This is a Python-based program that can classify periodic variable stars, which includes Miras, based on Machine learning. It needs mjd, mag and mag error as input data regardless of the filter chosen. As output, for each star that contains more than 80 data points, it gives us the variable type of the star, the probability with which it is sure that it is the variable type, and whether the classification was successful or the classification is suspicious – period is in period alias and/or period is very low. For our stars in the galactic halo, he determined that most of our stars are indeed Miras, and only 19 of them fall into a different category, namely the semi-regular variables (SRV) category, where this type is often confused with Miras. For stars in the galactic bulge, the program did not have enough points for most stars, so it determined the type of variability with very low probability, but those it was sure of it determined as Miras. In addition to designating stars as Miras, it was able to determine whether they were oxygen or carbon Miras, the distribution of which was unclear to us until this point because we did not have the necessary data to determine their distribution.

From the obtained $g-r$ and r we could then calculate the values for the unredening color ($(g-r)_0$), and also the absolute stellar size in the r filter (M_r) for each of our stars. The following relations were used for the calculation: 3.7 and 3.8, where d is the distance in parsecs, A_r is the extinction (mag), and $E(g-r)$ is the reddening, also called color extinction.

$$M_\mathrm{r} = r - 5\log(d) + 5 - A_\mathrm{r} \tag{3.7}$$

$$(g-r)_0 = (g-r) - E(g-r) \tag{3.8}$$

Due to the presence of interstellar material (dust and gas) between us and the galactic bulge, it is important to take these factors into account for a correct calculation. To calculate $(g-r)_0$ and M_r, however, we lacked knowledge of the magnitude of A_r and $E(g-r)$ for Miras. Since the ZTF is calibrated to Pan-STARRS1 (Ngeow, 2021), (Chambers, 2017), we were able to use the conversion relations associated with it since the ZTF does not have its own transformation relations between filters. The Johnson-Cousins filter system (Johnson, 1953), specifically extinction in the V filter (A_v) and reddening in the B and V filters ($E(B-V)$), seemed to be the most convenient for obtaining A_r and $E(g-r)$ because of the ease of transformation to Pan-STARRS1. We also obtained values for A_v and $E(B-V)$ using the IRSA DUST archive (35). These values were then converted to the g and r filters using the following relations; 3.9, 3.10 and 3.11. The values of 0.843 and 1.155 were taken from the transformation relations given in Wang (2019). The value of 2.617 corresponds to the quantity R_r, which is the extinction coefficient for the r filter, whose value is constant for a given color (Ngeow, 2021).

$$A_{\rm r} = 0.843 A_{\rm v} \tag{3.9}$$

$$A_{\rm g} = 1.155 A_{\rm v} \tag{3.10}$$

$$E(g-r) = \frac{A_{\rm r}}{2.617} \tag{3.11}$$

3.3.5 Obtaining quantities from isochrones

The calculated $M_{\rm r}$ and $(g-r)_0$ values for each star were then used as input values to the Stellar Isochrone Fitting Tool - StiFT (Supikova, 2021) in txt format, see Fig.3.3.6. It was also necessary to upload the input isochrone grid, which is freely available at Bressan (2012) and has many photometric systems to choose from, where the Pan-STARRS1 photometric system was chosen for our purpose. We then sorted this downloaded data for a large number of stars by age and entered the number of isochrones that corresponds to the age in the next column; i.e.; there is one isochrone for each age. We then create a txt file that contains $M_{\rm r}$ and $(g-r)_0$ (like our stars), and any 3 characteristics we are interested in - age, effective temperature, luminosity, mass, etc.) and the isochrone number. According to this interpolation isochrone grid, StiFT will calculate the values of the quantities we are looking for, such as luminosity, age, stellar mass and effective temperature.

As our input data, we put 88 Miras in bulge (only for this number we have values in the g and r filter) and 5 for clusters in bulge. We got results for 81 and 2 Miras in bulge, respectively. For the 348 Miras found in the halo, we had data in both g and r filters, including 1 in the cluster. We successfully counted data for 334 stars in the halo and unfortunately for none in the cluster.

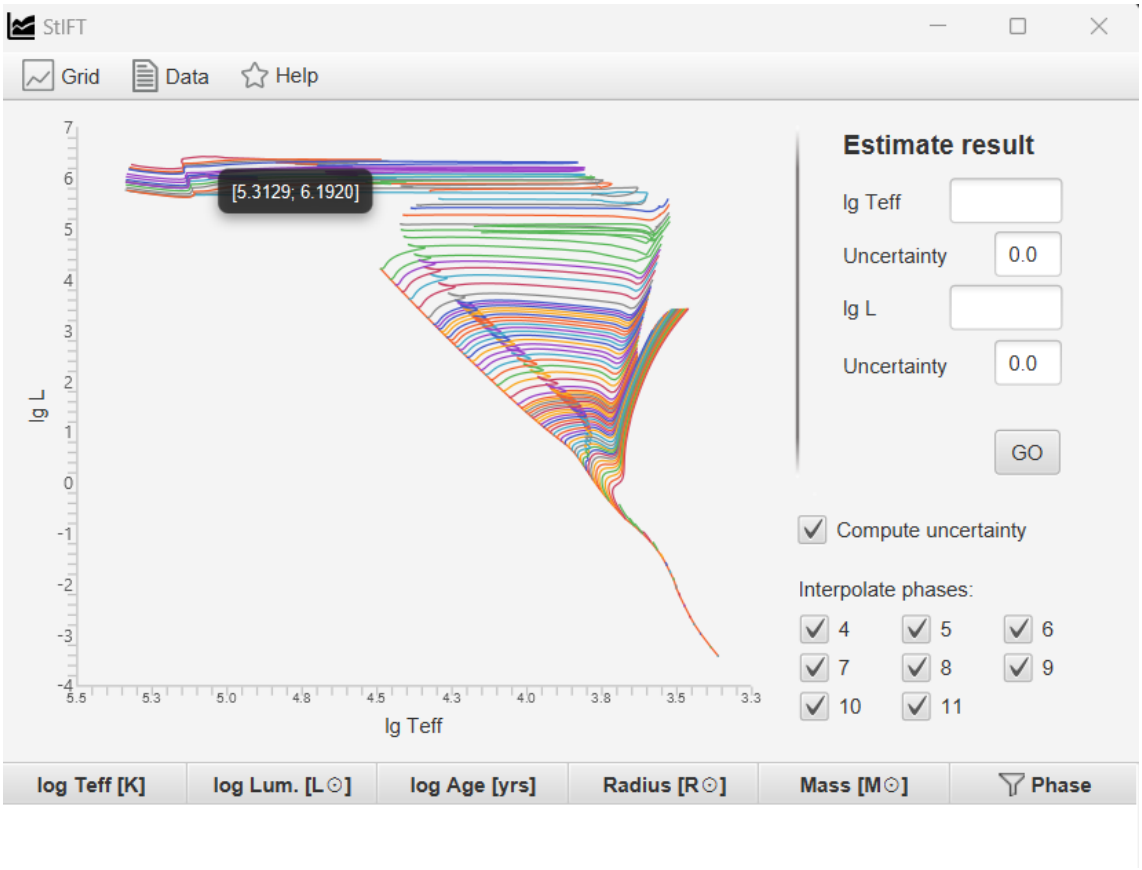

Figure 3.3.6: StiFT interface. In the upper left part, we upload the grid and our input data, or we can check only one star in the right part of the StiFT (Supikova, 2021).

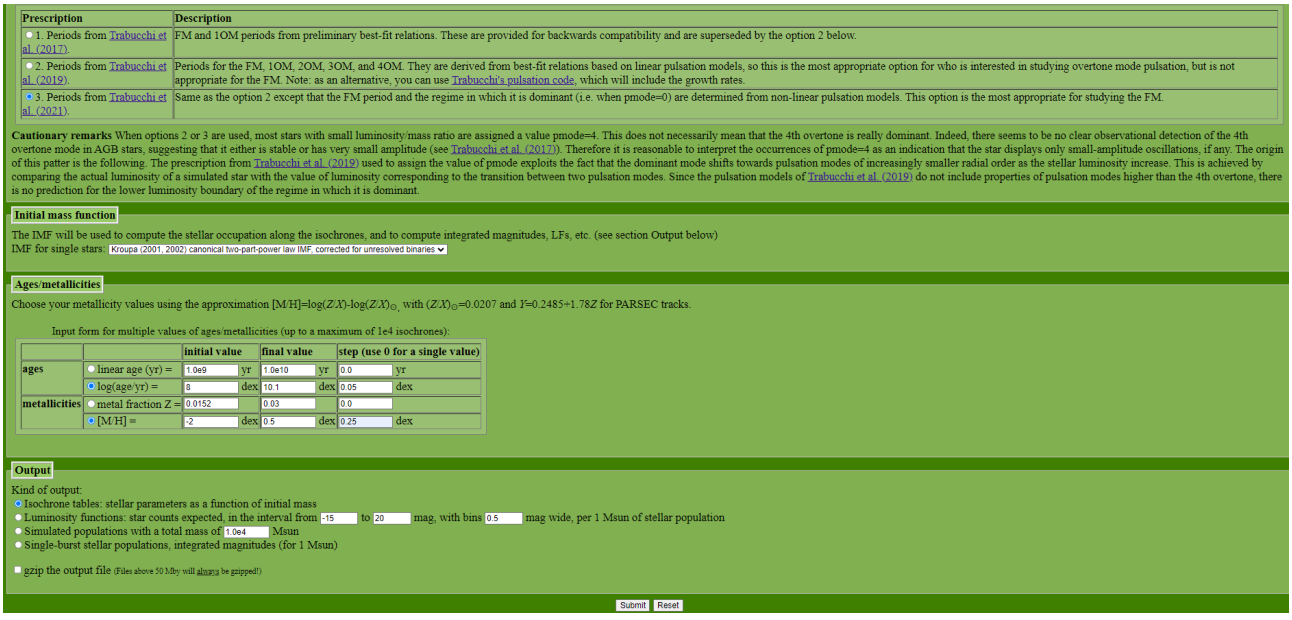

Figure 3.3.7: sample web interface for downloading isochrones (Bressan, 2012).

3.3.6 Extinction and reddening values

As mentioned in the text above, stars located in the bulge region are affected by interstellar reddening, see figure 3.3.8 of dust map. It was therefore desirable to obtain the filters we have already obtained, also their extinction and reddening values. The halo is not so affected by reddening (sometimes it is even assumed that there is no extinction), so it was problematic to obtain these values at all for some filters. We then compared the obtained values with those without extinction and looked at the correlations between them and between other parameters.

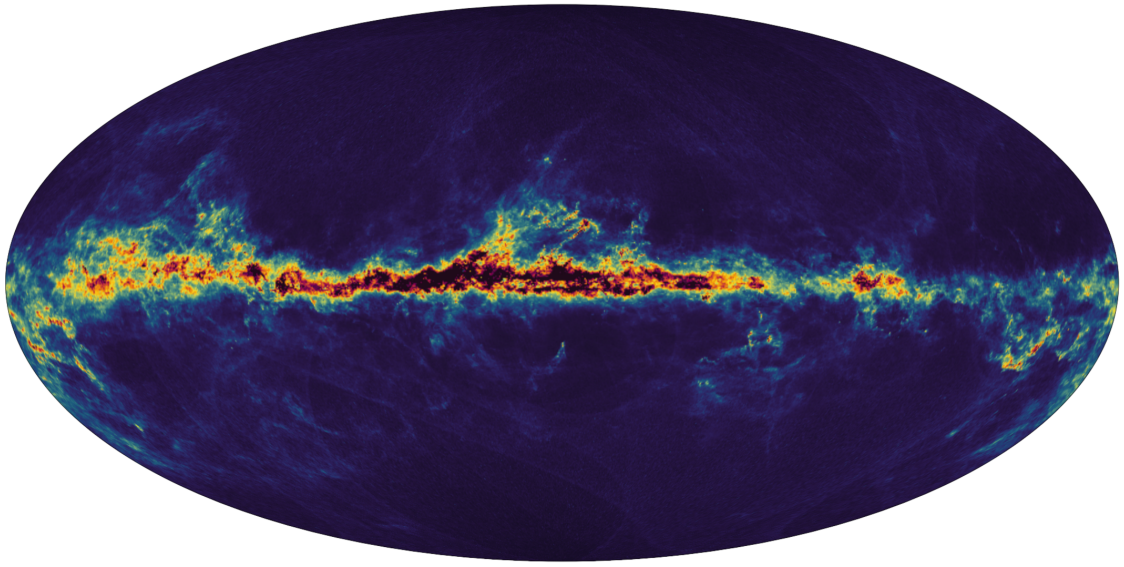

Figure 3.3.8: Dust map of Galaxy. We can see the amount of dust along the galactic plane and bulge, but not much dust in the halo (36).

The values of extinction and reddening in the V and I filters ($E(V-I), A_{\mathrm{I}}$) were obtained from OGLE-III (Soszyński, 2009), which has available values for both bulge and disk. It does not have these values for the halo, from the previously mentioned assumption of zero extinction in the Galactic halo. The optical gravitational lensing experiment (OGLE) also provided values for the extinction ratio between the V, I and J, K filters (R_{VIJK}), which allowed us to recalculate the extinction and reddening from the V and I filters to the J and K filters. To do this, we used the classical conversion 3.12 and 3.13, where the constants 0.36 and 1.36 were taken from (Layden, 2019).

$$E(J-K) = E(V-I)\,R_{\mathrm{VIJK}} \tag{3.12}$$

$$A_{\mathrm{K}} = \frac{0.36\,E(V-I)}{1.36} \tag{3.13}$$

We also used the Gaia DR3 VariSumarry catalogue, which provided us with their extinction and reddening values in addition to the G, BP, and RP colors, both for the mean

values and for the values at the minimum and maximum of the stellar brightness during the cycle.

Another way to deal with extinction, which affects stars mainly in the galactic bulge, is to use the Wesenheit function, also called Wesenheit magnitude or Wesenheit index, (Madore, 1976). Wesenheit magnitude is a function that is unaffected by extinction, thanks to the use of the ratio between two filters (bands). Since the attenuation of a star's light due to extinction is wavelength dependent, regardless of the filter, the attenuation will be similar in both filters (bands) since both bands measure light from the same star. Their ratio can therefore partially eliminate or minimize the extinction effect.

We calculate the Wesenheit magnitude as the magnitude difference in one filter and R times the difference in the two filters, where R is the ratio of total to selective absorption (Ngeow, 2005). Expressed numerically for the example of the V and I filters see equations 3.14 and 3.15, where in this case R is fixed as 1.55 (Ngeow, 2022). Similarly, we used the relation to determine the dereddening magnitude in the K filter, as figure 3.16. Finally, the values in the g, r, and i filters obtained from the ZTF archive were also recalculated by the previously mentioned adaptation to Pan-STARRS1. From 3.17, 3.18 and 3.19 relations, we were also able to calculate the absolute Wesenheit magnitude, as equation 3.20 in (Ngeow, 2021).

$$W_{\mathrm{I}} = I - R(V-I) \tag{3.14}$$
$$R = A_{\mathrm{I}}/E(V-I) \tag{3.15}$$
$$W_{\mathrm{K}} = K - 0.618(J-K) \tag{3.16}$$
$$W_{\mathrm{gi}} = g - 2.274(g-i) \tag{3.17}$$
$$W_{\mathrm{gr}} = r - 2.905(g-r) \tag{3.18}$$
$$W_{\mathrm{ri}} = r - 4.051(r-i) \tag{3.19}$$
$$M_{\mathrm{Wgr}} = W_{\mathrm{gr}} - 5\log(d) + 5 \tag{3.20}$$

Analysis

All the data were saved in Excel files and then processed in Python. For this, either existing code such as Upsilon was used, (Kim, 2016), or for the most part the data was processed with custom code. These results will be commented on in the following sections, first for the galactic bulge and then for the galactic halo.

4.1 Analysis of galactic bulge

4.1.1 Metallicity and period distribution of Miras (fundamental characteristics of Miras)

The bimodal distribution of metallicities for globular clusters has been known for some time and has been also verified. This bimodality of globular clusters is related to the period and place of their formation, see (Smith , 2000).

Our data for Miras in the Galactic bulge show a similar trend of bimodal metallicity distribution. In Fig. 4.1.1 we note the increased abundance of Miras for a metallicity of –0.4 dex and around +0.5 dex. This bimodality could be related to the evolution of the bulge itself and also tells us that Miras formed in two phases. According to article Rojas-Arriagada (2019), the more metal-rich stars (with a peak around metallicity of +0.5 dex) come from a period known as the secular evolution (a period of slow and steady evolution), when the thin disk evolved and the formation of a bar occurred. In contrast, the formation of metal-poorer stars (–0.5 dex) is not fully understood. It is thought to have originated during impulsive early star formation or during the evolution of the early thick disc.

On the other hand, the period distribution in Fig. 4.1.2 shows a classical Gaussian distribution with the highest frequency at a period of approximately 330 days. The average Miras period is generally reported to be around 300 days. Our value also agrees with the paper by Matsunaga (2017) where they obtained the same distribution for Miras in bulge with the same most frequent period, but where their data were obtained from the OGLE III catalogue. It is therefore a good comparison, where even across other catalogues we come to the same conclusion.

If we want to correlate the metallicity with the period and see if there is any dependence, as is the case for RR Lyrae stars or other pulsating variable stars, only a very slight dependence is seen in this case for Miras in the bulge, see Fig. 4.1.3. We can notice a slight dependence, where with increasing metallicity (decreasing age) we also identify a decreasing period (periods of brightness changes are more frequent). At the same time,

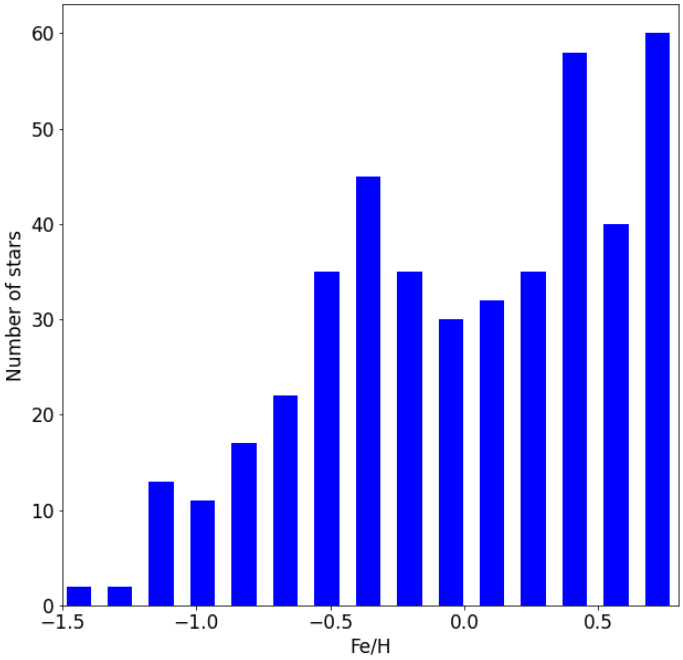

Figure 4.1.1: Abundace rate of metallicity. There is a noticeable bimodal distribution for Miras in the galactic bulge with peaks of –0.4 dex and +0.5 dex.

there is a slight trend for Miras in clusters, where these Miras have a period of brightness changes mostly above 250 days, while Miras located outside the cluster abundantly have periods even below 250 days.

Several papers are based on the view that there is no dependence between period and metallicity, e.g. paper by Feast (1996), but there is also a study Zijlstra (2003) where there is a decrease in period with time for the star R Hya. They explain it by the fact that there existed a gradual decrease in the mass loss of the star that caused this decrease in the period. The reason they give for the decrease in the mass-loss rate is that the star is at the very top of the AGB. However, they are inclined to the view that this decrease in period is isolated and most Miras do not show changes in period with time.

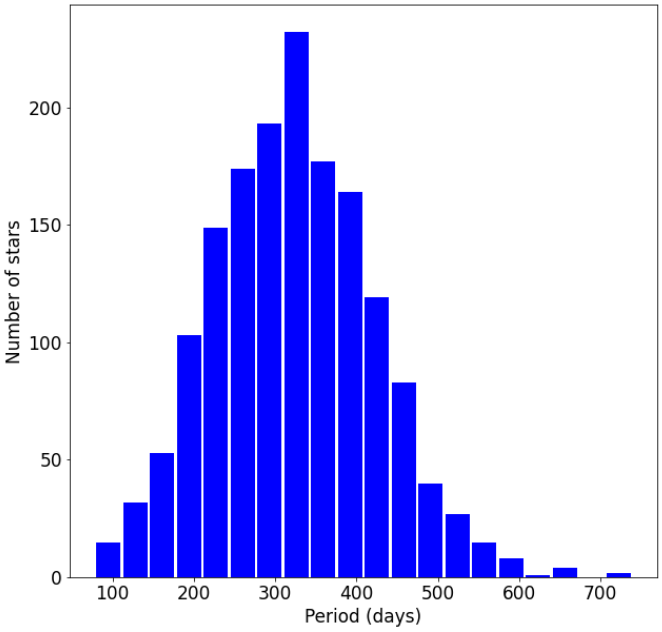

Figure 4.1.2: Abundance rate of the period showing Gaussian distribution with the peak around 300 days.

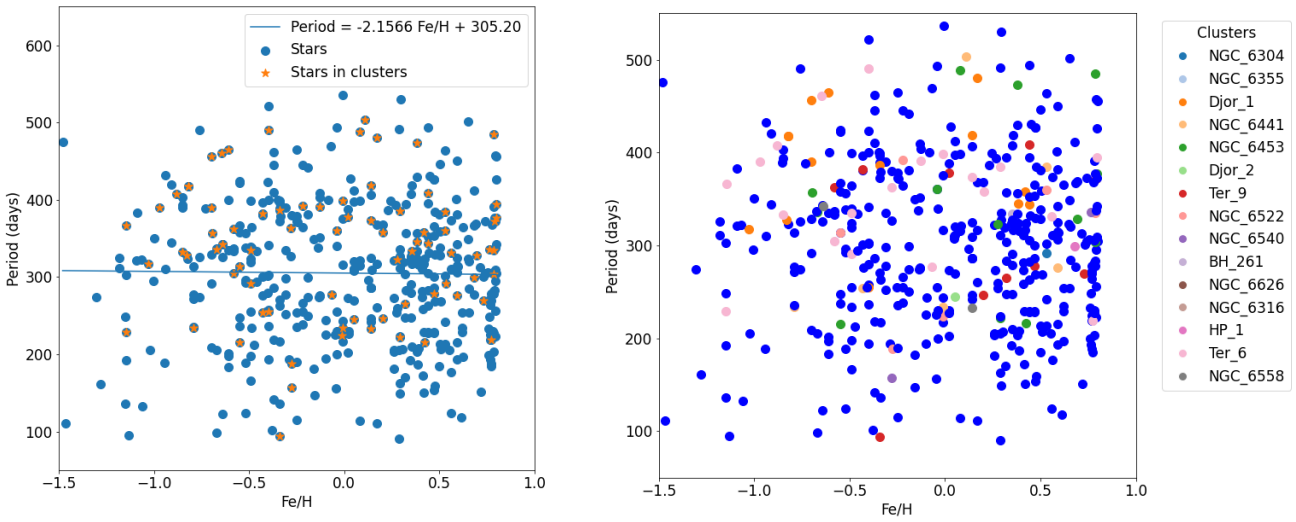

(a) Period–metallicity relation for Miras with weak linear dependence.

(b) Period–metallicity relation with location of stars belonging to clusters.

Figure 4.1.3: Period–metallicity relation.

We obtained the effective temperature of Miras in three ways, namely from the catalogue, by calculation and by isochrones. More detailed information on obtaining these values is given in the 3.3 section. It is clear from the Fig. 4.1.4. that the highest frequency for the effective temperature approximately matches both the calculated effective temperature and the effective temperature obtained from the catalogue, while the isochrones method gave us values completely outside our expectations. The Miras effective temperature according to Shore (2003) is supposed to be below 4000 K, which is in agreement with the effective temperatures obtained from the catalogue and the calculation. The effective temperatures obtained by the isochrones method may not fit due to the fact that we approximated the ZTF filters as Pan-STARRS1, and thus there may have been an error in determining the given values, and we will take them as indicative only.

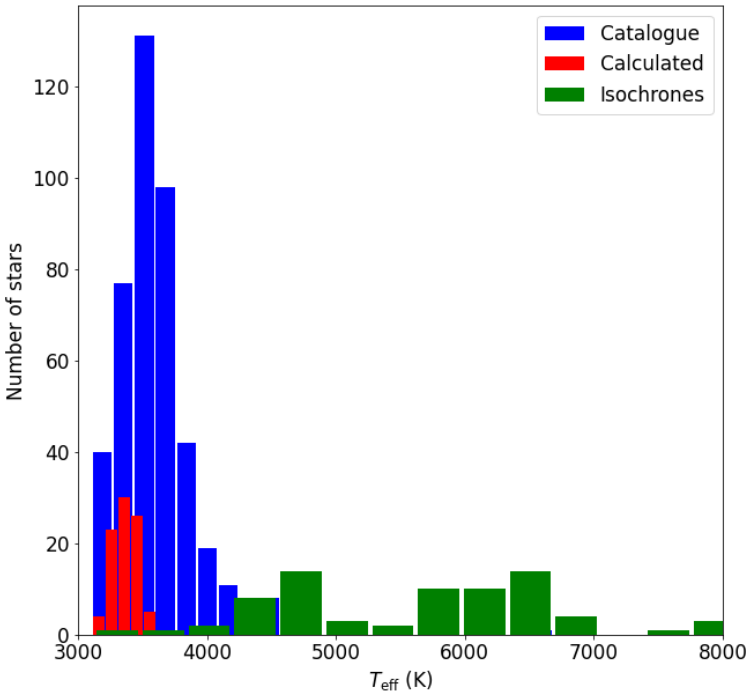

Figure 4.1.4: Frequency rate of effective temperature determined from catalogue, calculation and isochrones.

4.1.2 Color–magnitude and color–color relations

Since our stars are in the same region of the Galaxy – the bulge, and relatively close to each other, we settled for apparent magnitude and did not convert it to absolute magnitude.

From the Gaia catalogue, for the G, BP, and RP magnitudes, we obtained Fig. 4.1.5a. As expected, the stars are mostly placed together in the upper left part of the diagram. Higher $BP - RP$ color values indicate redder candidates (i.e. cooler stars), as we would expect for Miras. The scatter in G magnitudes is minimal, and if distance is included when converting to absolute magnitude, the scatter should decrease. In contrast, the scatter in color has several causes. One of them is the non-inclusion of extinction, which is evident in bulge stars and was therefore included in the 3.3.6 section. Another reason is that for $BP - RP$ values $BP - RP < 6.5$ mag we have crossed the threshold below which the Gaia values are not taken into account because they are unreliable. This limit can also be found for the G filter, where the limit is 16 mag and values above this magnitude are unreliable too, (Mowlavi , 2018). In our plot, we can also spot these data, and they are located in the lower left part of the plot and form a prominent part in an otherwise homogeneous cluster.

If we look at the graph 4.1.5b, where we can see the distribution of the stars in the clusters, is clear that Ter 6 and Djor 1 are located in areas with a higher color index, so they appear redder than the stars in NGC 6453 and NGC 6441, which are located below them. This is due to the previously mentioned reddening effect, where according to article Bica (2016), Ter 6 cluster has a higher reddening than NGC 6441. The reddening values for Djor 1 and NGC 6453 were taken from Harris (1976) and show the same reddening trend with respect to each other.

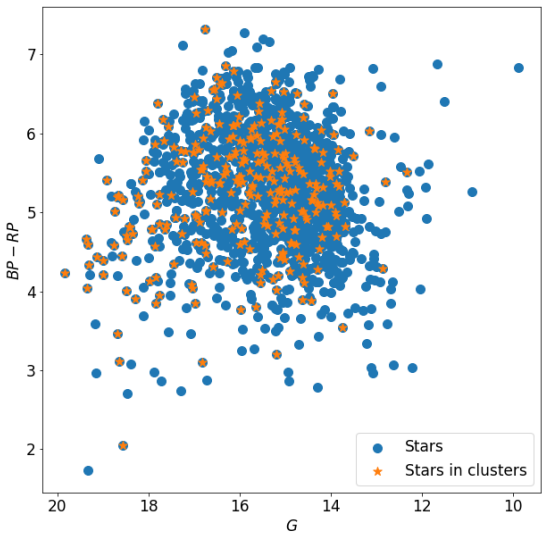

(a) Gaia color magnitudes used for Miras stars and Miras located in clusters

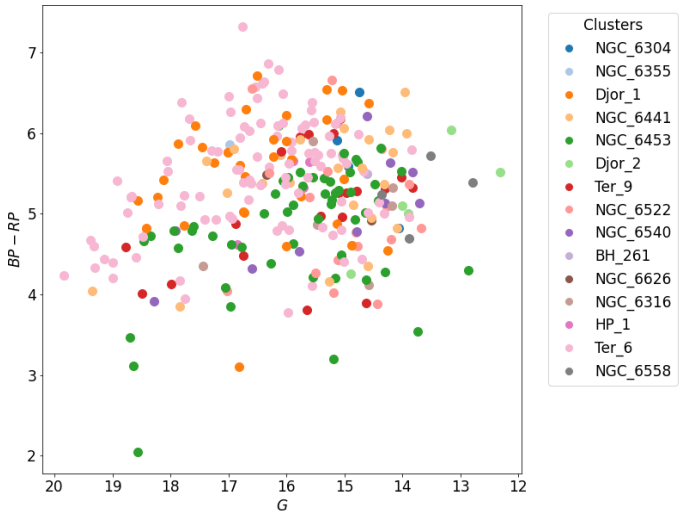

(b) Gaia color magnitudes used for color–magnitude diagram with location of Miras belonging to specific clusters.

Figure 4.1.5: Color–magnitude diagram for Gaia photometry.

For Gaia, in addition to the mean values for G, BP, and RP, we also obtained their minimum and maximum values, which are shown in Fig. 4.1.6. There is a noticeable dependence where we find brighter/hotter stars at the minimum of their radius and at the maximum of their luminosity, as we would expect for pulsating variable stars. While cool and low luminosity stars are found at the maximum of their radius.

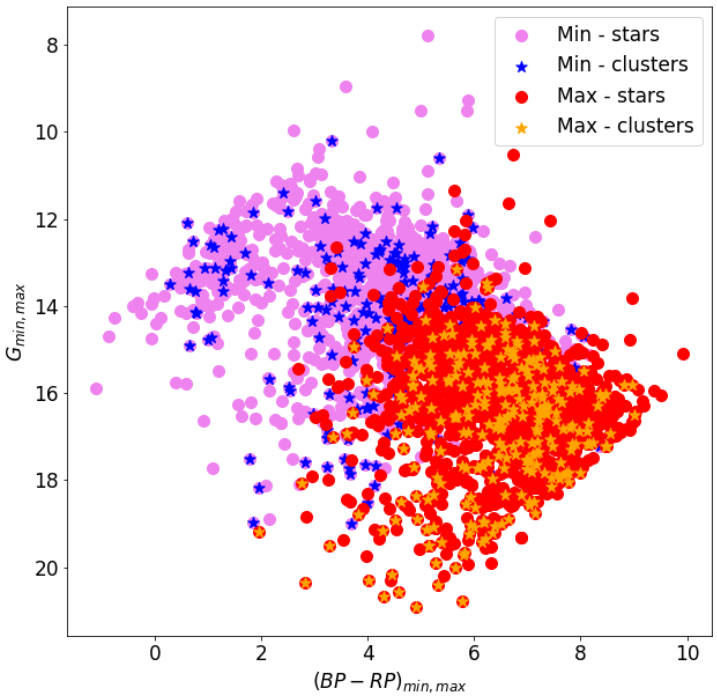

Figure 4.1.6: Shift of Miras in color–magnitude diagram during their pulsation cycle.

Since we have no information on their type for Miras in bulge – oxygen (O) vs carbon (C), we have to try to determine their type from the dependence of $J-K$ color on K magnitude. It has been found that carbon Miras have strong absorption bands in the CN and C2 molecules that affect the values in the J filter and shift them to higher values, while oxygen Miras are affected by the T_iO and H_2O molecules, which affect both the J and K bands (Matsunaga , 2017). They determined the cut-off region for the K filter to be $K < 9.5$ mag and for the $J-K$ color to be $J-K > 3.2$ mag by empirical observation and comparison with Miras in the Large Magellanic Cloud (LMC). This would correspond to about 40 Miras out of the total in our 4.1.7. However, this number may be lower since we have not included interstellar reddening in this graph.

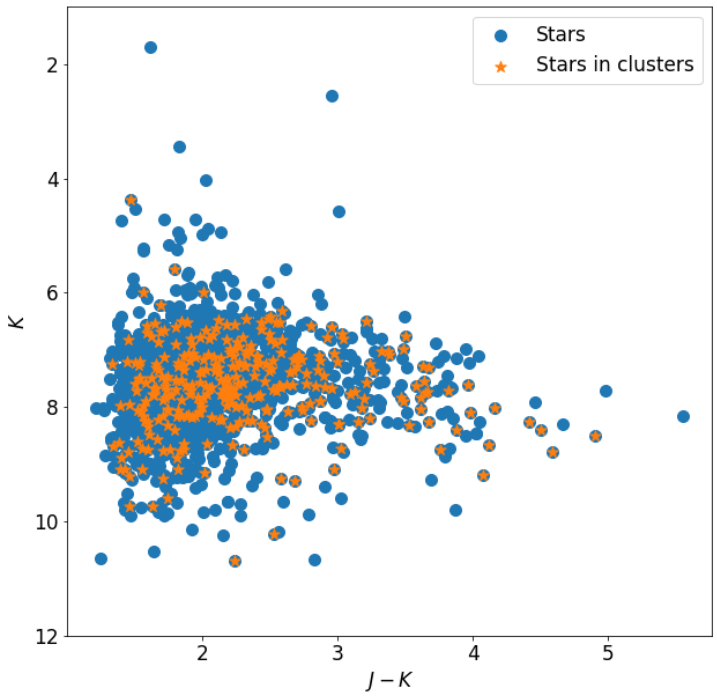

Figure 4.1.7: Location of Miras and Miras in clusters in color–magnitude diagram for 2MASS filters.

In addition to O and C Miras, SR variables are often mistakenly classified as Miras, but they have slightly lower amplitudes of brightness changes and also periods. However, based on the paper by Chen (2020), we are able to distinguish them, using the W_1 and W_2 filters from the WISE catalogue, which have, among other things, good signal-to-noise ratios. For $W_1 - W_2$ color greater than about 0.4, these should be SR variables according to the article. Like the previous filters in 2MASS, these values were determined based on Miras in LMC. In our Fig. 4.1.8, this would be about 1/3 of the stars, but at the same time, the article shows that this limit is quite overlapping and only very tentative. They take the dependence of W_1 on amplitude as the key, but these data are not available to us. However, our plot again shows that our stars are in the redder region, but since the wavelengths of W_1 and W_2 are very close to each other, the separation between Miras and SR becomes very blurred.

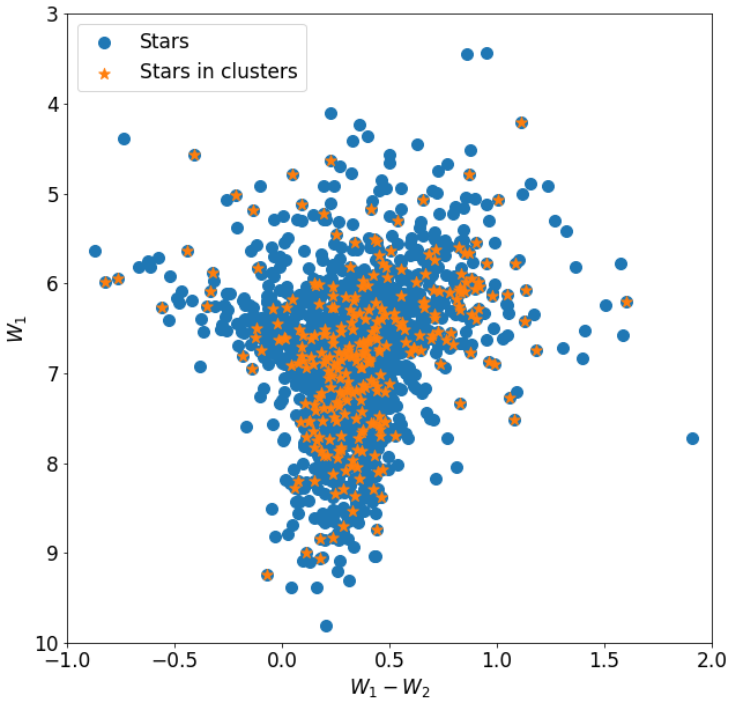

Figure 4.1.8: Location of Miras and Miras in clusters in color–magnitude diagram for filters W_1 and W_2 in WISE catalogue. These filtres belong to near infrared part of spectra

However, we could determine all these types of both O and C Miras and SR variables from the color diagram for the WISE catalogue, as in Fig. 4.1.9. This is based on papers by Chen (2020) and Iwanek (2021), both of which agree that for values of $-0.2 < W_1 - W_2 < 0.25$ and $W_2 - W_3 > 0$, these are oxygen Miras. However, the papers disagree on the type of variable star for $0.25 < W_1 - W_2 < 1.5$ and $W_2 - W_3 > 0$, with the first paper claiming that stars in this range are SR variables, while the second paper identified them as carbon Miras. It should be noted that the second paper discusses Miras on the LMC, which may introduce this confusion about the type determination.

However, the most common method to partition Miras based on chemical composition is a combination of photometric data from the Gaia catalogue and 2MASS. Where the J, K and BP, RP filters/magnitudes are converted to Wesenheit magnitudes according to the relations given in the methodology section, which reduces our influence to reddening. Simply distinguishing C/O Miras based on the 2MASS catalogue is not sufficient for stars in the bulge due to the large number of background stars and reddening compared to stars in the LMC and SMC, where it is sufficient to use the 2MASS catalogue values to distinguish them.

From the paper by Sun (2023) they determined the x-axis limit as approx 2.6 mag (parabole-shaped limit – decreasing color up to M_K = –7.5 mag, then the color increase again), based on the different absorption in the C and O Miras spectra. Stars with a value less than that belong to O Miras and C Miras, respectively. In Fig. 4.1.10, this is again

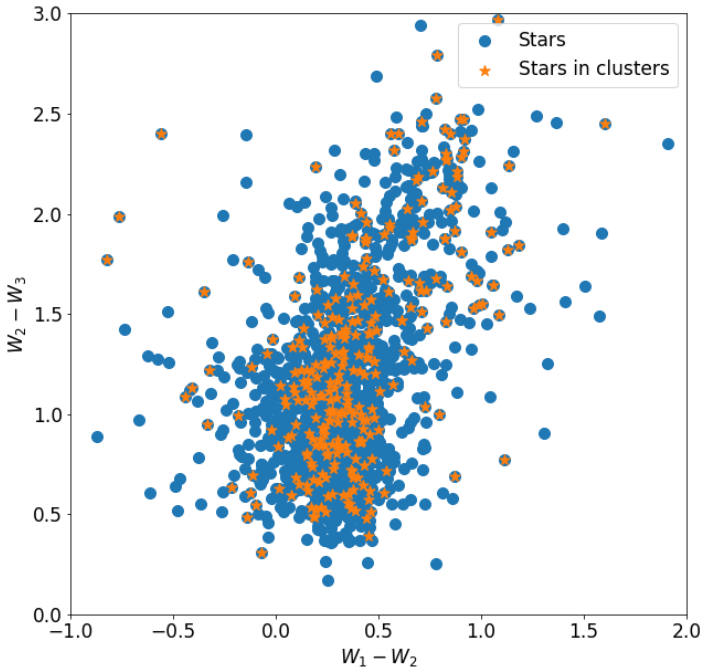

Figure 4.1.9: Location of Miras and Miras in clusters in color–color diagram for filters from WISE catalogue.To note, there is an extended linear dependence, whereas the color $W_1 - W_2$ grows, so does the color $W_2 - W_3$.

about 1/3 of the Miras falling into the C Miras category.

An interesting dependence can be seen in Fig. 4.1.11, where we used the V and I filters from the OGLE III survey. From the shape of the curve, we can conclude that these are RGB/AGB stars, as expected, but there is also a dependence on the period. We observe a trend where the period of Miras changes increases linearly with increasing color and decreasing magnitude. Thus, the redder and brighter the star, the longer the period. This phenomenon is typical of pulsating variable stars and is mostly known for Cepheids.

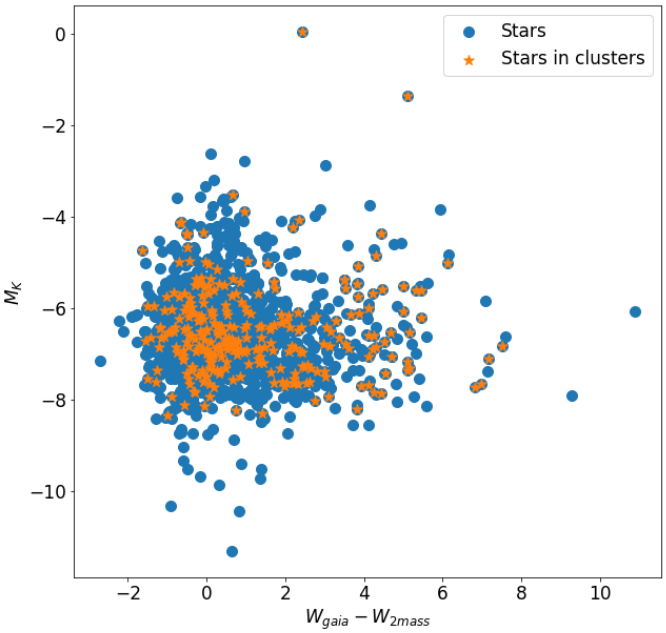

Figure 4.1.10: Comparing color with absolute magnitude from two different catalogues - 2MASS and Gaia.

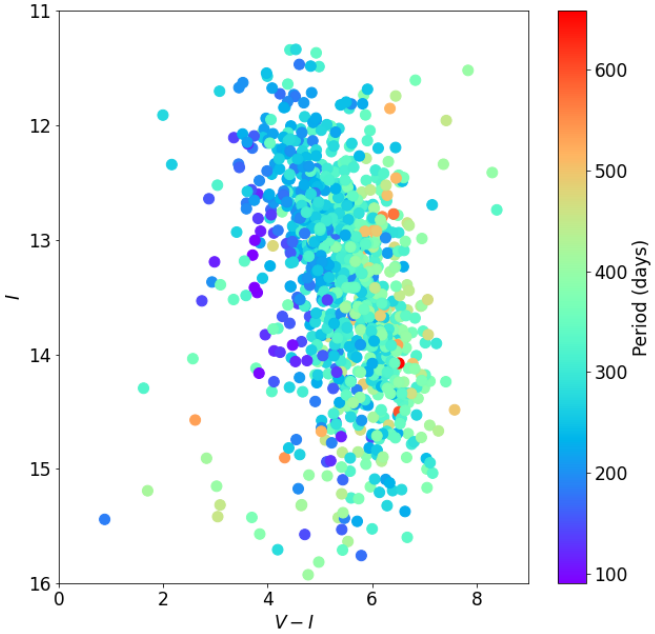

Figure 4.1.11: Comparing Miras in color–magnitude diagram for OGLE III filters. It is clear that there is color dependence on period, which changes with higher values of color.

4.1.3 Period magnitude and period color relations

Given the known relation showing the linear dependence of period on magnitude for pulsating stars, we expected a similar result in our case, as confirmed by 4.1.12, 4.1.13 and 4.1.14.

The dependence of the logarithm of base 10 on magnitude in the filter shows a linear dependence in Fig. 4.1.12. However, for log$P$ values of 2.4 to 2.8, we can notice an extension of the plot where we have multiple magnitudes for a given period. This may be because these are carbon Miras, which are typically characterized by larger spread of magnitude values and slightly longer periods. The same conclusion was reached in Soszynski (2005) and Yuan (2017), although for Miras located in thebLMC and SMC.

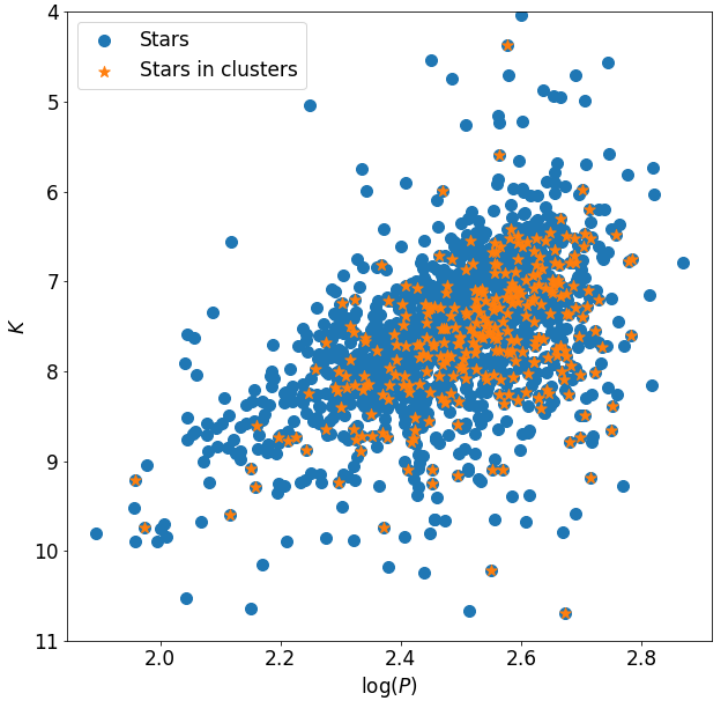

Figure 4.1.12: Period dependence on 2MASS filter log(P) on W_1.

The same dependence can be seen in the Fig. 4.1.13 that shows the dependence of log$P$ on W_1, but with the difference that the values are more compact and clustered together, compared to the previous graph. Our graph is quite comparable to the graph obtained in the paper by Schultheis (2008). There may be several reasons why we observe values closer together. Since Miras are cool red stars they will be detected more accurately and in more detail in the W filter, which includes redder wavelengths, and also this filter has a narrower wavelength coverage than the K filter.

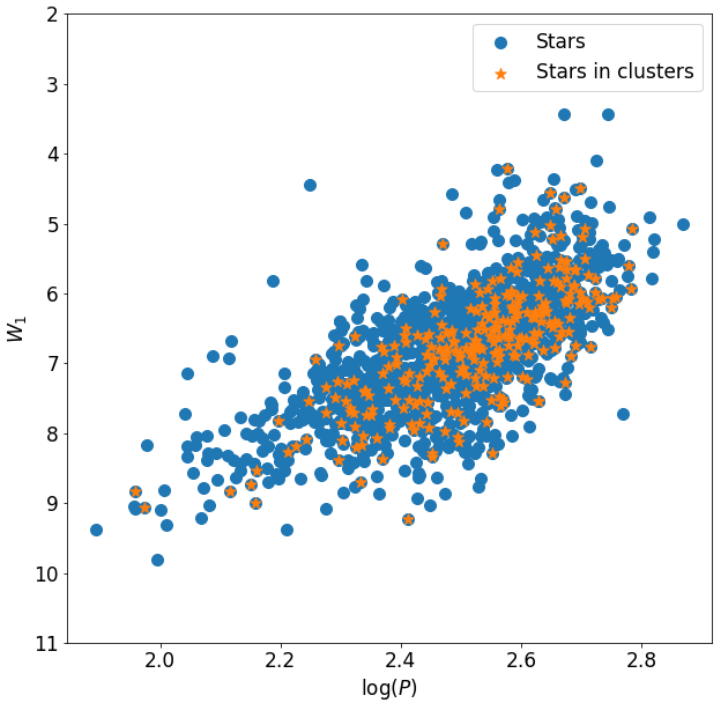

Figure 4.1.13: Linear dependence of log(P) on W_1 for Miras and Miras in bulge globular clusters.

Last, we took the dependence of the period on the $J-H$ color, from which, according to the paper by Yuan (2017), one can distinguish C/O Miras in the LMC. Our form of the Fig. 4.1.14 is in perfect agreement with that in the paper. Thus, we can adapt that in the range 0.5 to one for the $J-H$ color we find oxygen Miras and the rest are carbon Miras. Unfortunately, no paper has done the same with a sample of O/C Miras in the Galaxy, so we cannot take this conclusion as conclusive.

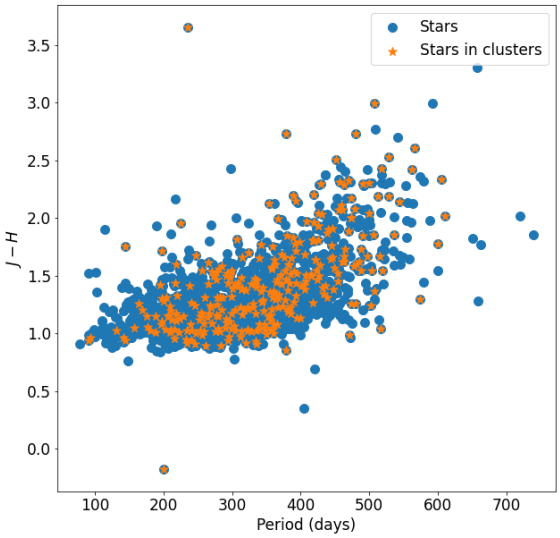

(a) Distribution of Miras in period–color relation.

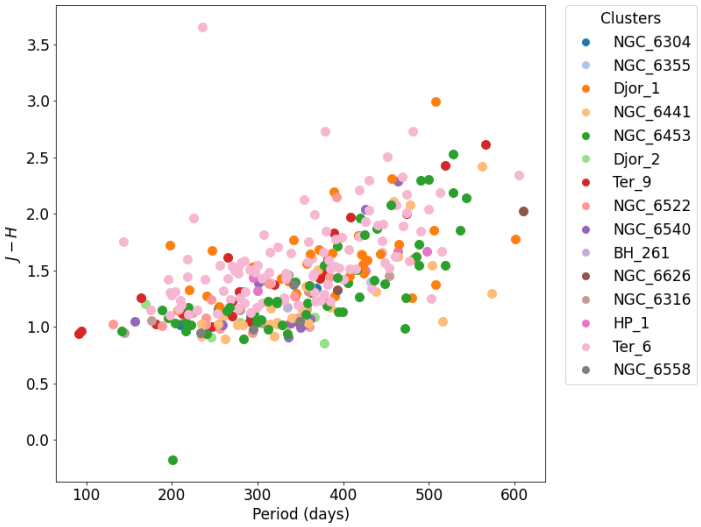

(b) Distribution of Miras according to cluster membership.

Figure 4.1.14: Period–color relation for $J - H$ color.

4.1.4 Lightcurves and moving color–magnitude diagram

From the ZTF catalogue, we have obtained for most stars their mjd and magnitude and the filter in which the star was measured. From this, we were able to construct light curves using code we wrote in Python. A sample of some of the light curves can be seen in the figures, where we can cross-reference the light curves of O and C Miras, which were determined using Upsilon. The period values were determined with Peranso using Lomb-Scargle methods, where we searched for periods in the range 100-1000 days. For O Miras, we determined the period with a deviation from the values obtained from the catalogue of 1 day in the case of the star whose light curve can be seen in Fig. 4.1.15. In contrast, for the star whose light curve is seen in Fig. 4.1.16, its period determination is off by 90 days. In the case of C Miras, its period differs by 17 days from that in the catalogue, see Fig. 4.1.17 . Unfortunately, the Upsilon program had a problem determining the type of stars in the bulge, so we do not have many stars to adequately compare. The Peranso program has always determined periods in the case of Miras in the bulge to be slightly longer than we found from the catalogue. It is also clear that the O Miras have larger amplitudes of brightness changes than the C Miras, as we would expect.

We also constructed a moving CMD, see Fig. 4.1.18, from the data obtained from the ZTF catalogue, as discussed in the 2.6 section. For these data, we did not consider extinction to calculate the absolute magnitude in the r band, as we did not have these data. The linear dependence of color on absolute magnitude remains the same as shown in Fig. 3.1.1, except that the trend is reversed. This is due to the previously discussed reversal of dependence when using a filter in the optical and infrared parts of the spectrum. In addition to this trend, we observe high amplitudes of luminosity changes associated with

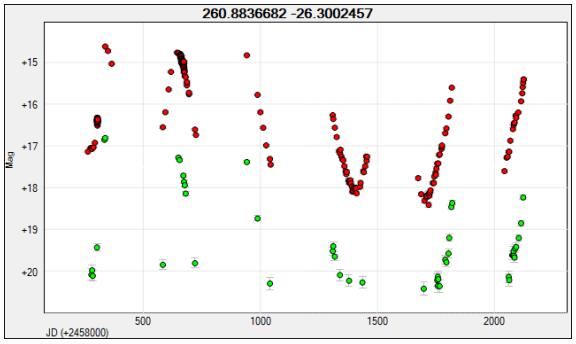

(a) Light curve of O Mira derived by Peranso using ZTF archive.

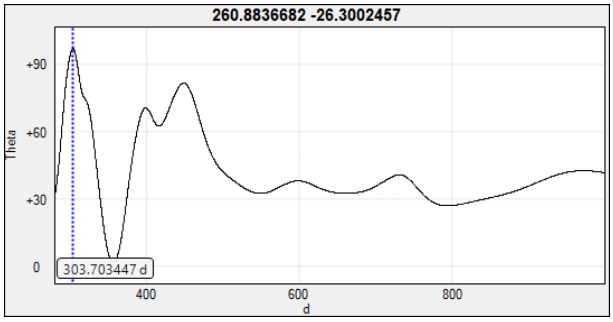

(b) Derived period by Lomb-Scargle method.

Figure 4.1.15: Light curves in *g* and *r* filters and derived period for O Mira with coordinates Ra = 260.8 deg, Dec = –26.30 deg.

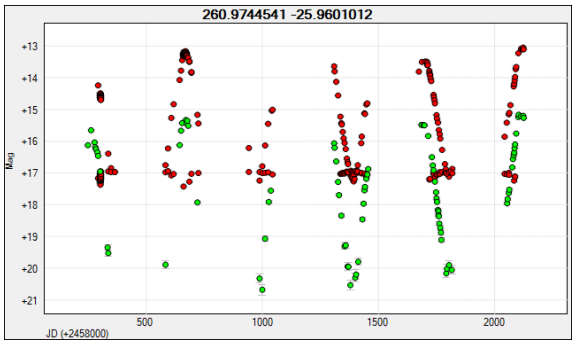

(a) Light curve of O Mira derived by Peranso using ZTF archive.

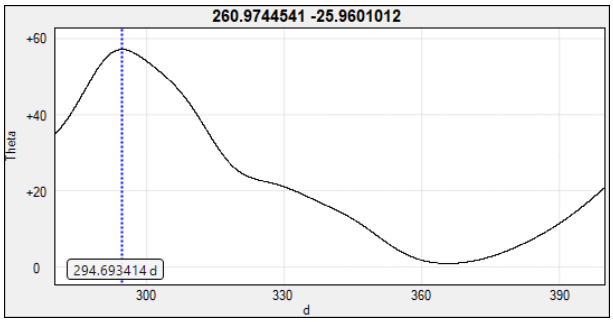

(b) Derived period by Lomb-Scargle method.

Figure 4.1.16: Light curves in *g* and *r* filters and derived period for O Mira with coordinates Ra = 260.97 deg, Dec = –25.96 deg.

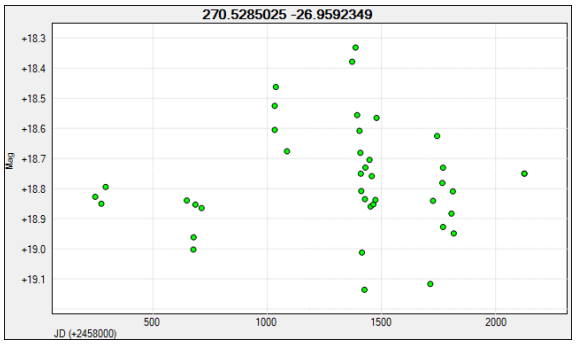

(a) Light curve of C Mira derived by Peranso using ZTF archive.

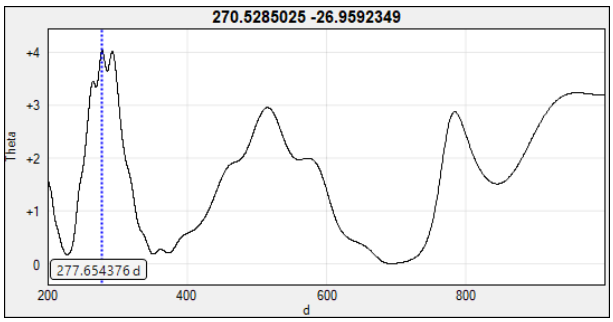

(b) Derived period by Lomb-Scargle method.

Figure 4.1.17: Light curve in *g* filter and derived period for C Mira with coordinates Ra = 270.5 deg, Dec = –26.96 deg.

strong pulsations of the star as a consequence of the effective temperature change of the star.

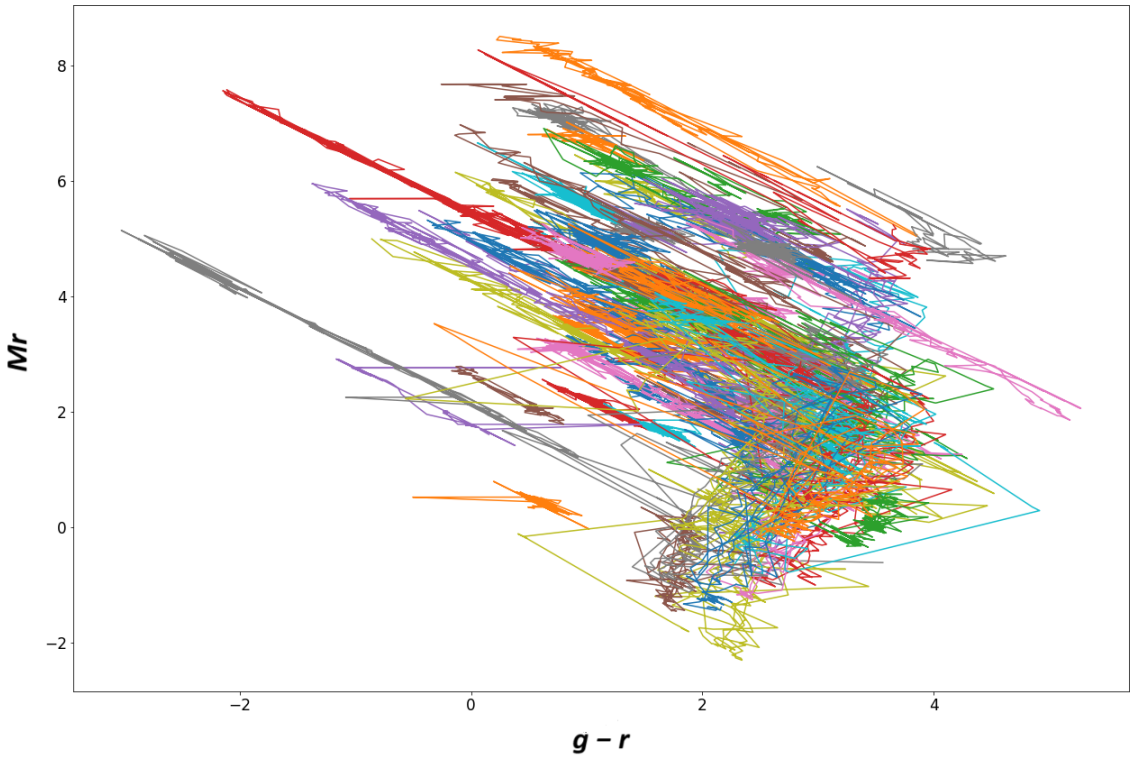

Figure 4.1.18: Moving CMD for bulge Miras. Different colors indicate different Mira stars.

4.1.5 Extinction and reddening dependence on location of stars in clusters

In the Fig. 4.1.19, 4.1.20 and 4.1.21 that show us the dependence of extinction on reddening for different filters, we can notice a linear dependence, where extinction increases with increasing reddening, as we would expect.

For the B, V and V, I filters we observe minimal point spread (these points are very close together) whereas for the J, K filters these points occupy a wider band of extinction for a single reddening value. The spread is related to the width of the J, K filters itself, which is larger than the B, V and V, I filters - its wavelength spread is wider.

All of these plots illustrate a consistent distribution of stars within a given extinction for a particular cluster. According to the graphs, stars belonging to the clusters NGC 6453 and NGC 6441 have low extinction and reddening values, while stars in the clusters Ter 6 and Djor 1 have high extinction and reddening values. This is consistent with the extinction

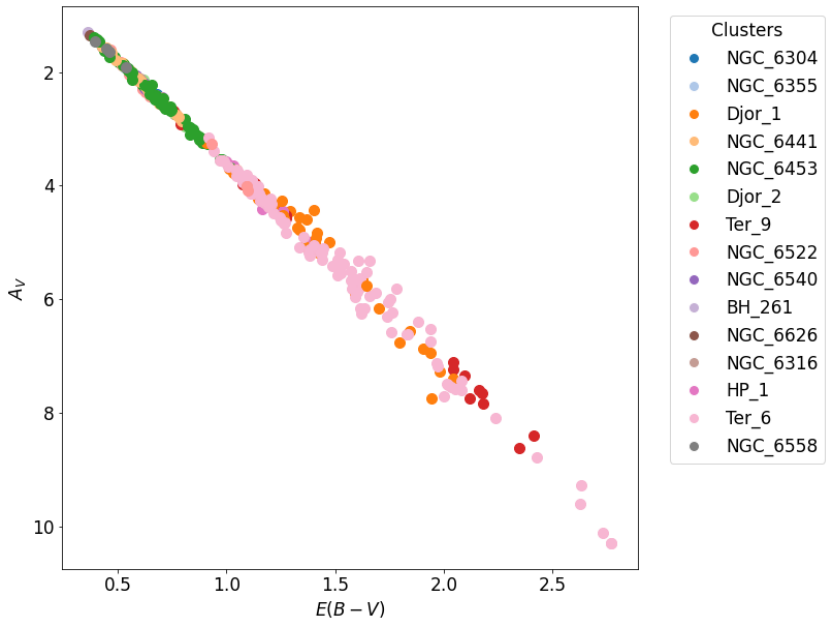

Figure 4.1.19: Extinction and reddening values in B and V filters.

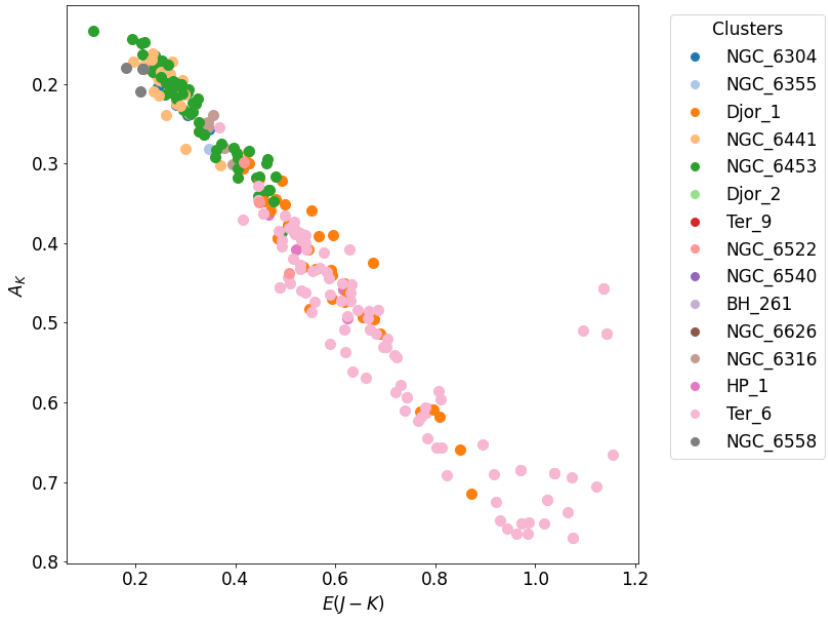

Figure 4.1.20: Extinction and reddening values in J and K filters.

values of the clusters in the Harris (1976) catalogue. The low extinction and reddening values refer to stars in clusters that have either $b > +5$ deg or $b < -5$ deg. However, for the case of the cluster NGC 6453, the paper by Bica (2016) claims that it is an outer bulge intruder that originally fell into the halo. The reason for their claim is the high space velocity of this cluster, which is typical of objects in a halo.

Just as we examined the color–magnitude diagram for the J and K filters in 4.1.2, because of the interstellar dust and gas, it was necessary to obtain values for extinction

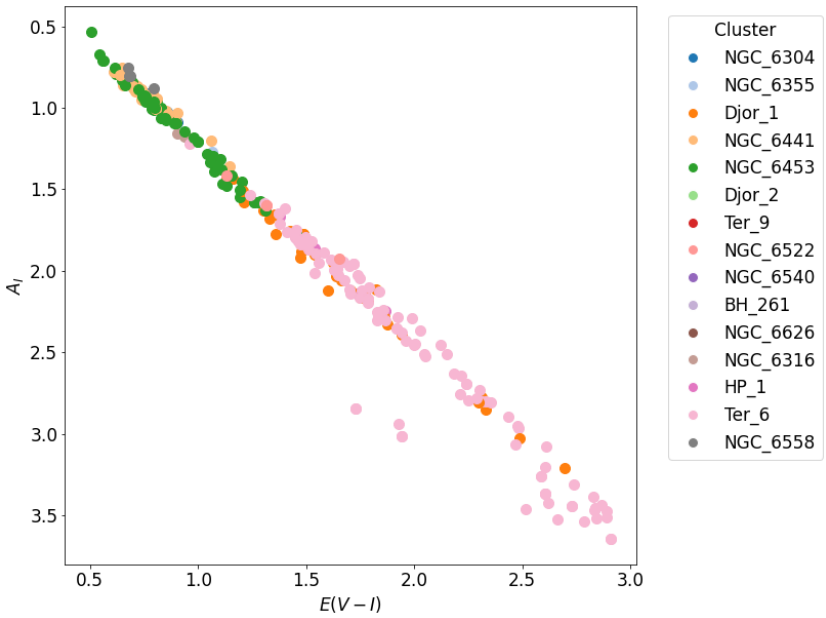

Figure 4.1.21: Extinction and reddening values in V and I filters.

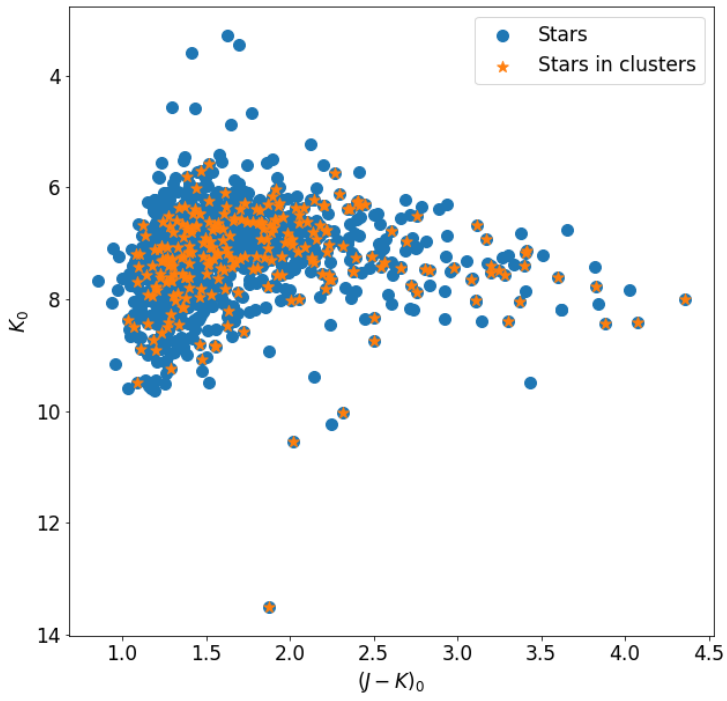

Figure 4.1.22: Dereddened 2MASS magnitudes for bulge Miras.

and reddening in these filters as well. From this, we were then able to convert these values to dereddening values of $(J-K)_0$ and K_0, the resulting dependence of which is shown in

4.1.22. Not surprisingly, we see the same point locations as in 4.1.7. just with different values on the axes. When we include the reddening, the stars have moved approximately 0.5 mag to the left bluer part of the graph. Thus, the interstellar material did indeed make the stars slightly redder than their true color. In contrast, there was no significant shift in the magnitude of K_0 on the y-axis.

4.1.6 Period dependence on extinction modified values

The linear dependence of the logarithm of the base 10 period on magnitude has already been demonstrated in 4.1.3 section. We have shown the same dependence in Fig. 4.1.23, this time using dereddened values of K_0. However, the range of dereddened magnitudes in the K filter is narrower here. This may be because stars in different parts of the bulge are affected differently by interstellar reddening and the dust/gas is not homogeneously distributed there.

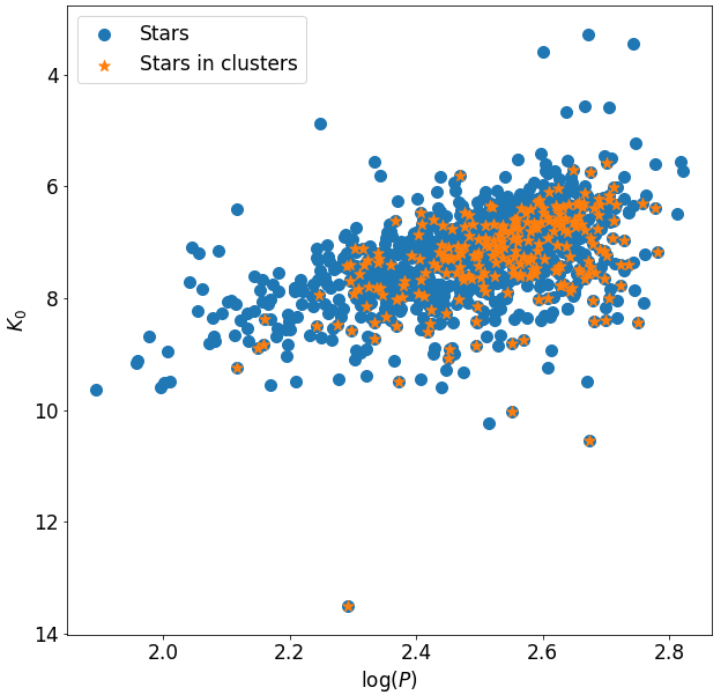

Figure 4.1.23: Period dependence on dereddened K_0 filter.

The same linear dependence can be seen if we convert the K filter to Wesenheit magnitude instead of accounting for extinction. This linear dependence differs for W_{JK} and K_0 in the slope and intercept values and hence the slope of the function is also different. In this case, the Fig. 4.1.24 rises faster for W_{JK} than it does for K_0. The reason for the differences may stem directly from the definition of the Wesenheit magnitude and its limitations, such as its dependence of the function on the choice of filter, which was discussed in 3.3 section.

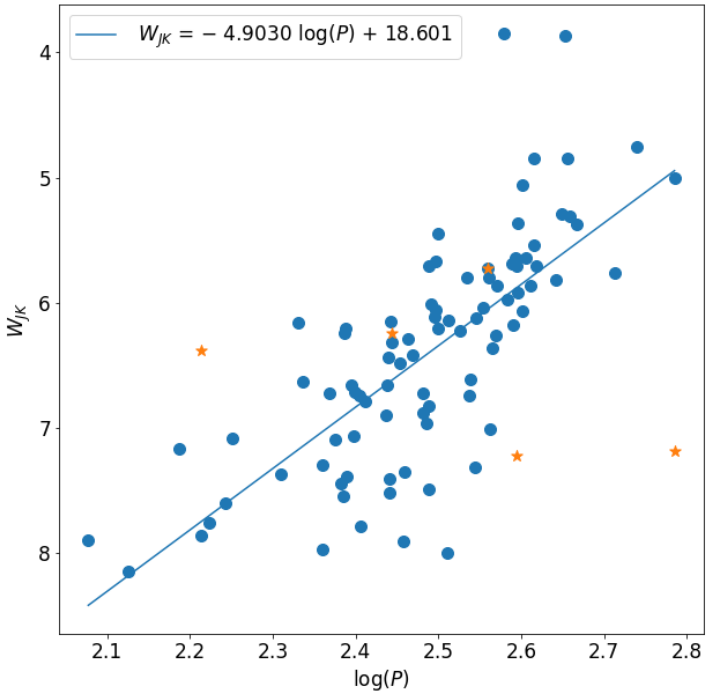

Figure 4.1.24: Dereddened 2MASS filters for bulge Miras with linear dependence Wesenheit magnitude on period.

4.2 Analysis of galactic halo

4.2.1 Metallicity and period distribution of Miras (Fundamental characteristics of Miras)

The distribution of metallicities by frequency does not have a bimodal distribution for the halo, as can be seen in Fig. 4.2.1. This may suggest that the stars in the halo were formed during one phase. We observe the highest metallicity abundance for Miras around +0.5 dex, suggesting that these Miras formed in a second phase when the Universe was already enriched with the material after the extinction of the primordial stars. A second peak for the bulge is also around this value, whereas the primordial one is around a metallicity of –0.5 dex, as discussed in section 4.1.1. This finding suggests that the halo might be slightly younger than the bulge, which is consistent with the paper by Morrison (1993) which reports its average age difference of about 1 Gyr.

In the case of the frequency-based period distribution, we found a Gaussian distribution with a peak for a period of approximately 300 days, see Fig. 4.2.2. This period is consistent with the period in the LMC for the paper by Matsunaga (2017) and for the Galactic halo from (37). This paper claims that this low period is due to a higher age than the bulge stars or lower metallicity. However, this is in contradiction with our metallicity results, where we found a double metallicity for Miras in the bulge, both metal-poor and metal-rich,

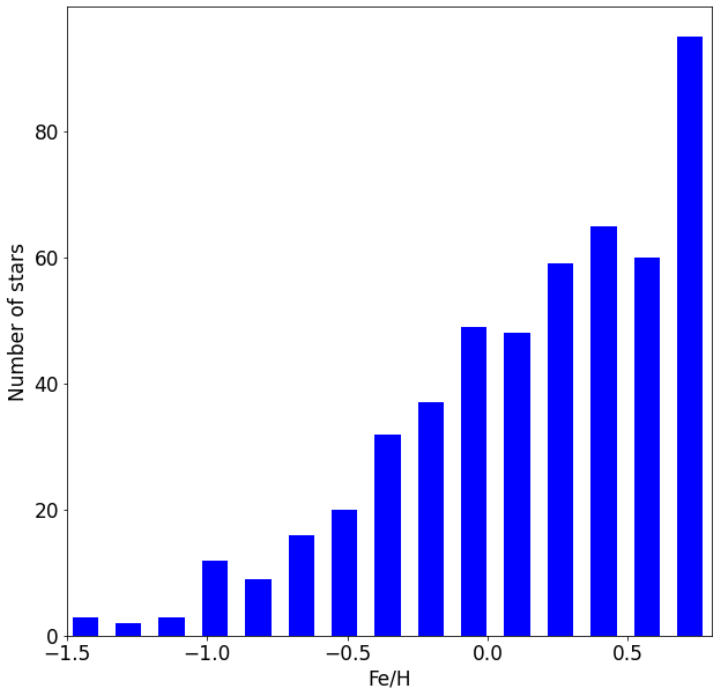

Figure 4.2.1: Metallicity distribution grows for metal rich Miras with peak at +0.5 dex.

while only one for the metal-rich halo. At the same time, the same result for the period distribution as for the LMC may indicate their similar ages, which is for halo, as we have already mentioned, approximately 1 Gyr younger than the bulge. Thus, the lower periods can be associated either with young stars on the AGB, their mass loss is just beginning, or with an excess of O Miras, which have on average lower periods than C Miras.

The dependence of the period on metallicity in the Fig.4.2.3 showed us a very slight dependence, where the period increases with increasing metallicity. The trend is indeed minimal and opposite to that for bulge. Thus, the significance is mainly due to the frequency of Miras for a given metallicity rather than any trend.

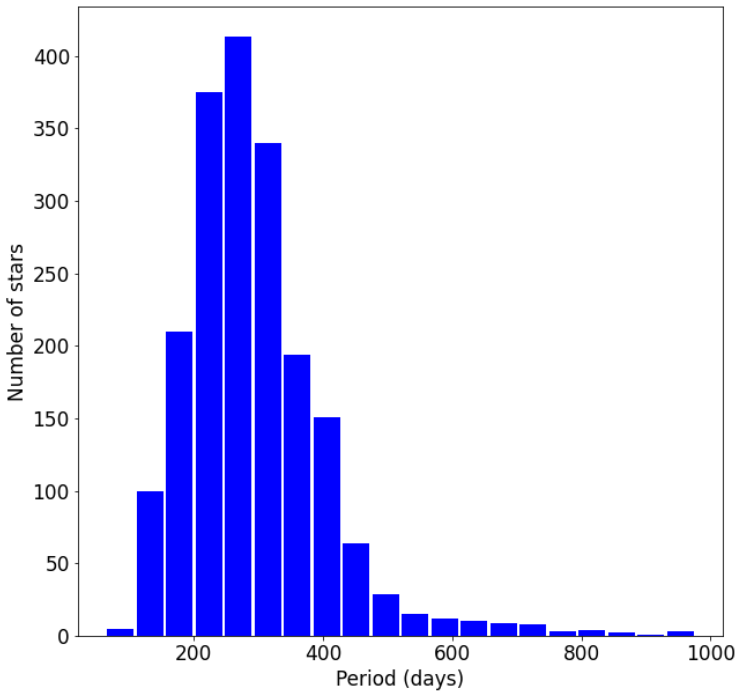

Figure 4.2.2: Gaussian distribution for Miras in galactic halo, with most frequent period around 300 days.

The values for the Miras effective temperatures were obtained, as mentioned in the bulge section, from the catalogue, by calculation and using isochrones. In Fig. 4.2.4. we can see the approximate correspondence in the effective temperature distribution regardless of its type of determination and the correspondence in the most common effective temperature, namely 3500 K. In this case, the approximation of the ZTF data to Pan-STARRS1 gave us an adequate and expected result. For this reason, we further investigated the dependence of the luminosity on effective temperature, as seen in Fig. 4.2.5. For effective temperatures between 2500 K and 3400 K, we obtained a linear increase in luminosity with effective temperature, while for effective temperatures above 3400 K, there is a decrease in luminosity, for the luminosity obtained with isochrones. This dependence is based on the definition of luminosity, where luminosity depends on the fourth power of effective temperature and the second power of radius. On the other hand, the luminosity obtained by calculation shows no trend.

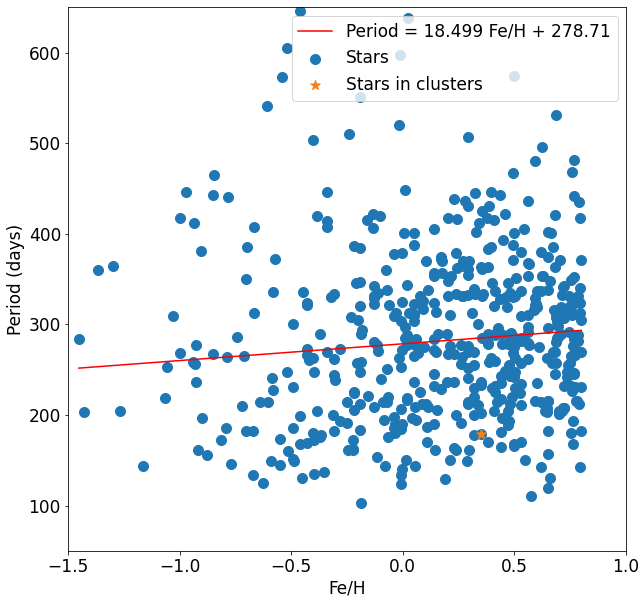

Figure 4.2.3: Dependence of metallicity on the period for halo Miras, do not show any strong correlation as is known for RR Lyrae variables.

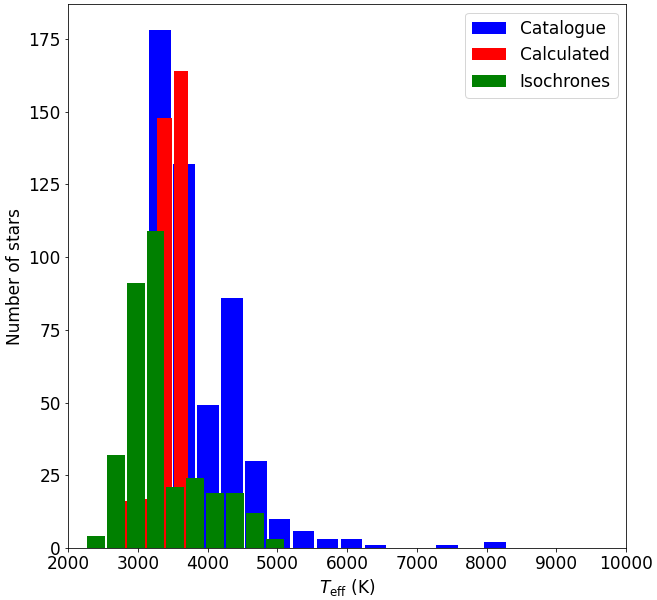

Figure 4.2.4: Histogram for effective temperatures whose derivation methods are shown in different colors.

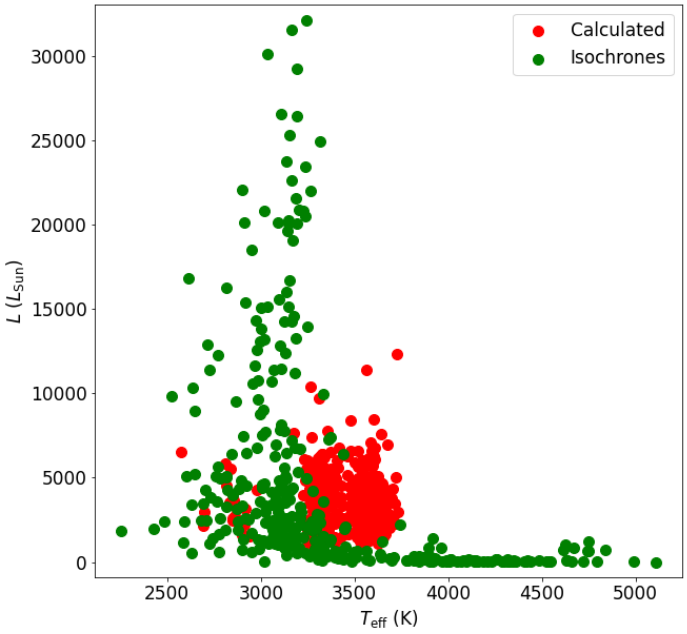

Figure 4.2.5: L (L_{Sun}) dependence on effective temperature. Different derivation methods for luminosity are tagged by different colors.

4.2.2 Color–magnitude and color–color relations

For the sake of a mutually consistent comparison of Miras in the halo with the bulge, we have not converted the magnitudes in the filters to absolute magnitudes either, although this would be convenient here because of the large range of distances for the galactic halo.

In the case of the Gaia magnitudes BP, RP, and G, which can be seen in 4.2.6a. a wide range of magnitudes in both the G and $BP - RP$ magnitudes can be seen. The same can be seen in the 4.2.6b, where we can observe the shift of the star at its pulsation minimum and maximum. The stars have a wide spread in G caused by large variations in parallaxes, yet there is a minimal shift in color. This is due to interstellar reddening, which is almost negligible for halo stars.

The claim of a wide range of values for magnitude in a particular filter can be verified in Fig. 4.2.7 showing filters from the 2MASS catalogue. It is clear that as we get a lower K value (brighter star), the distance the star is from us decreases, while the color of the stars does not change with distance. This tells us that extinction is minimal and the wide range in magnitude is caused by a distance. For K of approximately 11 mag, we see a larger scatter of values in the $J - K$ colors. This scatter should belong to the C Miras, also observed in the paper by Soszynski (2005), but for Miras in the LMC. In general, we can also say, based on the similarities mentioned earlier, that Miras in the halo and LMC show similar behaviour.

The type of Miras determined thanks to the Upsilon program could be verified with the paper by Sun (2023), where using the difference of the Wesenheit magnitude from

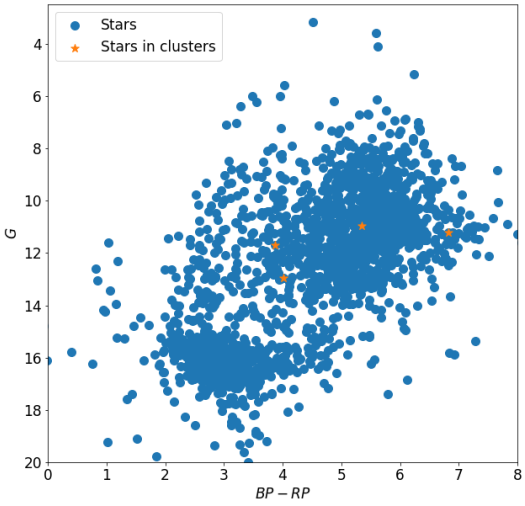

(a) Gaia color–magnitude diagram for halo Miras.

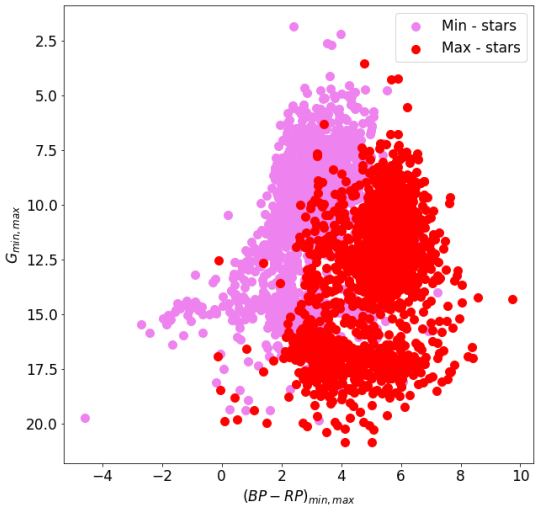

(b) Gaia color–magnitude diagram for Miras in their minimum and maximum magnitude/color.

Figure 4.2.6: Comparing mean values for Gaia magnitudes with their min and max values during pulsation.

the Gaia catalogue and 2MASS versus the absolute magnitude in the K filter, we were able to distinguish C/O Miras, see Fig. 4.2.8. We have already commented on this limit in the 4.1.2 section. It should be noted that the C/O Miras determined by us are only indicative based on the light curves, and a more precise determination would require our own spectral analysis and mass spectrography. The light curves obtained by us, based on ZTF data often have few points or are incomplete. We can note that most of the O Miras do indeed stay mostly within the region defined by the paper, but some C Miras are also within it. There is another trend to observe here, namely that C Miras generally show lower absolute magnitudes in the K filter for a given color than O Miras. Thus, they have slightly higher luminosities for a given color in the infrared region of the spectrum because of the circumstellar envelope that is typical of C Miras. In addition, O Miras begin to appear at lower color values, indicating that they are generally hotter than C Miras, which is consistent with the paper by Feast (2006).

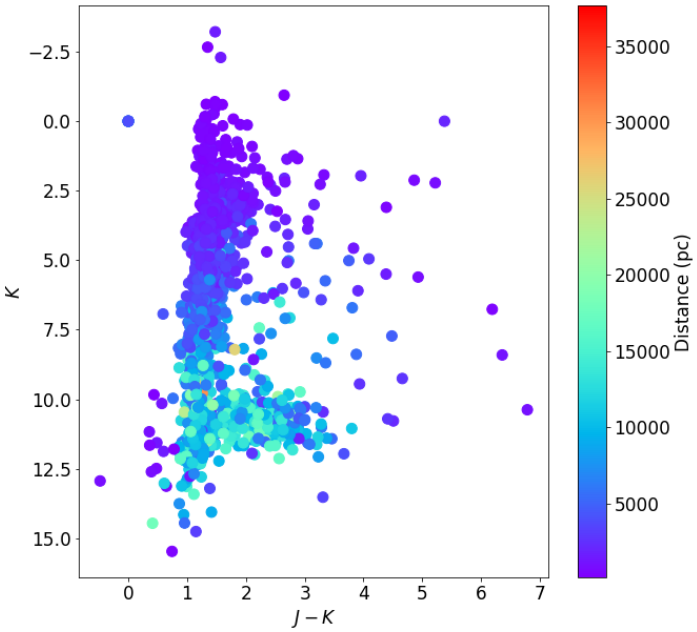

Figure 4.2.7: 2MASS color–magnitude diagram. It is obvious that as the magnitude increases, so does Miras distance from us.

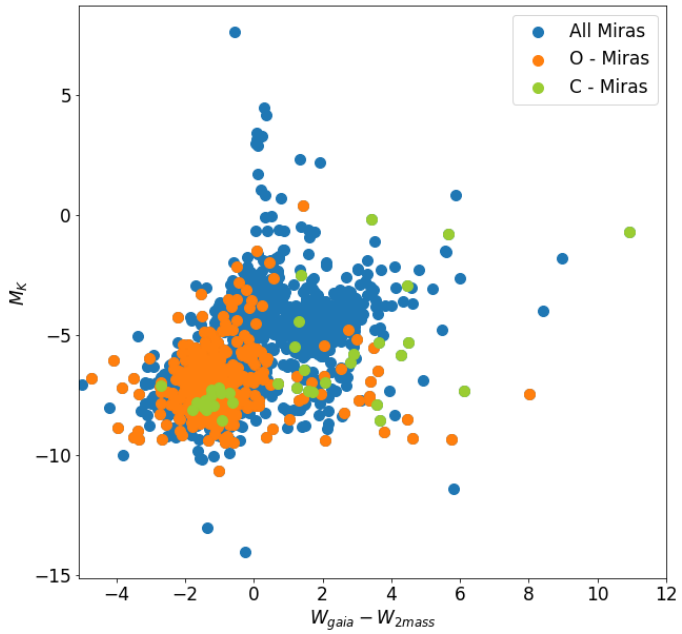

Figure 4.2.8: Color–magnitude diagram shows the distribution of different types Miras such as O/C Miras.

4.2.3 Period magnitude and period color relations

The dependence of the logarithm of the base 10 period on the K filter can be seen in the 4.2.9, wherein the left one it is again clear that the distribution in the two parts in magnitudes is due to distance and not to different types of stars. In addition, there is a linear dependence, where the brighter the object, the longer the period of brightness changes. The right one shows us, the same plot, but with the difference that we can see where the O/C Miras and SR variables are located. The graph shows that the C Miras have on average longer periods than the O Miras. This is related to their low age and higher mass loss and stellar winds that are driven by dust which is located around C Miras Feast (2006), Groenewegen (1996) and Groenewegen (1995). However, in the group of very young Miras, this distribution is very vague and cannot be relied upon, since stars can only become C Miras after the third dredge-up to the AGB.

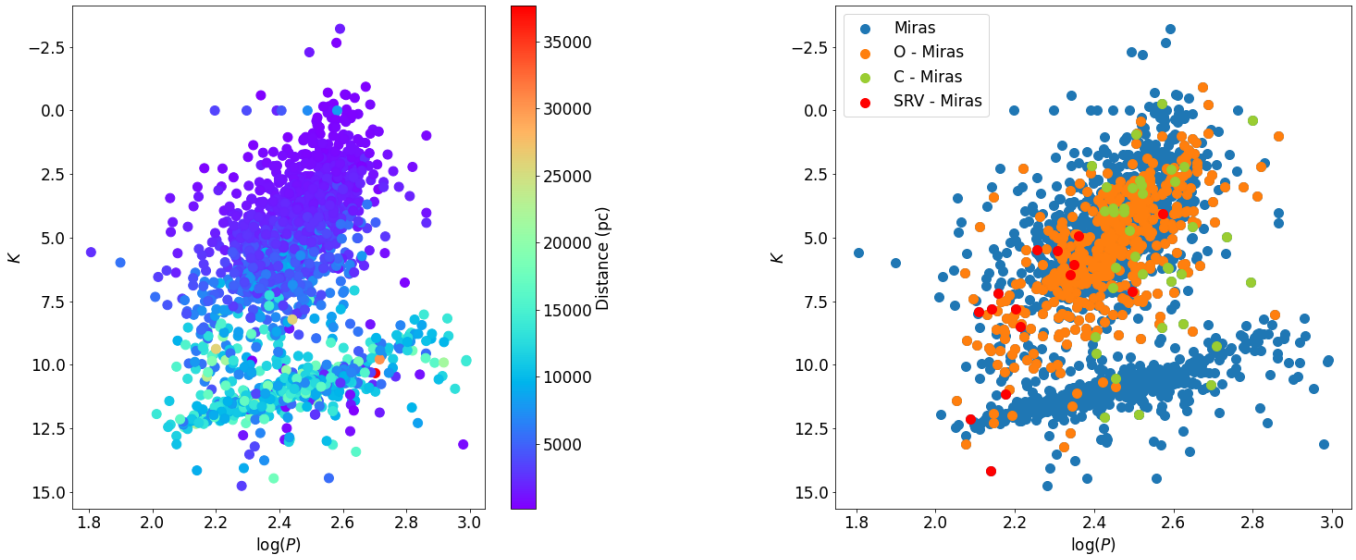

(a) Period–magnitude diagram for halo Miras with colorbar representing distance distribution. Large value of magnitude K the larger distance of Mira from us.

(b) Distribution of O/C Miras and SRV in period–magnitude diagram.

Figure 4.2.9: Period–magnitude diagrams for 2MASS filter K.

In the case of the dependence of the period on the $J-H$ color in Fig. 4.2.10, we observe the same distribution of Miras types based on the period. In addition, it is also noticeable that C Miras have a larger spread in color compared to SRV and O Miras. This spread into the red may be due to the thick circumstellar envelopes around these stars, as we would expect.

The period luminosity (PL) relation for Miras in the halo is shown in Fig. 4.2.11. that Miras with longer periods are fainter than those with shorter periods. This finding is in agreement with the paper by Ngeow (2023). At the same time, this dependence is exactly opposite to that found for the K, J, and H filters discussed above. This is because the r

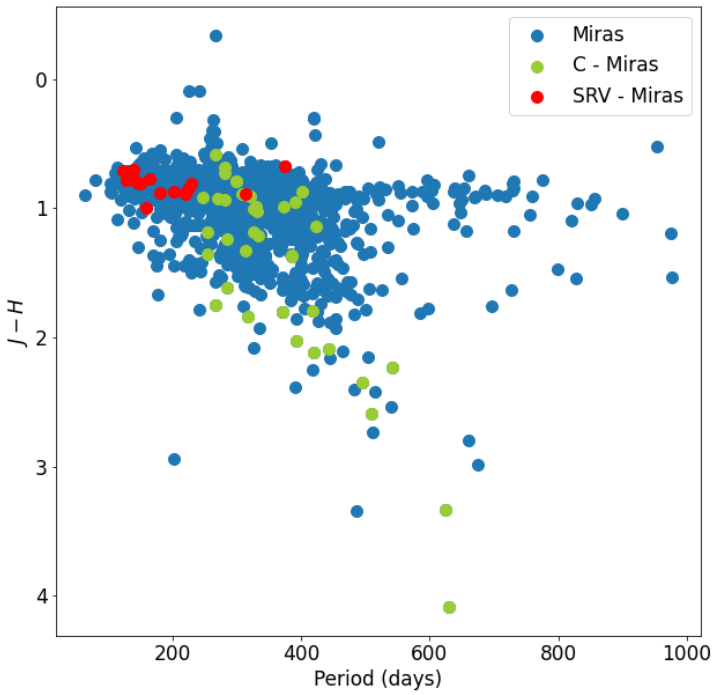

Figure 4.2.10: Period–magnitude diagram shows the distribution of different types Miras such as C Miras and SRV.

filter is more in the visible part of the spectrum, while K, J and H fall in the infrared part of the spectrum. Stars with longer periods in the visible spectrum show minimal emission in the plot, and as discussed, the longer period stars are mostly C Miras. These stars have circumstellar envelopes around them that emit in the infrared spectrum, and therefore we observe a decrease in the visible part for longer periods.

The linear dependence of the period on the filter confirms to us that indeed Miras can be used as standard candles to determine distances, especially in older galaxies such as ellipticals, or in spiral galaxy haloes where Cepheids are scarce.

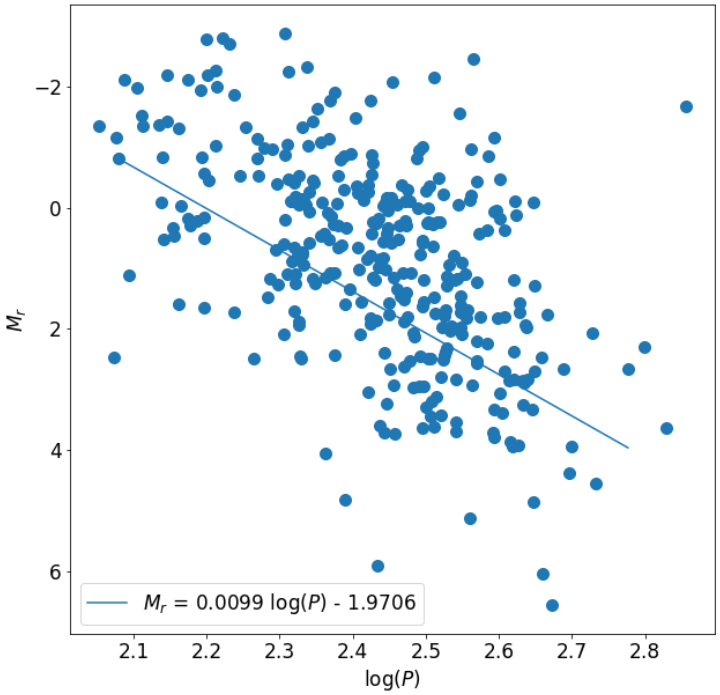

Figure 4.2.11: Period–luminosity diagram for ZTF *r* filter shows linear dependence which is described by the equation in this figure.

4.2.4 Lightcurves and moving color–magnitude diagram

We discussed the method of obtaining light curves and moving CMDs in Sect. 4.1.4. We followed the same procedure for the galactic halo. In this case, we knew the O/C distribution of Miras determined by Upsilon for multiple stars. The period determination was more in agreement with the period obtained from the catalogue, where the average deviation was 10 days. The exception was C Mira, see Fig. 4.2.14. where the period determined by Peranso was 100 days longer than that determined by the catalogue. In contrast, C Mira, see Fig. 4.2.15, has a deviation between periods of 10 days, as does O Miras. In the case of O Miras, the period determined by Peranso was in approximate agreement with the period obtained from the catalogue, whose light curves can be seen in Fig. 4.2.12 and Fig. 4.2.13 . Here we can also observe higher amplitudes of luminosity changes for O Miras, as we would expect, but the periods are similar for our chosen Miras.

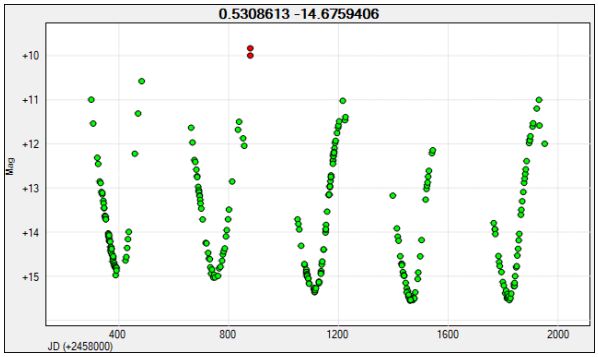

(a) Light curve of O Mira derived by Peranso using ZTF archive.

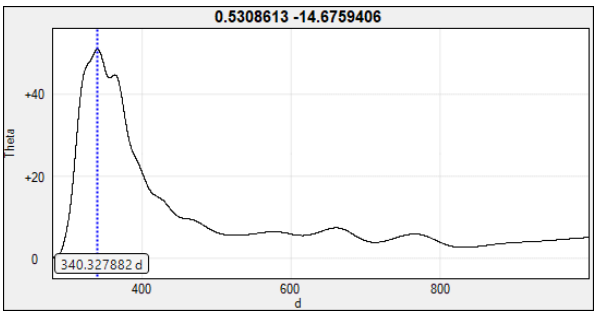

(b) Derived period by Lomb-Scargle method.

Figure 4.2.12: Light curve in *g* filter and derived period for O Mira with coordinates Ra = 0.531 deg, Dec = –14.68 deg.

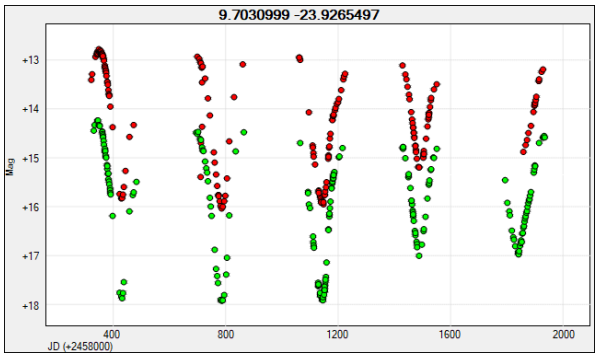

(a) Light curve of O Mira derived by Peranso using ZTF archive.

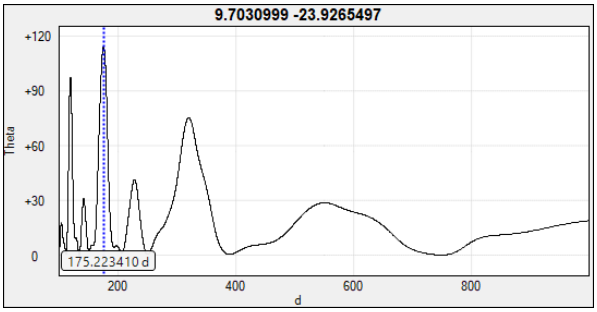

(b) Derived period by Lomb-Scargle method.

Figure 4.2.13: Light curves in *g* and *r* filters and derived period for O Mira with coordinates Ra = 9.703 deg, Dec = –23.93 deg.

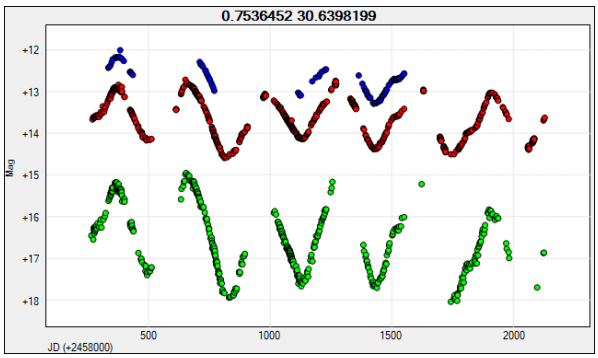

(a) Light curve of C Mira derived by Peranso using ZTF archive.

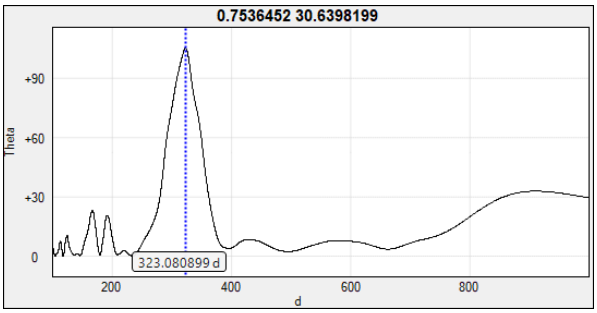

(b) Derived period by Lomb-Scargle method.

Figure 4.2.14: Light curves in *g*, *r* and *i* filters and derived period for O Mira with coordinates Ra = 0.754 deg, Dec = 30.64 deg.

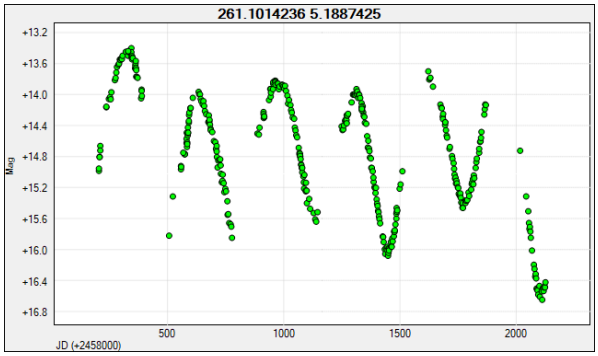

(a) Light curve of C Mira derived by Peranso using ZTF archive.

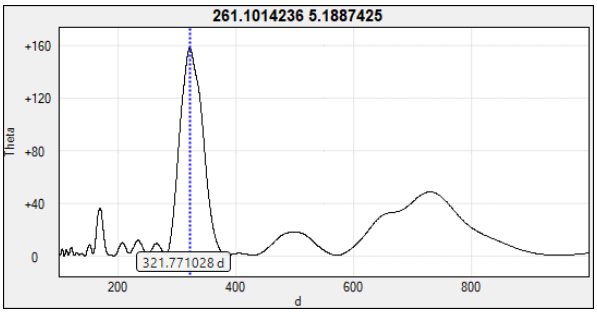

(b) Derived period by Lomb-Scargle method.

Figure 4.2.15: Light curve in *g* filter and derived period for O Mira with coordinates Ra = 261.1 deg, Dec = 5.189 deg.

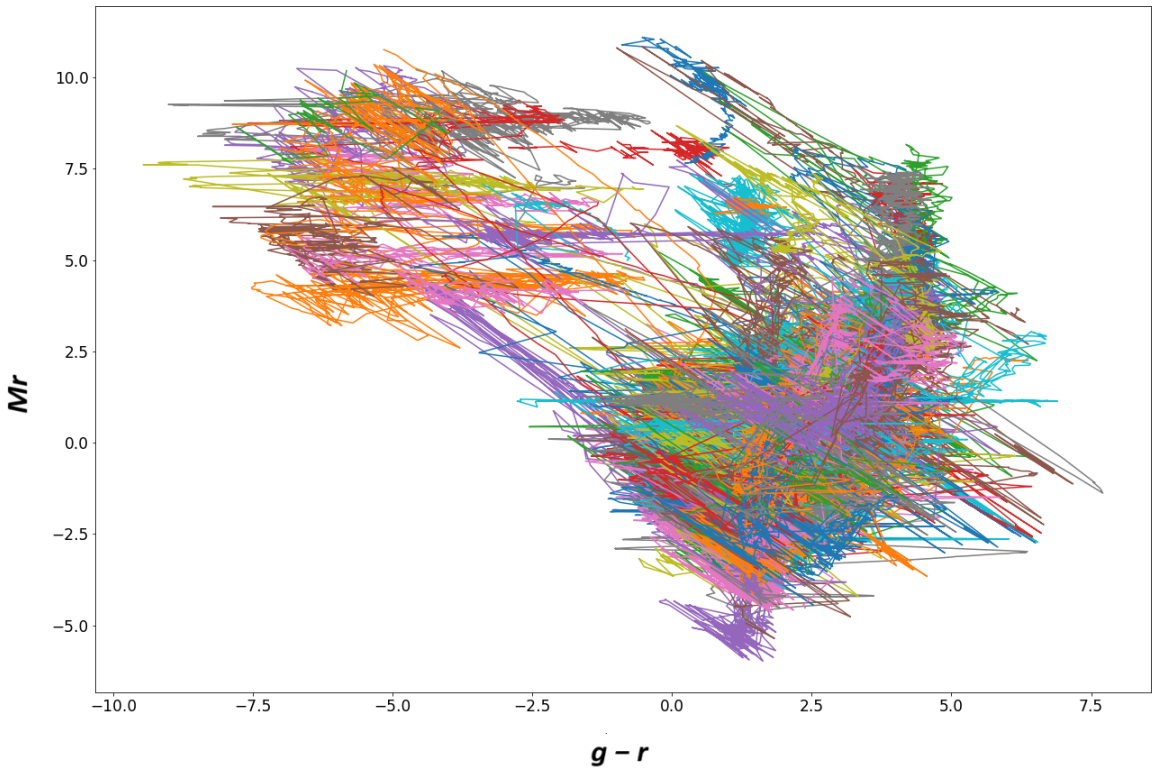

Figure 4.2.16: Moving CMD for Miras in the galactic halo. We can notice two separate groups for different color ranges.

The processed moving CMD can be seen in Fig. 4.2.16, where we observe the same trend as for the Miras in the bulge. However, the difference is noticeable in the color index. For several stars located in the upper left part of the diagram, this color index is extremely low, which would indicate their high effective temperature. However, a search of the effective temperatures obtained from the catalogue found no dependence that would tell us that these Miras are hotter. The type of Miras, the dependence on parallax, metallicity and location in the galaxy was also investigated. All of these characteristics appear to be independent of location in the diagram and computational error has been ruled out. It would therefore be worth further investigation as to why these stars are located in regions typical of extremely hot stars.

4.2.5 Period dependence on extinction modified values

For Miras in the halo, we did not have enough data to obtain extinction values for the different filters, as most of the catalogue focuses on extinction values for bulge and disc. For this reason, we only recalculated the values of g, r, and i from the ZTF catalogue and J, K from the 2MASS catalogue to Wesenheit dereddened magnitudes. For the ZTF filters, the dependence of the logarithm of the base 10 period on the Wesenheit magnitudes is evident, as seen in Fig. 4.2.17, where for each filter combination we obtained a linear dependence. We have the steepest dependence for the $g-r$ color and the flattest dependence for the g, i filters. Since the g, r band is in the optical band, where we expect a linear dependence opposite to the infrared band, as discussed above, the g, i bands lie on the boundary between the optical and infrared bands, causing a flatter dependence that reverses when using more infrared bands.

Thus, for the K filter we expect and find an inverse linear dependence in Fig. 4.2.18 than for the g, r and i filters. This finding is also in agreement with the paper by Soszynski (2005) in which this dependence, albeit steeper, was found for Miras in the LMC.

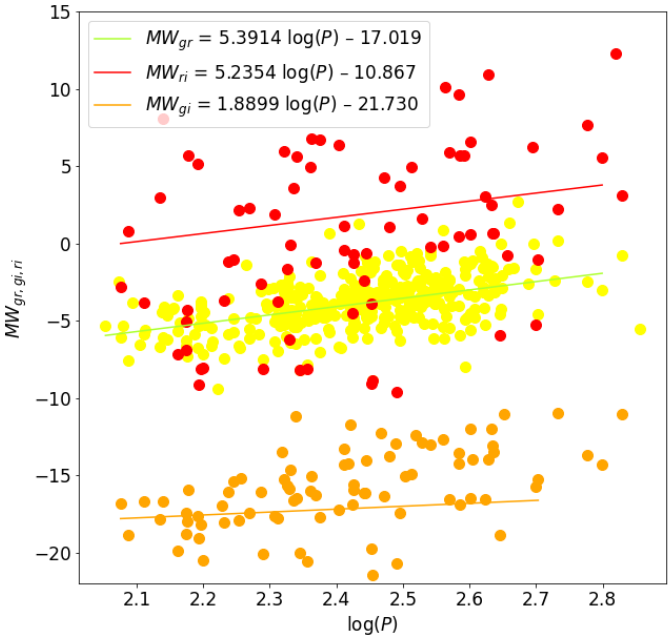

Figure 4.2.17: Relation of absolute magnitude in ZTF filters g, r, and i on log$P$. For each filter, we obtain a similar slope value and linear function.

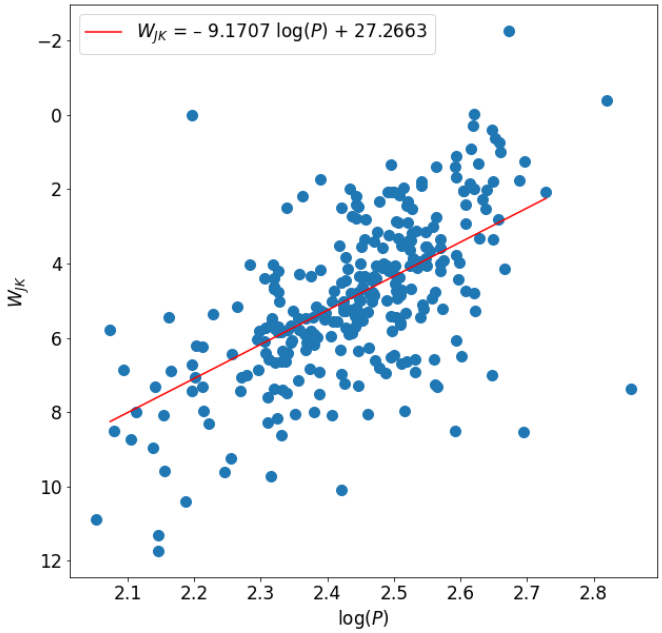

Figure 4.2.18: Dependence of Wesenheit dereddened magnitude in K filter on log$P$. We also obtain linear dependence with equation described in the graph.

Conclusion and summary

This work aimed to study Mira variable stars, including those in globular clusters. Because of the investigation of Miras in globular clusters, we focused only on those Miras that are located in the Galactic halo and bulge. As a condition to determine whether a Mira belongs to a cluster, it had to satisfy that its coordinates Ra, Dec do not differ by more than 1 deg from clusters, and the deviation from the proper motion of the star and the cluster is no more than 5 sigma. For the galactic bulge, we obtained 1608 Miras of which 308 are located in 15 clusters. For the galactic halo, we obtained data for 1954 Miras, but only 4 were located in 3 globular clusters. Thus, we conclude that Miras are not abundant in globular clusters and occur predominantly outside of these clusters. The reason for the disproportion of Miras in the bulge and halo clusters may be that the bulge is a very dense and relatively small area, so their inclusion in the clusters may not be correct. To be more certain about the classification, we would need to know the metallicity of the star and cluster or investigate the density and mass profile more deeply. All the data concerning Miras and clusters were obtained from the AAVSO, VSX, Gaia, 2MASS, Wise, OGLE-III, ZTF, Pan-STARRS1, isochrones, Harris, Holger Baumgardt catalogues or were complemented with the data obtained by calculation. Data were then saved in excel files and processed in Python using custom codes or the adopted Upsilon code for Mira type identification. Since Miras in clusters shows the same dependencies as those outside clusters, we will discuss Miras in general in the following lines for better clarity.

For Miras in the Galactic bulge, we found a bimodal metallicity distribution with the highest abundances for metallicities of -0.4 dex and $+0.5$ dex. In contrast, for Miras in the Galactic halo we obtained a gradually increasing abundance of Miras for higher metallicities, with a peak around $+0.5$ dex. This may be due to the different formation times of Miras in the halo and bulge, with the halo possibly being up to 1 Gyr younger, as suggested in the Morrison (1993).

The period distribution for Miras in the bulge and halo shows a classical Gaussian curve, where the highest frequency was found for periods of 330 days and 300 days, respectively. Lower periods of brightness changes may be associated with younger Miras, which would be consistent with the previous finding of metallicity/age Miras. In addition, in bulge, there may be an excess of O Miras, which have on average lower periods at the same age than C Miras.

The dependence of metallicity on the period of brightness changes in time did not show us a satisfactory dependence in either case, and we assume that there is no significant change in the period with metallicity. Thus, in the case of Miras in bulge clusters, most of them tend to lie at periods above 250 days, while those outside the clusters are also abundant at lower periods.

The highest abundance of Miras for effective temperatures obtained from the catalogue, by calculation, and from isochrones was found to be 3500 K in the case of the halo. In the case of bulge stars, the effective temperatures obtained from isochrones diverged from those obtained by calculation and from the catalogue, which also had the highest abundance around 3500 K. The reason is that we used ZTF data to calculate the isochrones but used data from Pan-STARRS1 as sample isochrones since sample isochrones were not available for ZTF.

By comparing the Miras bulge and halo in the color–color and color–magnitude diagrams, we found that the Miras in the halo have a larger spread in magnitudes for different filters but a similar spread in colors. The large range in magnitude values is explained by the fact that the Miras in the halo have large distances between them, which contrasts with their location in the bulge, where they are close together. The range in color for Miras in the bulge is due to the non-inclusion of interstellar extinction and reddening, which is typical for this region of the galaxy. In contrast, there is minimal interstellar extinction in the halo, so this spread in color may be due to the greater abundance of different types of Miras (O/C/SRV), while in the bulge are mostly O Miras, (Feast , 2007).

When studying the dependence of the G filter on the color $BP - RP$ (magnitudes from Gaia catalogue), we notice the same pattern for both halo and bulge, namely that at the minimum radius the object is bluer and brighter compared to the maximum. The bulge clusters Ter 6 and Djor 1 showed the highest color values, while NGC 6453 and NGC 6441 showed the lowest ones. Comparing with the catalogues and our obtained data, extinction affected their color values, whereas for higher color these stars/clusters had higher extinction.

Since we did not have information on the type of Miras for the bulge from the Upsilon program, we had to rely on the articles, whereby comparing the 2MASS filter K and the $J - K$ color they can distinguish O/C Miras, or by using the $W1$, $W2$ and $W3$ filters they can distinguish O/C Miras and SRV. This separation is only approximate but at least as a basic separation it was sufficient for us. From these inferred distributions, we found that less than 1/3 of the Miras in the bulge should be of type C, which is consistent with the expectation of a more abundant O Miras in the bulge. However, the filters from the 2MASS catalogue are insufficient to identify C/O Miras in the Galaxy, mainly because of the high reddening and the large number of background stars. Therefore, we examined photometric data from both the Gaia and 2MASS catalogues converted to the Wesenheit dereddened magnitude relative to the absolute magnitude in the K filter. We again took the O/C limits of Miras for the bulge based on the articles mentioned in the analysis part. For Miras in the halo, however, we had the type determined and could compare it with the prediction in the paper. This prediction fits our data very well and can therefore be taken as adequate for Miras in bulge as well. In addition, we found that C Miras in the halo have a lower magnitude and are thus brighter in the K filter for a given $J - K$ color than O Miras. This is due to the strong circumstellar envelope around C Miras, which emits in the longer infrared part of the spectrum.

When examining the V and I filters from the OGLE-III catalogue, which gave us enough data only for Miras in the bulge, we found a magnitude dependence on color with a third parameter that distinguished the color change periods. When Miras is redder and brighter, its period of brightness changes increases, as is known for pulsating Cepheid-type stars.

Miras can therefore also be good distance identifiers, for example in old elliptical galaxies, or in the halo of spiral galaxies.

By examining the dependence of the filter on the logarithm of the period, we obtained a linear dependence, where the star appears brighter in the infrared part of the spectrum with an increasing period. This dependence is narrower the more the filter falls in the infrared part of the spectrum, while the dependence is reversed if we use a filter from the optical part of the spectrum. The reason for this is that Miras are cool stars, which causes the predominant type of radiation to be longer wavelengths. In the case of C Miras, which generally have longer periods than O Miras and are surrounded by a circumstellar envelope, the radiation is further shifted to even longer wavelengths, which significantly limits the optical part of the spectrum. We have also verified this claim for the dependence of the magnitude in the K filter on the logarithm of the base 10 period for Miras in the halo. SRVs were distributed at the shortest periods, while C Miras were at the longest ones with generally higher luminosity.

From the ZTF catalogue we obtained time series data for a large fraction of our stars, from which we were able to construct a light curve and determine the periods. The program Peranso was used to determine the periods, with the Lomb-Scargle method, which in most cases gave us periods similar to those obtained from the catalogue. From the light curves, we also checked for the selected Miras that the Upsilon program correctly determined the type of Miras, since C Miras have lower amplitudes than O Miras. Periods are not crucial as we would have to compare Miras of the same age. In addition, we were able to construct a moving CMD for Miras in the bulge and halo using the color $g-r$ and the absolute magnitude in the filter r. Since these filters fall more in the optical part of the spectrum, we found the opposite dependence to that for the filter in the infrared part of the spectrum, as we commented above. At the same time, it is worth noting the high amplitudes of the luminosity changes associated with the strong Miras pulsations, and this prevails as a consequence of the change in the effective temperature of the star. In addition, we found a double distribution in the halo of Miras, with one part of the stars occupying a very hot region of the diagram. Unfortunately, no correlation was found with the effective temperature obtained from the catalogue or with other quantities such as metallicity, period, parallax, and position in the galaxy.

From the dependence of extinction on reddening, we verified that stars belonging to the same clusters have similar extinction and are in the same region of the graph. The low extinction in the bulge is shown by Miras with $b > +5$ deg and $b < -5$ deg, from which we can conclude that the extinction is strong only in the range $-5 < b < +5$ deg. For the Galactic bulge, we also had extinction data, so we recalculated the data from the J and K filters to dereddened values, which, compared to the plot without including extinction, shifted the color by 0.5 mag to the hotter part, while there was no shift in the K filter. Thus, extinction affected the stars in the bulge, especially in the J filter, as there was no shift in the K filter.

We compared the values for the bulge for the dereddened values with the values converted to Wesenheit magnitudes. As expected we obtained a linear dependence but with the difference that the dependence in this case increases faster for W_{JK} than it does for K_0. The reason for the differences may stem directly from the definition of the Wesenheit magnitude and its limitation, or from the data obtained for the extinction and reddening

values. For the halo, we did not have data for extinction and reddening, so we had to be satisfied with only the conversion to Wesenheit magnitudes for the ZTF filters and the K filter. For halo we observe a steeper dependence of the Wesenheit K magnitude on the logarithm of the base 10 period than for the same plot but for Miras in bulge. This difference may be due to, among other things, a more accurate determination of the linear fit for the halo, due to knowing more data for Miras in the halo. For the ZTF catalogue filters, we obtained the steepest dependence for the $g-r$ color and the flattest dependence for the $g-i$ color. The g, r bands lying in the optical spectrum show a linear dependence, as expected. On the contrary, the g, i bands are located at the boundary of the optical and infrared spectra, which causes a flatter dependence. When using infrared bands with longer wavelengths, this dependence changes.

For future research, it would be useful to determine more Miras their type and possibly compare this with the actual determination from the spectra. It would also be worth investigating the mass-loss rate and its dependence on Miras type or other parameters, as these stars have high values for mass loss. It would be convenient to obtain extinction values for the ZTF filters and sample isochrones for the ZTF filters, rather than having to approximate these filters to Pan-STARRS1.

References

Sources

Aarseth, S. Gravitational N-Body Simulations: Tools and Algorithms (Cambridge Monographs on Mathematical Physics). (Cambridge University Press,2003,11,10)

Adams, Alyssa M., Exploring the Properties of Mira-Type Stars with Spectropolarimetry, 2013, Undergraduate Honors Theses, Paper 118.,https://dc.etsu.edu/honors/118

Andriantsaralaza, M., Ramstedt, S., Vlemmings, W. & De Beck, E. Distance estimates for AGB stars from parallax measurements. *Astron. Astrophys.*. **667** pp. A74 (2022,11)

Angus, R., Morton, T., Foreman-Mackey, D., Saders, J., Curtis, J., Kane, S., Bedell, M., Kiman, R., Hogg, D. & Brewer, J. Toward Precise Stellar Ages: Combining Isochrone Fitting with Empirical Gyrochronology. *The Astronomical Journal*. **158**, 173 (2019,10), https://doi.org/10.3847/1538-3881/ab3c53

Bastian, N. & Mink, S. The effect of stellar rotation on colour-magnitude diagrams: on the apparent presence of multiple populations in intermediate age stellar clusters. *Monthly Notices Of The Royal Astronomical Society: Letters*. **398**, L11-L15 (2009,9), https://doi.org/10.1111/j.1745-3933.2009.00696.x

Bedding, T. & Zijlstra, A. HIPPARCOS Period-Luminosity Relations for Mira and Semiregular variables. . **506**, L47-L50 (1998,10)

Bellazzini, M., Ferraro, F. & Ibata, R. Building Up the Globular Cluster System of the Milky Way: The Contribution of the Sagittarius Galaxy. *The Astronomical Journal*. **125**, 188-196 (2003,1), https://doi.org/10.1086/344072

Berlioz-Arthaud, P. Mira Variables explained by a planetary companion interaction: A means to drop the pulsation paradigm?. *Astronomy ampAstrophysics*. **397**, 943-950 (2003,1),https://doi.org/10.1051/0004-6361:20021540

Bica, E., Ortolani, S. & Barbuy, B. Globular Clusters in the Galactic Bulge. *Publications Of The Astronomical Society Of Australia*. **33** (2016), http://dx.doi.org/10.1017/pasa.2015.47

Binney, J. & Tremaine, S. Galactic Dynamics: Second Edition (Princeton Series in Astrophysics, 13). (Princeton University Press,2008,1,27)

Boyd, D. Spectroscopic and photometric study of the Mira stars SU Camelopardalis and RY Cephei. (arXiv,2021),https://arxiv.org/abs/2107.10061

Bressan, A., Marigo, P., Girardi, L., Salasnich, B., Dal Cero, C., Rubele, S. & Nanni, A. PARSEC: stellar tracks and isochrones with the PAdova and TRieste Stellar Evolution Code. . **427**, 127-145 (2012,11)

Carlson, M. & Holtzman, J. Measuring Sizes of Marginally Resolved Young Globular Clusters with theSpace Telescope/i. *Publications Of The Astronomical Society Of The Pacific*. **113**, 1522-1540 (2001,12), https://doi.org/10.1086/324417

Carroll, B. & Ostlie, D. An Introduction to Modern Astrophysics. (Cambridge University Press,2017), https://books.google.cz/books?id=PY0wDwAAQBAJ

Chambers, K. & Et al. VizieR Online Data Catalog: The Pan-STARRS release 1 (PS1) Survey - DR1 (Chambers+, 2016). *VizieR Online Data Catalog*. pp. eII/349 (2017,7)

Charbonnel, C., Krause, M., Decressin, T., Meynet, G., Prantzos, N. & Diehl, R. How did globular clusters lose their gas?. *Proceedings Of The International Astronomical Union*. **10**, 255-256 (2012,8), https://doi.org/10.1017/s1743921314005663

Chen, X., Wang, S., Deng, L., Grijs, R., Yang, M. & Tian, H. The Zwicky Transient Facility Catalog of Periodic Variable Stars. *The Astrophysical Journal Supplement Series*. **249**, 18 (2020,7), http://dx.doi.org/10.3847/1538-4365/ab9cae

Clement, C., Muzzin, A., Dufton, Q., Ponnampalam, T., Wang, J., Burford, J., Richardson, A., Rosebery, T., Rowe, J. & Hogg, H. Variable Stars in Galactic Globular Clusters. *The Astronomical Journal*. **122**, 2587-2599 (2001,11), https://doi.org/10.1086/323719

Cutri, R., Wright, E., Conrow, T., Fowler, J., Eisenhardt, P., Grillmair, C., Kirkpatrick, J., Masci, F., McCallon, H., Wheelock, S., Fajardo-Acosta, S., Yan, L., Benford, D., Harbut, M., Jarrett, T., Lake, S., Leisawitz, D., Ressler, M., Stanford, S., Tsai, C., Liu, F., Helou, G., Mainzer, A., Gettngs, D., Gonzalez, A., Hoffman, D., Marsh, K., Padgett, D., Skrutskie, M., Beck, R., Papin, M. & Wittman, M. VizieR Online Data Catalog: AllWISE Data Release (Cutri+ 2013). *VizieR Online Data Catalog*. pp. eII/328 (2021,2)

Clement, C. Catalogue of variable stars in Milky Way globular clusters. *EPJ Web Of Conferences*. **152** pp. 01021 (2017), https://doi.org/10.1051/epjconf/201715201021

Da-run, X. Turbulent Convection and Pulsation Stability of Stars. *Chinese Astronomy And Astrophysics*. **41**, 471-494 (2017,10),https://doi.org/10.1016/j.chinastron.2017.11.001

Deliyannis, C., Anthony-Twarog, B., Lee-Brown, D. & Twarog, B. Li Evolution and the Open Cluster NGC 6819: A Correlation between Li Depletion and Spindown in Dwarfs More Massive Than the F-Dwarf Li-Dip. *The Astronomical Journal*. **158**, 163 (2019,9),https://doi.org/10.3847/1538-3881/ab3fad

Eggen, O. Photoelectric Studies. V. Magnitudes and Colors of Classical Cepheid Variable Stars.. *The Astrophysical Journal*. **113** pp. 367 (1951,3),https://doi.org/10.1086/145405

Eyer, L. & Mowlavi, N. Variable stars across the observational HR diagram. (2007), https://api.semanticscholar.org/CorpusID:118367005

L. Eyer, Rimoldini, L., Audard, M., Anderson... /iRelease 2. *Astronomy ampAstrophysics*. **623** pp. A110 (2019,3),https://doi.org/10.1051/0004-6361/201833304

Eyer, L., Audard, M., Holl, B., Rimoldini, L., Carnerero, M., Clementini, G., De Ridder, J., Distefano, E., Evans, D., Gavras, P., Gomel, R., Lebzelter, T., Marton, G., Mowlavi, N., Panahi, A., Ripepi, V., Wyrzykowski, L., Nienartowicz, K., Jevardat de Fombelle, G., Lecoeur-Taibi, I., Rohrbasser, L., Riello, M., Garcıa-Lario, P., Lanzafame, A., Mazeh, T., Raiteri, C., Zucker, S., Ábrahám, P., Aerts, C., Aguado, J., Anderson, R., Bashi, D., Binnenfeld, A., Faigler, S., Garofalo, A., Karbevska, L., Kóspál, Á., Kruszyńska, K., Kun, M., Lanza, A., Leccia, S., Marconi, M., Messina, S., Molinaro, R., Molnár, L., Muraveva, T., Musella, I., Nagy, Z., Pagano, I., Palaversa, L., Plachy, E., Prša, A., Rybicki, K., Shahaf, S., Szabados, L., Szegedi-Elek, E., Trabucchi, M., Barblan, F., Grenon, M., Roelens, M. & Süveges, M. Gaia Data Release 3. Summary of the variability processing and analysis. . **674** pp. eA13 (2023,6)

Fabas, N., Lèbre, A. & Gillet, D. Shock-induced polarized H emission lines in the Mira star/i. *Astronomy ampAstrophysics*. **535** pp. A12 (2011,10),https://doi.org/10.1051/0004-6361/201117748

Feast, M. The pulsation, temperatures and metallicities of Mira and semiregular variables in different stellar systems. *Monthly Notices Of The Royal Astronomical Society*. **278**, 11-21 (1996,1), http://dx.doi.org/10.1093/mnras/278.1.11

Feast, M., Whitelock, P. & Menzies, J. Carbon-rich Mira variables: kinematics and absolute magnitudes: C-Mira kinematics. *Monthly Notices Of The Royal Astronomical Society*. **369**, 791-797 (2006,5), http://dx.doi.org/10.1111/j.1365-2966.2006.10324.x

Feast, M. C– and O–Rich Miras and Galactic Structure. *Why Galaxies Care About AGB Stars: Their Importance As Actors And Probes*. **378** pp. 479 (2007,11)

Feast, M. The Ages, Masses, Evolution and Kinematics of Mira variable. (arXiv,2008), https://arxiv.org/abs/0812.0250

Forbes, D. & Bridges, T. Accreted versussitu/iWay globular clusters. *Monthly Notices Of The Royal Astronomical Society*. (2010,2), https://doi.org/10.1111/j.1365-2966.2010.16373.x

Forbes, D., Bastian, N., Gieles, M., Crain, R., Kruijssen, J., Larsen, S., Ploeckinger, S., Agertz, O., Trenti, M., Ferguson, A., Pfeffer, J. & Gnedin, O. Globular cluster formation and evolution in the context of cosmological galaxy assembly: open questions. *Proceedings Of The Royal Society A: Mathematical, Physical And Engineering Sciences*. **474**, 20170616 (2018,2), https://doi.org/10.1098/rspa.2017.0616

Fukugita, M., Yasuda, N., Doi, M., Gunn, J. & York, D. Characterization of Sloan digital sky survey stellar photometry. *Astron. J.*. **141**, 47 (2011,2)

Gaia Collaboration, Brown, A., Vallenari, A., Prusti, T., De Bruijne, J., Babusiaux, C., Biermann, M., Creevey, O., Evans, D., Eyer, L., Hutton, A., Jansen, F., Jordi, C., Klioner, S., Lammers, U., Lindegren, L., Luri, X., Mignard, F., Panem, C., Pourbaix, D., Randich, S., Sartoretti, P., Soubiran, C., Walton, N., Arenou, F., Bailer-Jones, T. Gaia Early Data Release 3. Summary of the contents and survey properties. . **649** pp. eA1 (2021,5)

Gaia Collaboration VizieR Online Data Catalog: Gaia DR3 Part 1. Main source (Gaia Collaboration, 2022). *VizieR Online Data Catalog*. pp. eI/355 (2022,5)

Groenewegen, M. The circumstellar shells of carbon miras. *Astrophysics And Space Science*. **224**, 321-324 (1995,2), http://dx.doi.org/10.1007/BF00667864

Groenewegen, M., Van den Hoek, L. & De Jong, T. The evolution of galactic carbon stars.. . **293** pp. 381-395 (1995,1)

Groenewegen, M. & Whitelock, P. A revised period-luminosity relation for carbon Miras. *Monthly Notices Of The Royal Astronomical Society*. **281**, 1347-1351 (1996,8), http://dx.doi.org/10.1093/mnras/281.4.1347

Habing, H. AGB and POST-AGB STARS: an Overview. *Science With The VLT Interferometer*. pp. 183-191 (1997), https://doi.org/10.1007/978-3-540-69398-7-23

Harris, G. & Deupree, R. Effects of heavy-element abundances on the color-magnitude diagrams of young clusters in the Galaxy and the Magellanic Clouds. *The Astrophysical Journal*. **209** pp. 402 (1976,10), https://doi.org/10.1086/154733

Herbig, G. Identification of Aluminum Hydride as the Emitter of Bright Lines Observed in Cygni Near Minimum Light. *Publications Of The Astronomical Society Of The Pacific*. **68** pp. 204 (1956,6), https://doi.org/10.1086/126916

Iwanek, P., Kozlowski, S., Gromadzki, M., Soszyński, I., Wrona, M., Skowron, J., Ratajczak, M., Udalski, A., Szymański, M., Pietrukowicz, P., Ulaczyk, K., Poleski, R., Mróz, P., Skowron, D. & Rybicki, K. Multiwavelength Properties of Miras. *The Astrophysical Journal Supplement Series*. **257**, 23 (2021,11), http://dx.doi.org/10.3847/1538-4365/ac1797

Jetsu, L. & Porceddu, S. Shifting Milestones of Natural Sciences: The Ancient Egyptian Discovery of Algol's Period Confirmed. *PLOS ONE*. **10**, e0144140 (2015,12), https://doi.org/10.1371/journal.pone.0144140

Johnson, H. & Morgan, W. Fundamental stellar photometry for standards of spectral type on the revised system of the Yerkes spectral atlas. *The Astrophysical Journal*. **117** pp. 313 (1953,5),https://doi.org/10.1086/145697

Keenan, P. Classification of the S-Type Stars.. *The Astrophysical Journal*. **120** pp. 484 (1954,11),https://doi.org/10.1086/145937

Kim, D. & Bailer-Jones, C. A package for the automated classification of periodic variable stars. *Astronomy amp; Astrophysics*. **587** pp. A18 (2016,2), http://dx.doi.org/10.1051/0004-6361/201527188

King, I. The structure of star clusters. I. an empirical density law. *The Astronomical Journal*. **67** pp. 471 (1962,10), https://doi.org/10.1086/108756

Kruijssen, J. Globular clusters as the relics of regular star formation in 'normal' high-redshift galaxies. *Monthly Notices Of The Royal Astronomical Society*. **454**, 1658-1686 (2015,10), https://doi.org/10.1093/mnras/stv2026

Layden, A., Tiede, G., Chaboyer, B., Bunner, C. & Smitka, M. Infrared K-band Photometry of Field RR Lyrae Variable Stars. . **158**, e105 (2019,9)

Mackey, A. & Gilmore, G. Comparing the properties of local globular cluster systems: implications for the formation of the Galactic halo. *Monthly Notices Of The Royal Astronomical Society*. **355**, 504-534 (2004,12), https://doi.org/10.1111/j.1365-2966.2004.08343.x

Madore, B. A Reddening-independent Formulation of the Period-Luminosity Relation: the Wesenheit Function. *The Galaxy And The Local Group*. **182** pp. 153 (1976,1)

Mardling, R. & Aarseth, S. Tidal interactions in star cluster simulations. *Monthly Notices Of The Royal Astronomical Society*. **321**, 398-420 (2001,3), https://doi.org/10.1046/j.1365-8711.2001.03974.x

Mamajek, E., Torres, G., Prsa, A., Harmanec, P., Asplund, M., Bennett, P., Capitaine, N., Christensen-Dalsgaard, J., Depagne, E., Folkner, W., Haberreiter, M., Hekker, S., Hilton, J., Kostov, V., Kurtz, D., Laskar, J., Mason, B., Milone, E., Montgomery, M., Richards, M., Schou, J. & Stewart, S. IAU 2015 Resolution B2 on Recommended Zero Points for the Absolute and Apparent Bolometric Magnitude Scales. *ArXiv E-prints*. pp. earXiv:1510.06262 (2015,10)

Masci, F., Laher, R., Rusholme, B., Shupe, D., Groom, S., Surace, J., Jackson, E., Monkewitz, S., Beck, R., Flynn, D., Terek, S., Landry, W., Hacopians, E., Desai, V., Howell, J., Brooke, T., Imel, D., Wachter, S., Ye, Q., Lin, H., Cenko, S., Cunningham, V., Rebbapragada, U., Bue, B., Miller, A., Mahabal, A., Bellm, E., Patterson, M., Jurić, M., Golkhou, V., Ofek, E., Walters, R., Graham, M., Kasliwal, M., Dekany, R., Kupfer, T., Burdge, K., Cannella, C., Barlow, T., Sistine, A., Giomi, M., Fremling, C., Blagorodnova, N., Levitan, D., Riddle, R., Smith, R., Helou, G., Prince, T. & Kulkarni, S. The Zwicky Transient Facility: Data Processing, Products, and Archive. *Publications Of The Astronomical Society Of The Pacific*. **131**, 018003 (2018,12), https://doi.org/10.1088/1538-3873/aae8ac

Matsunaga, N., Menzies, J., Feast, M., Whitelock, P., Onozato, H., Barway, S. & Aydi, E. Discovery of carbon-rich Miras in the Galactic bulge. *Monthly Notices Of The Royal Astronomical Society*. **469**, 4949-4956 (2017,5), http://dx.doi.org/10.1093/mnras/stx1213

Mattei, J. Introducing Mira Variables. . **25**, 57-62 (1997,1)

Meyers, R. Encyclopedia of Physical Science and Technology, Eighteen-Volume Set. (Cambridge University Press,2001)

Minniti, D., Geisler, D., Alonso-Garcıa, J., Palma, T., Beamın, J., Borissova, J., Catelan, M., Clariá, J., Cohen, R., Contreras Ramos, R., Dias, B., Fernández-Trincado, J., Gómez, M., Hempel, M., Ivanov, V., Kurtev, R., Lucas, P., Moni-Bidin, C., Pullen, J., Ramırez Alegrıa, S., Saito, R. & Valenti, E. New VVV Survey Globular Cluster Candidates in the Milky Way Bulge. . **849**, eL24 (2017,11)

Morrison, H. & Harding, P. The Galactic bulge and halo. *Publications Of The Astronomical Society Of The Pacific*. **105** pp. 977 (1993,9), http://dx.doi.org/10.1086/133267

Mowlavi, N., Lecoeur-Taïbi, I., Lebzelter, T., Rimoldini, L., Lorenz, D., Audard, M., De Ridder, J., Eyer, L., Guy, L., Holl, B., Fombelle, G., Marchal, O., Nienartowicz, K., Regibo, S., Roelens, M. & Sarro, L. Gaia Data Release 2: The first Gaia catalogue of long-period variable candidates. *Astronomy amp; Astrophysics*. **618** pp. A58 (2018,10), http://dx.doi.org/10.1051/0004-6361/201833366

Ngeow, C. & Kanbur, S. The linearity of the Wesenheit function for the Large Magellanic Cloud Cepheids. . **360**, 1033-1039 (2005,7)

Ngeow, C., Liao, S., Bellm, E., Duev, D., Graham, M., Mahabal, A., Masci, F., Medford, M., Riddle, R. & Rusholme, B. Zwicky transient facility and globular clusters: The period–luminosity and period–luminosity–color relations for late-type contact binaries. *Astron. J.*. **162**, 63 (2021,8)

Ngeow, C., Bhardwaj, A., Henderson, J., Graham, M., Laher, R., Medford, M., Purdum, J. & Rusholme, B. Zwicky Transient Facility and Globular Clusters: The Period-Luminosity and Period-Wesenheit Relations for Type II Cepheids. . **164**, e154 (2022,10)

Ngeow, C., Ou, J., Bhardwaj, A., Purdum, J., Rusholme, B. & Wold, A. Zwicky Transient Facility and Globular Clusters: The gr-band Period–Luminosity Relations for Mira Variables at Maximum Light and their Applications to Local Galaxies. *The Astronomical Journal*. **166**, 96 (2023,8), http://dx.doi.org/10.3847/1538-3881/ace7b4

Peebles, P. & Dicke, R. Origin of the Globular Star Clusters. *The Astrophysical Journal*. **154** pp. 891 (1968,12), https://doi.org/10.1086/149811

Percy, J. Rotating Variable Stars. . **72** pp. 162 (1978,6)

Polster, J. Analýza světelných křivek uhlíkových mirid [online]. (Masarykova univerzita, Přírodovědecká fakulta, Brno), https://is.muni.cz/th/uw7xe/, SUPERVISOR : Zdeněk Mikulášek

Qin, W., Nataf, D., Zakamska, N., Wood, P. & Casagrande, L. The Mira-based Distance to the Galactic Center. *The Astrophysical Journal*. **865**, 47 (2018,9), http://dx.doi.org/10.3847/1538-4357/aad7fb

Ragland, S., Traub, W., Berger, J., Danchi, W., Monnier, J., Willson, L., Carleton, N., Lacasse, M., Millan-Gabet, R., Pedretti, E., Schloerb, F., Cotton, W., Townes, C., Brewer, M., Haguenauer, P., Kern, P., Labeye, P., Malbet, F., Malin, D., Pearlman, M., Perraut, K., Souccar, K. & Wallace, G. First Surface-resolved Results with the Infrared Optical Telescope Array Imaging Interferometer: Detection of Asymmetries in Asymptotic Giant Branch Stars. *The Astrophysical Journal*. **652**, 650-660 (2006,11), https://doi.org/10.1086/507453

Reid, M. & Peek, J. How Mira Variables Change Visual Light by a Thousandfold. *The Astrophysical Journal*. **568**, 931-938 (2002,4), https://doi.org/10.1086/338947

Reid, M. & Brunthaler, A. The Proper Motion of Sagittarius A*. II. The Mass of Sagittarius A*. *The Astrophysical Journal*. **616**, 872-884 (2004,12), http://dx.doi.org/10.1086/424960

Renzini, A. & Pecci, F. Tests of Evolutionary Sequences Using Color-Magnitude Diagrams of Globular Clusters. *Annual Review Of Astronomy And Astrophysics*. **26**, 199-244 (1988,9),https://doi.org/10.1146/annurev.aa.26.090188.001215

Rojas-Arriagada, A., Zoccali, M., Schultheis, M., Recio-Blanco, A., Zasowski, G., Minniti, D., Jönsson, H. & Cohen, R. The bimodal [Mg/Fe] versus [Fe/H] bulge sequence as revealed by APOGEE DR14. *Astronomy amp; Astrophysics*. **626** pp. A16 (2019,6), http://dx.doi.org/10.1051/0004-6361/201834126

Schultheis, M., Sellgren, K., Ramírez, S., Stolovy, S., Ganesh, S., Glass, I. & Girardi, L. Interstellar extinction and long-period variables in the Galactic centre. *Astronomy amp; Astrophysics*. **495**, 157-168 (2008,12), http://dx.doi.org/10.1051/0004-6361:200810342

Shore, S. Stars, Variable. *Encyclopedia Of Physical Science And Technology*. pp. 737-747 (2003), http://dx.doi.org/10.1016/B0-12-227410-5/00726-2

Skrutskie, M., Schneider, S., Stiening, R., Strom, S., Weinberg, M., Beichman, C., Chester, T., Cutri, R., Lonsdale, C., Elias, J., Elston, R., Capps, R., Carpenter, J., Huchra, J., Liebert, J., Monet, D., Price, S. & Seitzer, P. VizieR Online Data Catalog: 2MASS Catalog Incremental Data Release (IPAC/UMass, 2000). *VizieR Online Data Catalog*. pp. eII/241 (2000,9)

Smith, G. The Metal Contents of Milky Way Globular Clusters. *Publications Of The Astronomical Society Of The Pacific*. **112**, 12-17 (2000,1), http://dx.doi.org/10.1086/316498

Soszynski, I., Udalski, A., Kubiak, M., Szymanski, M., Pietrzynski, G., Zebrun, K., Szewczyk, O., Wyrzykowski, L. & Ulaczyk, K. The Optical Gravitational Lensing Experiment. Miras and Semiregular Variables in the Large Magellanic Cloud. (arXiv,2005), https://arxiv.org/abs/astro-ph/0512578

Soszyński, I. The OGLE-III catalog of variable stars: First results. *The Magellanic System: Stars, Gas, And Galaxies*. **256** pp. 30-35 (2009,3)

Sun, Y., Zhang, J., Zhang, B., Xu, S., Mai, X., Ding, H., Chen, W. & Wen, S. Miras as a distance indicator in the CSST, JWST, and Gaia era. *Frontiers In Astronomy And Space Sciences*. **10** (2023,7), http://dx.doi.org/10.3389/fspas.2023.1232151

Supikova, J. & Paunzen, E. Estimating stellar parameters. *OBA Stars: Variability And Magnetic Fields*. pp. e1 (2021,4)

Uttenthaler, S., Lebzelter, T., Busso, M., Palmerini, S., Aringer, B. & Schultheis, M. Lithium destruction and production observed in red giant stars. (arXiv,2012), https://arxiv.org/abs/1206.2759

Viani, L. & Basu, S. Isochrones of M67 with an Expanded Set of Parameters. *EPJ Web Of Conferences*. **160** pp. 05005 (2017), https://doi.org/10.1051/epjconf/201716005005

Wang, S. & Chen, X. The Optical to Mid-infrared Extinction Law Based on the APOGEE, Gaia DR2, Pan-STARRS1, SDSS, APASS, 2MASS, and WISE Surveys. . **877**, e116 (2019,6)

Watson, C., Henden, A. & Price, A. VizieR Online Data Catalog: AAVSO International Variable Star Index VSX (Watson+, 2006-). *VizieR Online Data Catalog*. pp. eB/vsx (2022,5)

Willson, L. & Marengo, M. Miras. (arXiv,2012), https://arxiv.org/abs/1207.4094

Wood, P. Convection and pulsation in red giant stars. *Proceedings Of The International Astronomical Union*. **2**, 343-348 (2006,8),https://doi.org/10.1017/s1743921307000701

Yamamura, I., Dominik, C., De Jong, T., Waters, L. & Molster, F. The origin of silicate carbon stars: ISO/SWS observation of V778 Cygni. . **363** pp. 629-639 (2000,11)

Yuan, W., Macri, L., He, S., Huang, J., Kanbur, S. & Ngeow, C. Large Magellanic Cloud Near-infrared Synoptic Survey. V. Period–Luminosity Relations of Miras. *The Astronomical Journal*. **154**, 149 (2017,9), http://dx.doi.org/10.3847/1538-3881/aa86f1

Zijlstra, A., Matsuura, M. & Bedding, T. Period Evolution in Mira Variables. *Astrophysics And Space Science Library*. pp. 91-94 (2003), http://dx.doi.org/10.1007/978-94-010-0139-7-13

Electronic sources

[1] https://esahubble.org/wordbank/globular-cluster/

[2] http://spider.seds.org/spider/MWGC/mwgc.html

[3] https://sites.astro.caltech.edu/~george/ay20/eaa-galhalo.pdf

[4] https://ned.ipac.caltech.edu/level5/ESSAYS/Cudworth/cudworth.html

[5] https://www.eso.org/public/france/images/b09/?lang

[6] https://esahubble.org/wordbank/globular-cluster/

[7] https://www.nasa.gov/mission_pages/hubble/main/index.html

[8] https://webb.nasa.gov/

[9] https://courses.lumenlearning.com/suny-astronomy/chapter/checking-out-the-theory/

[10] https://www.space.com/15396-variable-stars.html

[11] https://earthsky.org/tonight/spica-guide-to-omega-centauri/

[12] https://chandra.harvard.edu/graphics/edu/earth_scientist_stars.pdf

[13] https://imagine.gsfc.nasa.gov/science/objects/cataclysmic_variables.html

[14] https://heasarc.gsfc.nasa.gov/W3Browse/all/gcvs.html

[15] https://www.aavso.org/variables-what-are-they-why-observe-them

[16] https://astrobites.org/2012/07/18/understanding-the-dynamical-state-of-globular-clusters/

[17] https://www.aavso.org/mira-variables-period-changes

[18] http://www.sai.msu.su/gcvs/gcvs/vartype.htm

[19] https://academic-accelerator.com/encyclopedia/helium-flash

[20] https://ogle.astrouw.edu.pl/atlas/Miras.html

[21] https://chandra.harvard.edu/edu/formal/variable_stars/bg_info.html

[22] https://www.atnf.csiro.au/outreach/education/senior/astrophysics/stellarevolution_postmain.html

[23] https://www.atnf.csiro.au/outreach/education/senior/astrophysics/stellarevolution_hrintro.html

[24] http://astro.vaporia.com/start/colormagnitudediagram.html

[25] https://www.cosmos.esa.int/web/gaia/iow_20180316

[26] https://www.ipac.caltech.edu/page/history

[27] https://www.ipac.caltech.edu/project/irsa

[28] https://www.ipac.caltech.edu/page/mission

[29] https://irsa.ipac.caltech.edu/data/ZTF/docs/releases/ztf_release_notes_latest

[30] https://astronomy.ua.edu/undergraduate-program/course-resources-astronomy/lab-exercise-8-cosmic-distributions-and-the-galactic-ecology/1293-2/

[31] https://www.sdss4.org/surveys/segue/

[32] https://web.njit.edu/~gary/321/Lecture18.html

[33] https://physics.mcmaster.ca/~harris/mwgc.dat

[34] https://people.smp.uq.edu.au/HolgerBaumgardt/globular/orbits_table.txt

[35] https://irsa.ipac.caltech.edu/applications/DUST/

[36] https://www.esa.int/ESA_Multimedia/Images/2022/06/Gaia_map_of_interstellar_dust_in_the_Milky_Way

[37] http://www.ioa.s.u-tokyo.ac.jp/kisohp/RESEARCH/symp2012/Sakamoto.pdf

[38] https://astronomy.swin.edu.au/cosmos/h/Half-light+Radius

[39] https://slideplayer.com/slide/13529497/